รหัสโครงการ SUT1-105-42-24-22

รายงานการวิจัย

การประลัยระหว่างโปรตอนและแอนไทโปรตอน กลายเป็น 2 และ 3 เมซอน ขณะหยุดนิ่ง

(Proton-Antiproton Annihilation at Rest into Two and Three Mesons)

คณะผู้วิจัย

หัวหน้าโครงการ

Asst.Prof.Dr. Yupeng Yan

สาขาวิชาฟิสิกส์

สำนักวิชาวิทยาศาสตร์

มหาวิทยาลัยเทคโนโลยีสุรนารี

ได้รับทุนอุดหนุนการวิจัยจากมหาวิทยาลัยเทคโนโลยีสุรนารี ปีงบประมาณ พ.ศ. 2542-43

งานวิจัยเป็นความรับผิดชอบของหัวหน้าโครงการวิจัยแต่เพียงผู้เดียว

ตุลาคม 2545

Acknowledgement

I would like to express my deep appreciation of the research grant provided by Suranaree University of Technology which made this project possible and successful. It is indeed a pleasure to acknowledge Dr. Worasit Uchai, Dr. Chinorat Kobdaj, Mr. Kem Pumsa-ard and Ms. Nopmanee Supanam for their participation in the research. The author is grateful for helps from his colleagues.

บทคัดย่อ

ไดอะแกรมชนิดต่างๆ ของอันตรกริยาของการประลัยระหว่างนิวคลิออน-แอนไทนิวคลิออน กลายเป็น 2 และ 3 เมซอน ได้รับการวิเคราะห์ การเปรียบเทียบระหว่างผลการทำนายทางทฤษฎีกับผลการทดลองแสดงให้เห็นว่ากลไกของการสร้างและการทำลายของควาก-แอนไทควากแบบ $^3P_0$ ดูสมเหตุผลมากกว่ากลไกของการประลัยระหว่างนิวคลิออน-แอนไทนิวคลิออนแบบ $^3S_1$ และไดอะแกรม A2 และ A3 เป็นชนิดที่เกิดขึ้นมากกว่ากระบวนอื่นๆ ในด้านการประลัยของนิวคลิออน-แอนไทนิวคลิออน กลายเป็น 2 และ 3 เมซอน การประเมินค่าของขนาดของทรานซิชันและพลังงานศักย์เชิงแสงของการประลัยระหว่างนิวคลิออน-แอนไทนิวคลิออนกลายเป็น 2 เมซอน ได้รับการแสดงไว้อย่างละเอียดในไดอะแกรม A2 ค่าพลังงานเชิงแสงจากไดอะแกรมแบบ A2 และ A3 ที่หาค่าได้ ได้รับการนำมาประยุกต์เพื่อศึกษาระดับพลังงานของอะตอมของนิวคลิออน-แอนไทนิวคลิออน

เพื่อทำการพิสูจน์ข้อถกเถียงที่ว่ากลไกของการสร้างและการทำลายของควาก-แอนไทควาก แบบ $^3P_0$ ดูสมเหตุผลมากกว่ากลไกของการประลัยระหว่างนิวคลิออน-แอนไทนิวคลิออน เราได้ทำการศึกษาอันตรกริยาของการประลัยของอิเล็กตรอน-โพซิตรอนกลายเป็นคู่ของนิวคลิออน แบบ $^3P_0$ ข้อมูลจากการทดลองสอดคล้องกับทฤษฎีอย่างสมเหตุผล

Abstract

Various diagrams of the reactions of nucleon-antinucleon annihilation into two and three mesons have been analyzed. The comparison of the theoretical predictions by different diagrams with experimental data show that the $^3P_0$ quark-antiquark creation and destruction mechanism is more reasonable than the $^3S_1$ mechanism in nucleon-antinucleon annihilations, and the $A2$ and $A3$ diagrams are dominant over other processes for the nucleon-antinucleon annihilation into respectively two and three mesons. Illustrated in details are the evaluations of the transition amplitude and the corresponding optical potential of the nucleon-antinucleon annihilation into two mesons in the $A2$ diagram. The derived optical potentials from the $A2$ and $A3$ diagrams have been applied to study the nucleon-antinucleon atomic states.

To further verify the argument that the $^3P_0$ quark-antiquark creation and destruction mechanism is more reasonable than the $^3S_1$ mechanism in nucleon-antinucleon annihilations, we have also studied the reactions of electron-position annihilation into nucleon-antinucleon pairs in the $^3P_0$ model. The experimental data are reasonably produced.

Contents

Chapter 1

Introduction

The consistent description of the strong interaction at low and intermediate energies is still a prominent problem in theoretical physics. Although the basic theory, Quantumchromodynamics (QCD), was already developed in the early 70's[1, 2, 3, 4], at present we are far from a fundamental understanding of the phenomenology of strongly interacting hadrons at low energy.

The QCD describes the interactions between the constituents of the hadrons, quarks and gluons, in the framework of a nonabelian gauge theory. Due to this nonabelian structure of the theory, the gauge bosons (gluons) are allowed to interact with each other which in turn leads to a strong momentum dependence of the coupling constant α_s. At small distances (or at large momentum transfers) α_s becomes small, leading to the so-called asymptotic freedom[5, 4], hence a perturbative treatment of QCD is possible and quite successful. At large distances (or at small momentum transfers) the quark-quark couplings become large and presumably give rise to quark confinement[6]. Hence in the low and intermediate energy domain of hadron physics the perturbative treatment of QCD fails.

Based on the lack of effective methods in obtaining solutions to QCD in the nonperturbative confinement region, one has to resort to the development of effective models. An important ingredient in model building is to reduce the degrees of freedom of QCD and to determine the effective interactions between them. In doing so, several approaches have been developed.

In the more traditional meson-exchange-models, the strong interaction is de-

scribed in the framework of the observable, physical degrees of freedom, such as baryons and mesons. The idea here is that quark degrees of freedom are negligible, whereas the extended structure of hadrons can be described by effective form factors, which are fitted to experimental data.

In the nonrelativistic constituent quark model, quarks and antiquarks are kept as the relevant degrees of freedom, whereas the interaction between the quarks, particularly the confinement, is described by effective, QCD inspired potentials. The gluonic degrees of freedom are eliminated by introducing the notion of dressed, i.e. "constituent", quarks as compared to the naked, i.e. "current", quarks as originally defined in perturbative QCD. The original success of the nonrelativistic constituent quark model is based on the classification and description of the baryon and meson spectrum and of particular properties, such as magnetic moments and rms radii[7, 8]. Successful descriptions of nucleon-nucleon observables have been advanced in the nonrelativistic quark model[9, 10, 11, 12] as well as in the meson-exchange picture. Thereby, the advantage of the quark model is based on the fact that a large number of experimental observables can be understood qualitatively and quantitatively by a low number of free parameters.

Other aspects of the strong interaction can be studied in the nucleon-antinucleon ($N\overline{N}$) system. Antinucleons used as probes for the study of the strong force dynamics are particularly, with respect to the annihilation, without counterpart in the matter-matter interaction. An antinucleon can annihilate with a nucleon into any energetically allowed system with total baryon number $B = 0$ ($B = +1$ for N, -1 for $\overline{N}$, and 0 for mesons). In $\overline{N}N$ annihilation at rest a substantial energy $2m_Nc^2 \simeq 1.88$ GeV/c^2 is available, thus one can populate a variety of multi-meson final states. The complexity of the $\overline{N}N$ system as compared to the NN system is also enhanced by the fact that N and $\overline{N}$ are distinguishable particles, hence the $\overline{N}N$ wave function does not have to be antisymmetrized. Thus for $\overline{N}N$ twice the number of partial wave states are allowed as for the NN system, where $I + L + S =$ odd (I = total isospin, S = total spin, and L = relative orbital angular momentum) due to the Pauli principle. This enhanced complexity and the multi-channel nature of $\overline{N}N$ annihilation offer a richness of dynamical content which poses a considerable challenge to microscopic theories.

The first decisive evidence for the existence of the antiproton ($\overline{p}$) was obtained at the Berkeley Bevatron in 1955[13], with the first experimental observation of an $\overline{N}N$ annihilation being detected soon thereafter in 1956[14]. These early experiments reported the electric charge of the antiproton to be opposite to the one of the proton and the mass of the antiproton to be equal to the one of the proton, essentially confirming Dirac's hypothesis of a "charge conjugate" particle (antiparticle) for a strongly interacting particle.

In the 1960s and 1970s, bubble chamber experiments for $\overline{N}N$ annihilations were carried out at Brookhaven and CERN. In this work, bubble chambers of liquid hydrogen and deuterium were used, thus the reactions were essentially dominated by initial $\overline{N}N$ atomic states with orbital angular momentum $L = 0$. The results[15, 16, 17] coming from these experiments are the earliest hints of so-called dynamical selection rules (DSR). Dynamical selection rules relate to the fact that certain channels in the transition $\overline{N}N \rightarrow M_1 M_2$ (where $M_i = \pi, \eta, \rho, \omega$, etc), which are allowed by conservation of the $I^G(J^{PC})$ quantum numbers, are suppressed. The observed dynamical selection rules cannot be explained by simple geometric or statistical models, therefore, provide critical constraints on microscopic models for the annihilation dynamics.

A strong boost in the study of $\overline{N}N$ interactions at low energies followed the operation of the Low Energy Antiproton Ring (LEAR) at CERN, which started producing first experimental results in 1983. LEAR provides beams of $\overline{p}'s$ at very low momentum with high intensity and good momentum resolution. The most important advantage of LEAR was probably its ability to separate the contributions of different initial partial waves of the $\overline{p}p$ atom to the annihilation. The new technique to distinguish annihilation from orbital angular momentum S- and P-wave states is crucial. It confirmed and also extended the experimental observation of DSR in the mechanism of $\overline{N}N$ annihilation into mesons, which yield key signatures for the underlying annihilation dynamics. The experimental program at LEAR contains the following main items:

1. measurements of total, annihilation, elastic and charge-exchange $\overline{N}N$ cross sections, as well as spin observables.
2. measurements of a variety of annihiiation channels, particularly the determina-

tion of branching ratios for two-body decay modes such as $\pi^+\pi^-$, K^+K^-, $\pi\rho$, etc. in dependence on the initial $\overline{p}p$ atomic states ($L = 0, 1$).

3. measurements of energy shifts and width broadenings of the $\overline{N}N$ atomic states due to the strong interaction.

4. meson spectroscopy: understanding of the mass spectrum and of dynamical properties, such as decay modes for the meson states below a mass scale of about 2 GeV. This includes the search for new meson states which lie outside the known SU(3) nonets of quark-antiquark $\overline{Q}Q$ mesons. These new meson states are "exotics" (glueballs ggg, hybrids $Q\overline{Q}g$, quark molecules $Q^2\overline{Q}^2$) predicted by QCD, but also more "conventional" resonances, such as $\overline{N}N$ unclear bound states or meson-meson molecules.

Particularly with respect to the latter point, LEAR experiments have yielded evidence for broad mesonic resonances X with a width $\Gamma > 50 - 100$ MeV, which can not be explained by the standard flavor SU(3) $\overline{Q}Q$ picture. Two solidly established examples of such resonances are the $AX(1565)$ and $E(1410)$ seen in annihilation reactions of the type $\overline{N}N \to \pi X$, $\pi\pi X$. The ability of the LEAR facility to distinguish annihilation from initial S and P-wave $\overline{N}N$ states was essential to determine their quantum numbers ($J^G(J^{PC}) = 0^+(2^{++})$ and $0^+(0^{-+})$ for the AX and E, respectively).

On the other side, theoretical attempts in understanding antiproton physics soon followed after the discovery of the antiproton and the emergence of the few experimental data on $\overline{N}N$ reactions. It was soon realized that in the framework of meson-exchange theory the NN and the $\overline{N}N$ interactions are intimately related by the so-called G-parity rule[18]. This close connection between the NN and $\overline{N}N$ force encouraged early hopes that an analysis of $\overline{N}N$ observables could possibly provide additional information on the meson-exchange model of the NN potential.

However, the applicability of the G-parity transformation is only limited to the long and intermediate range elastic part of the $\overline{N}N$ potential. At short distances, typically at around $r \simeq 1$ fm, where the nucleon and antinucleon as objects of finite size overlap, the annihilation mechanism sets in. The annihilation process is a dominant feature in the $\overline{N}N$ interaction. For instance, in low energy $\overline{N}N$ scattering, the annihilation cross section is about twice as large as the elastic[19, 20, 21].

The central idea in describing the short-ranged annihilation processes for the $\overline{N}N$ system consists of replacing the multi-channel problem by an effective optical potential V_{opt}. V_{opt} is a complex potential of the form $V_{opt} = V_{ann} + iW_{ann}$, where W_{ann} is the absorptive part and V_{ann} the dispersive real part due to annihilation. In general, this optical potential is non-local in coordinate space, thereby possessing an explicit state and energy dependence.

In earlier works[22, 23, 24, 25] the annihilation was parameterized by a local, energy-independent optical potential of simple forms, such as Gaussian or Woods-Saxon. The elastic medium and long range part of the $\overline{N}N$ interaction was obtained by G-parity transformation of realistic meson-exchange potentials for the NN system, for example such as the so-called Bonn[26] and Paris[27, 28, 29] potentials. These models are very successful in fitting experimental data of $\overline{N}N$ scattering (integrated, differential cross sections and spin observables) with few free parameters[22, 25]. A more refined version of such an approach, which allows additional state and energy dependence of the optical potential, thereby doing a fine-tuning to the recently acquired scattering data, is pursued by the Paris group[30, 31]. In the one channel optical model for the $\overline{N}N$ system, all information about individual mesonic annihilation channels has been sacrificed. Thus, one is able to calculate the cross section for $\overline{N}N$ annihilation. However, all the information about individual annihilation channels has been integrated over.

A further step in describing the annihilation processes in more detail is the investigation of statistical models, which are able to describe pion multiplicity and charge distributions for the final annihilation products[32, 33, 34]. The basis of these models is the idea that when the proton and antiproton are close together, the total energy of the system is concentrated in the region of the three-quark and three-antiquark object. Each final state is created according to its statistical weight. The description of the annihilation by theses models is based on a simple phenomenological ansatz, however they fail to reproduce special branching ratios of $\overline{N}N$ into mesons, particularly with respect to the DSR.

Microscopic derivations of the annihilation potential for the $\overline{N}N$ system are essentially based on two approaches: the baryon-exchange model and the nonrelativistic constituent quark model. Both models make basic assumptions about the

relevant degrees of freedom in the $\overline{N}N$ transition into final state mesons, thereby fixing the underlying dynamics with a certain amount of free parameters. The aim here is to work out a theoretical foundation which at the same time is able to describe the detailed annihilation mechanism (such as annihilation cross sections for $\overline{N}N$ into specific meson channels or branching ratios for $\overline{N}N$ annihilation from atomic states) as well as global $\overline{N}N$ observables (such as $\overline{N}N$ scattering cross sections).

In the more traditional approach of hadronic models, where for example the NN interaction is set up in the framework of meson-exchange, the $\overline{N}N$ annihilation into mesons is described by baryon-exchange[35, 36, 37]. The relevant inputs here are the baryon-baryon-meson vertices, which are taken in analogy to the ones obtained from the meson-exchange picture of the NN force. The vertex form factors, which account for the off-shell behavior of the exchanged baryon, are distinct from those applied to t-channel exchange, where the meson is off-shell. Much of the phenomenological success of the baryon exchange picture at low energies is due to the introduction of arbitrary form factors at the hadronic vertices, which are given no interpretation in terms of the underlying quark-gluon degrees of freedom.

For a short range process such as $\overline{N}N$ annihilation, which involves appreciable overlap of the N and $\overline{N}$, a description in terms of quark-gluon degrees of freedom seems more appropriate. However, for low energy $\overline{N}N$ processes we are in the strong coupling regime of QCD, where a first principle calculation is beyond our realm at present. Thus, a phenomenological approach was chosen in which one considers $\overline{N}N$ transitions into mesons corresponding to different quark line diagrams, describing the flavor flux from the initial $\overline{N}N$ to the final meson states. At the same time, a prescription for the effective $\overline{Q}Q$ dynamics in terms of color, spin and flavor dependence must be adopted. In the absence of a firm guiding principle, this phenomenological prescription is by no means unique and a number of possibilities have been explored in the past.

Quark line diagram models have been investigated by the Helsinki group[38, 39, 40], the Osaka group[41, 42] and the Tübingen group[43, 44, 45], among others. An overview of the various quark models with a detailed discussion can be found in ref.[46]. The picture emerging from the phenomenological analysis is that quark line diagrams with so-called planar topology for the $\overline{N}N$ annihilation into two and three

mesons (denoted as A2 and A3, respectively), maximizing the number of nonperturbative $\overline{Q}Q$ interaction vertices, provide a reasonable account of the annihilation data. Here the spin-flavor-orbital structure of the $\overline{Q}Q$ dynamics is described by the $^3P_0$ model, where $\overline{Q}Q$ pairs are created or destroyed with vacuum quantum numbers $I^G(J^{PC}) = 0^+(0^{++})$, $^3P_0$ in LS-coupling. The optical potential due to the annihilation diagrams A2 and A3, together with a suitable medium and long range elastic potential, based on meson-exchange theory, has also been applied to $\overline{N}N$ scattering observables, thereby being able to explain the data far better than previous microscopic quark model calculations [47, 48].

There is another exciting point about the $\overline{N}N$ system, namely the possibility of $\overline{N}N$ bound states or resonances. In contrast to the NN counterpart, for which no bound states exist (with the exception of the loosely bound deuteron), the $\overline{N}N$ interaction is strongly attractive, particularly at short and intermediate distances, and does not have a repulsive core. While the NN force is ultimately repulsive due to the Pauli principle, the $\overline{N}N$ force is dominated by short range annihilation. The range and the strength of the annihilation potential determine the width of these bound states of the $\overline{N}N$ system: a strong longer range annihilation would broaden the states to the extent that they are essentially unobservable. The $\overline{N}N$ bound states have been studied in the quark annihilation model in which the short range annihilation potential is derived in the diagrams A2 and A3 [49]. The model predicts a reasonable results.

The aim of the current work is to study (1) the $\overline{N}N$ annihilation diagram A2 in details; (2) the $\overline{N}N$ atomic states, which are mainly bound by the Coulomb interaction, in a powerful numerical method, the Sturmian function method; (3) the processes of electron-position annihilation into nucleon-antinucleon pairs in the nonrelativistic $^3P_0$ quark model; (4) proton-proton high energy elastic scattering; (5) and proton-neutron high-energy charge exchange scattering.

Chapter 2

Analysis of Annihilation Mechanism

For a short range process such as the $\overline{N}N$ annihilation, where the baryons have considerable overlap, a description in terms of quark-gluon degrees of freedom seems most appropriate. However, for low energy $\overline{N}N$ processes we are in the strong coupling regime of QCD, where the perturbative theories developed in high-energy particle physics become useless. Thus we have to choose a phenomenological approach, in which one considers transitions for $\overline{N}N$ into mesons corresponding to different quark line diagrams (describing the flavor flux topology), as summarized in Fig. 2.1. At the same time a prescription for the effective $Q\overline{Q}$ dynamics in terms of color, spin and flavor dependence has to be adopted.

2.1 $^3P_0$ or $^3S_1$

Quark-antiquark pairs can be created or destroyed with vacuum quantum numbers $I^G(J^{PC}) = 0^+(0^{++})$ ($^3P_0$ in LS-coupling) or with effective gluon quantum numbers ($^{33}S_1$, in color $\{8\}$). Experimental data on the relative branching ratios for $\overline{N}N$ annihilation into two and three mesons provide strong constraints on the dynamical models. Particularly the observation of Dynamical Selection Rules (DSR), in which certain annihilation transitions are suppressed, although allowed by $I^G(J^{PC})$

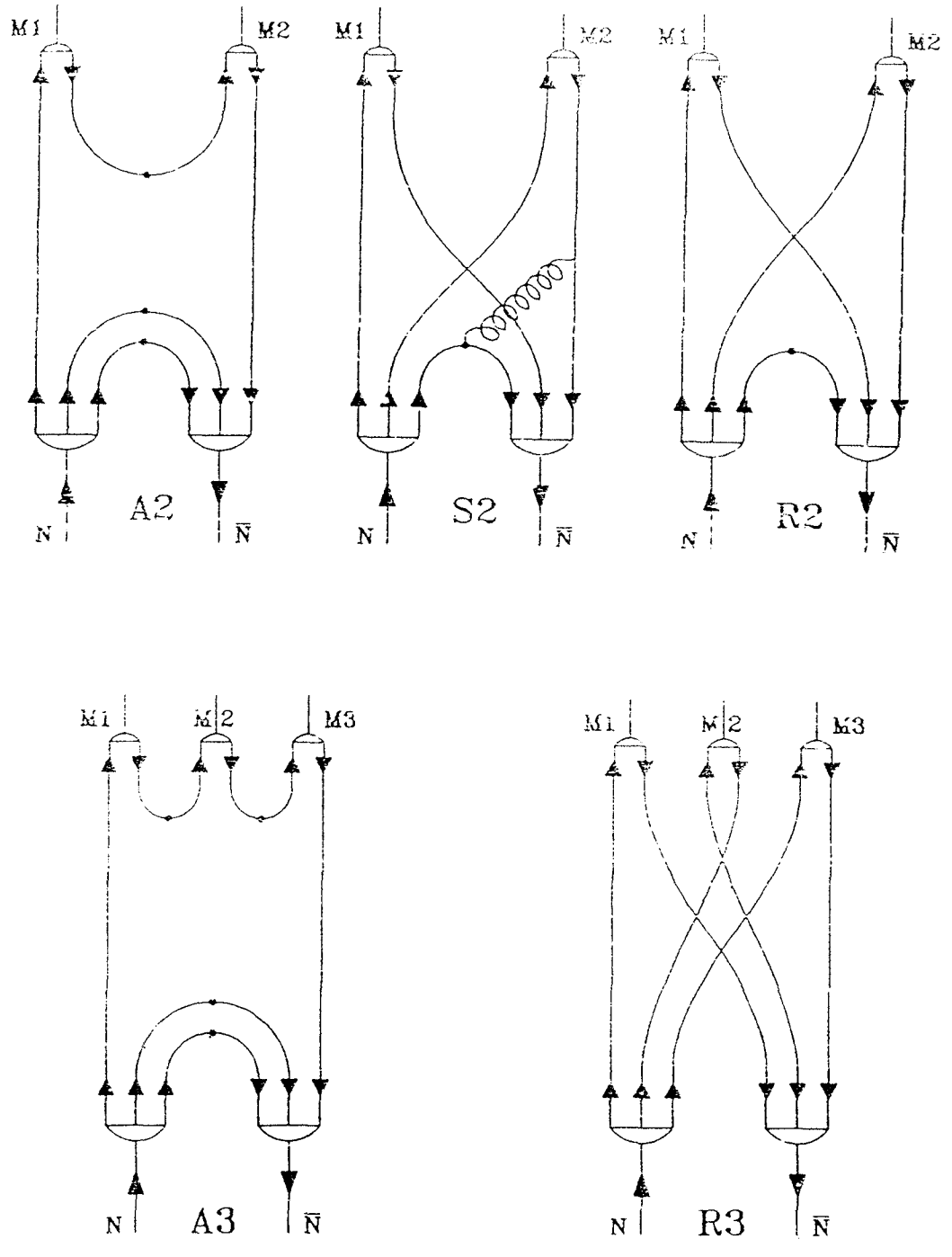

Fig. 2.1 Quark diagrams for nucleon-antinucleon annihilation into two and three mesons.

conservation, offer key tests on the annihilation dynamics[50, 46]. Different annihilation topologies with an effective $Q\overline{Q}$ dynamics lead to distinct predictions for the DSR in different quark models. The phenomenological analysis indicates that quark line diagrams with planar topology applying the ${}^3P_0$ $\overline{Q}Q$ vertices are the dominant processes in $\overline{N}N$ annihilation into mesons. A good description of $\overline{N}N$ annihilation data over a range of energies can be achieved within this approach, although discrepancies remain in particular channels[43, 44, 45, 46]. The viewpoint developed here is, that $\overline{N}N$ annihilation can be treated in an analogous fashion to meson decay, which can be well described phenomenologically using an effective ${}^3P_0$ vertex[51]. The connection between the ${}^3P_0$ dynamics and strong coupling QCD has been well established[52, 53, 54, 55]. The $\overline{N}N$ system shares the same quantum numbers as a $Q\overline{Q}$ state, differing only in mass and internal quark structure, hence it seems consistent to apply the ${}^3P_0$ model to the $\overline{N}N$ annihilation dynamics. In the following we will substantiate the claim that diagrams with planar topology are effectively the dominant quark mechanism in describing the $\overline{N}N$ annihilation process.

The transition of a $\overline{N}N$ system to two or three meson final states must obey the conservation of $I^G(J^{PC})$ (I, J, G, P and C are the total isospin, total angular momentum, G parity, parity and charge conjugation of a system, respectively) quantum numbers, which will forbid some annihilation channels for a certain initial $\overline{N}N$ state. Let us, for instance, consider parity (P) conservation here. An $\overline{N}N$ initial state has the parity:

$$P_{\overline{N}N} = (-1)^{L+1} \tag{2.1}$$

while the two-meson final state has parity

$$P_{M_1M_2} = P_{M_1}P_{M_2}(-1)^l \tag{2.2}$$

where L and l are the orbital angular momenta for the initial $\overline{N}N$ and the final two-meson states, respectively, and P_{M_i} is the intrinsic parity of the meson i. An accessible annihilation process $\overline{N}N \to M_1\,M_2$ must satisfy the relation

$$P_{\overline{N}N} = P_{M_1M_2}. \tag{2.3}$$

The parity conservation implies following transitions from orbital angular momentum S-, P-, and D-wave $\overline{N}N$ states to two s-wave mesons or one s-wave and one

p-wave meson final states:

$$\begin{aligned} S &\to ss(l = odd) \quad and \quad sp(l = even) \\ P &\to ss(l = even) \quad and \quad sp(l = odd) \\ D &\to ss(l = odd) \quad and \quad sp(l = even) \end{aligned} \tag{2.4}$$

where s denotes a s-wave meson $(Q\overline{Q})_{l=0}$, p a p-wave meson $(Q\overline{Q})_{l=1}$.

As for the G-parity conservation, an accessible annihilation process $\overline{N}N \to M_1 M_2$ must satisfy the relation

$$G_{\overline{N}N} = G_{M_1 M_2}. \tag{2.5}$$

where $G_{\overline{N}N}$ is the G-parity of the $\overline{N}N$ initial system and $G_{M_1 M_2}$ the G-parity of two-meson final states defined as

$$G_{M_1 M_2} = G_{M_1} G_{M_2} \tag{2.6}$$

with

$$G_M = (-1)^{i+l+s} \tag{2.7}$$

where i, l and s are the isospin, orbital angular momentum and spin of an individual meson, respectively.

In summary, we list in Table 2.1 the allowed $\overline{N}N \to ss$ process with the total angular momentum $J = 0$ and 1 by $I^G(J^{PC})$ conservation

2.2 Experimental Evidence for Dynamical Selection Rules

Different quark diagrams for $\overline{N}N$ annihilation, as indicated in Fig. 2.1, will possess dynamical selection rules, which restrict or suppress the possible transitions in eq.2.4 and Table 2.1. These theoretically predicted dynamical selection rules allow in comparison with experimental data to rule out certain models. Here we give selected examples for some annihilation channels, which show striking deviations from the expected behavior based on $I^G(J^{PC})$ conservation laws.

	J=0	J=1
$s_1 = 0,\ s_2 = 0$	${}^3P_0 \to {}^1S_0$	${}^3S_1 \to {}^1P_1$ ${}^3D_1 \to {}^1P_1$
$s_1 = 1,\ s_2 = 0$	${}^1S_0 \to {}^3P_0$	${}^3S_1 \to {}^3P_1$ ${}^1P_1 \to {}^3S_1, {}^3D_1$ ${}^3P_1 \to {}^3S_1, {}^3D_1$ ${}^3D_1 \to {}^3P_1$
$s_1 = 1,\ s_2 = 1$	${}^1S_0 \to {}^3P_0$ ${}^3P_0 \to {}^1S_0, {}^5D_0$	${}^3S_1 \to {}^1P_1, {}^5P_1, {}^5F_1$ ${}^1P_1 \to {}^3S_1, {}^3D_1$ ${}^3P_1 \to {}^5D_1$ ${}^3D_1 \to {}^1P_1, {}^5P_1, {}^5F_1$

Table 2.1: Allowed lowest $\overline{N}N \to ss$ process by $I^G(J^{PC})$ conservation. The states are labelled as ${}^{2S+1}L_J$ with S the total spin, L the total orbital angular momentum and J the total angular momentum. s_i is the spin of the ith meson.

May *et al.*[56] presented relative decay branching ratios for $\overline{N}N$ annihilation from atomic S- and P-wave states to the final state $\pi^+\pi^-\pi^0$ as shown in Table 2.2 and Table 2.3. From these tables, we obtain the following ratios for the production rates:

$$\frac{BR\,(\bar{p}p({}^3S_1) \to \pi^{\pm}\rho^{\mp})}{BR\,(\bar{p}p({}^1S_0) \to \pi^{\pm}\rho^{\mp})} \simeq 40 \tag{2.8}$$

$$\frac{BR\,(\bar{p}p({}^3P_1) \to \pi^0 f_2)}{BR\,(\bar{p}p({}^3P_2) \to \pi^0 f_2)} \simeq 11 \tag{2.9}$$

$$\frac{BR\,(\bar{p}p({}^3P_1) \to \pi^{\pm}\rho^{\mp})}{BR\,(\bar{p}p({}^3P_2) \to \pi^{\pm}\rho^{\mp})} \simeq 25 \tag{2.10}$$

Also from ASTERIX [57] it is found that

$$\frac{BR\,(\bar{p}p({}^3S_1) \to \pi^+\pi^-\eta)}{BR\,(\bar{p}p({}^1S_0) \to \pi^+\pi^-\eta)} \simeq 0.5 \tag{2.11}$$

All of the above ratios are in disagreement with the naive expectations based on the statistical relative weight given by $(2J_1+1)/(2J_2+1)$, where J_1, J_2 is the total

Transitions	Branching Ratios (%)
$^1S_0 \to \pi^{\pm}\rho^{\mp}$	1.3 ± 0.6
$^1S_0 \to \pi^0 f_2$	3.4 ± 0.5
$^1S_0 \to (3\pi)_{PS}$	11.7 ± 1.8
$^3S_1 \to \pi\rho$	76.8 ± 4.1
$^3S_1 \to \pi\rho(1600)$	6.9 ± 0.7

Table 2.2: Relative branching ratios $\bar{p}p \to \pi^+\pi^-\pi^0$ from S waves

angular momentum of the initial $p\bar{p}$ state. Hence for the ratios of eqs.2.8 and 2.11 the statistical ratio is 3, compared to the experimental values of 40 and 0.5, respectively. Accordingly, for the ratios of eqs.2.9 and 2.10 the statistical relative weight would only be $3/5 = 0.6$, differing by a factor of 18-42 from experiment.

The deviation from naive expectation comes from the detailed dynamics of the underlying annihilation mechanism, hence the name 'dynamical selection rules'. The detailed extraction of the underlying dynamics can sensitively depend on initial and possibly final state interactions, in other words, the wave functions of the initial and final states. Initial $\overline{N}N$ atomic states are dominated by the Coulomb interaction between the proton and antiproton. Due to the short-ranged distortion induced by the nuclear force, however, the $\overline{N}N$ atomic states can greatly differ from the hydrogen-like wave functions in the strong interaction region. For instance, the $\overline{N}N$ atomic state must have an additional node if there exists a $\overline{N}N$ deep bound state with the same quantum numbers. Therefore, the extraction of the underlying quark dynamics strongly depends on our knowledge of the $\overline{N}N$ interaction, for instance the meson-exchange potential. For a theoretical explanation of the "$\pi\rho$" puzzle of eqs.2.8 and 2.10 in terms of the planar annihilation diagram A2, where the proper treatment of the initial state interaction plays a decisive role, see ref.[43]. Previous examples were meant to illustrate the occurrence of dynamical selection rules in experiment. Now we will concentrate on discussing the various theoretical approaches in working out the underlying annihilation dynamics on the quark level.

Transitions	Branching ratios (%)
$^1P_1 \to \pi\rho(l=0)$	17.6 ± 3.4
$^1P_1 \to \pi\rho(l=2)$	9.3 ± 3.1
$^1P_1 \to (3\pi)_{PS}$	3.4 ± 0.4
$^3P_1 \to \pi^{\pm}\rho^{\mp}$	14.8 ± 1.5
$^3P_1 \to \pi^0 f_2$	21.1 ± 0.7
$^3P_1 \to (3\pi)_{PS}$	10.0 ± 0.8
$^3P_1 \to \pi^0 AX$	5.3 ± 0.6
$^3P_2 \to \pi^{\pm}\rho^{\mp}(l=2)$	0.6 ± 0.2
$^3P_2 \to \pi^0 f_2$	2.0 ± 0.6
$^3P_2 \to (3\pi)_{PS}$	12.9 ± 0.6
$^3P_2 \to \pi^0 AX$	3.0 ± 0.4

Table 2.3: Relative branching ratios $\bar{p}p \to \pi^+\pi^-\pi^0$ from P waves, where l is the relative orbital angular momentum of the two meson system.

2.3 Theoretical Analysis of Annihilation Mechanisms

Based on the $I^G(J^{PC})$ conservation laws, the R2, R3, and S2 topologies of Fig. 2.1 yield rather strong selection rules for the $\overline{N}N \to M_1M_2(M_1M_2M_3)$ processes. Especially for the R2 and R3 diagrams, a large number of annihilation channels is forbidden. In the R3 topology, an S-wave or P-wave $\overline{N}N$ system can only decay into three s-wave mesons or two s-wave mesons and one p-wave meson, respectively. The selection rules for the R2 and S2 topologies[41, 42, 50] are much more complicated, as listed in Table 2.4 and Table 2.5.

Table 2.4 shows that very few channels are allowed for the transition of a $\overline{N}N$ state to two s-wave mesons in the R2 topology. In particular, all S-wave $\overline{N}N$ states are forbidden to decay into two s-wave mesons. There is no evidence for the R2 selection rules in experiment. In recent years, a large number of reliable branching ratios for $\overline{N}N \to$ *mesons* have been measured. In Table 2.6 we list the collected

	$^{11}S_0$	$^{31}S_0$	$^{13}S_1$	$^{33}S_1$	$^{11}P_1$	$^{31}P_1$	$^{13}P_0$	$^{33}P_0$	$^{13}P_1$	$^{33}P_1$	$^{13}P_2$	$^{33}P_2$
$\pi\pi$	-	-	-	$\ominus$	-	-	+	-	-	-	$\ominus$	-
$\pi^0\eta$	-	-	-	-	-	-	-	+	-	-	-	$\ominus$
$\eta\eta$	-	-	-	-	-	-	+	-	-	-	$\ominus$	-
$\rho\rho$	$\ominus$	-	-	$\ominus$	-	$\ominus$	+	-	-	-	+	-
$\rho^0\omega$	-	$\ominus$	-	-	-	-	-	+	-	+	-	+
$\omega\omega$	$\ominus$	-	-	-	-	$\ominus$	+	-	-	-	+	-
$\pi\rho$	-	$\ominus$	$\ominus$	-	+	-	-	-	-	$\ominus$	-	$\ominus$
$\pi^0\omega$	-	-	-	$\ominus$	-	+	-	-	-	-	-	-
$\eta\rho^0$	-	-	-	$\ominus$	-	+	-	-	-	-	-	-
$\eta\omega$	-	-	$\ominus$	-	+	-	-	-	-	-	-	-

Table 2.4: $\overline{N}N$ annihilation into two s-wave meson in the R2 topology. + and - mean allowed and forbidden transitions, respectively. $\ominus$ indicates a channel which is allowed by the conservation of the quantum numbers $I^G(J^{PC})$, but forbidden in the R2 topology.

	$^{11}S_0$	$^{31}S_0$	$^{13}S_1$	$^{33}S_1$	$^{11}P_1$	$^{31}P_1$	$^{13}P_0$	$^{33}P_0$	$^{13}P_1$	$^{33}P_1$	$^{13}P_2$	$^{33}P_2$
$\pi\pi$	-	-	-	+	-	-	$\ominus$	-	-	-	$\ominus$	-
$\pi^0\eta$	-	-	-	-	-	-	-	$\ominus$	-	-	-	$\ominus$
$\eta\eta$	-	-	-	-	-	-	$\ominus$	-	-	-	$\ominus$	-
$\rho\rho$	+	-	-	+	-	+	$\ominus$	-	-	-	+	-
$\rho^0\omega$	-	+	-	-	-	-	-	+	-	+	-	+
$\omega\omega$	+	-	-	-	-	$\ominus$	+	-	-	-	+	-
$\pi\rho$	-	+	+	-	+	-	-	-	-	+	-	$\ominus$
$\pi^0\omega$	-	-	-	+	-	+	-	-	-	-	-	-
$\eta\rho^0$	-	-	-	+	-	+	-	-	-	-	-	-
$\eta\omega$	-	-	+	-	+	-	-	-	-	-	-	-

Table 2.5: $\overline{N}N$ annihilation into two s-wave meson in the S2 topology. + and - mean allowed and forbidden transitions, respectively. $\ominus$ indicates a channel which is allowed by the conservation of the quantum numbers $I^G(J^{PC})$, but forbidden in the S2 topology.

	S	P
K^+K^-	1.08±0.05	0.278±0.051
$K^0\overline{K^0}$	0.83±0.5	0.088±0.023
$\pi^+\pi^-$	3.19±0.20	4.81±0.49
$\rho^\mp\pi^\pm$	32.1±4.2	15.0±2.0
$\rho^0\pi^0$	15.6±2.1	4.0±0.9
$f_2\pi^0$	3.9±1.1	18.3±2.3
$\pi^+\pi^-\pi^0$	66±8	45±6
$\eta\pi^+\pi^-$	13.7±1.5	3.35±0.84
$\eta'\pi^+\pi^-$	3.46±0.67	0.61±0.33
$a_2^\pm\pi^\mp$	26.9±6.0	9.03±4.76
$\eta\rho$	3.29±0.90	0.94±0.53
$f_2\eta$	0.15±0.15	1.1±0.5
$\eta'\rho$	1.81±0.44	∼0.3
$\pi^+\pi^-\omega$	65.5±6.8	70.5±10.5
$\rho\omega$	19.1±3.7	63.8±12.8
$\pi^\pm b_1^\mp$	8.3±1.2	6.7±1.8

Table 2.6: Branching ratios at rest for S-wave and P-wave $\bar{p}p$ annihilation into mesons. The unit is 10^{-4}

data measured by the ASTERIX collaboration[58]. We find that for most two s-wave meson channels the branching ratios in the S-wave $\bar{p}p$ annihilation are at least comparable with those in the P-wave $\bar{p}p$ annihilation, and that the total annihilation rate for $\bar{p}p(S-wave) \to M_1(s)M_2(s)$ and $\bar{p}p(S-wave) \to M_1(s)M_2(p)$ are of the same order. If the S2 topology were a dominant process in $\bar{p}p$ annihilation into mesons, then the rate for $\bar{p}p(S-wave) \to M_1(s)M_2(s)$ would have to be rather small. This is not the case.

The selection rules for the S2 topology of Table 2.5 are not as strong as for the R2 diagram. However, since the 2π channel of P-wave $\bar{p}p$ annihilation is forbidden, we would observe a much larger rate for the annihilation $\bar{p}p(S-wave) \to \pi\pi$ than

for $\bar{p}p(P-wave) \rightarrow \pi\pi$, if the S2 diagram were dominant. The experimental results in Table 2.6 rule out the S2 topology as a dominant process.

As for the R3 topology, the predicted selection rules are also in conflict with experimental observations. For example, the R3 model forbids the production of a 3π final state in P-wave $\overline{N}N$ annihilation, which is in disagreement with the sizable branching ratio of Table 2.6.

The A2 model offers relatively loose selection rules, as indicated in Table 2.7[50, 46]. Unlike the R2 and S2 topologies, where many two-meson channels allowed by the fundamental conservation laws are forbidden, none of these channels is forbidden for either S-wave or P-wave $\bar{p}p$ initial states. In the full analysis of two-meson branching ratios it is shown that the A2 model agrees far better with experimental data than the corresponding R2 and S2 models[43]. Similarly, three-meson annihilation data are consistent with an annihilation dynamics dominated by the A3 model of Fig. 2.1. Again, the A3 topology possesses essentially no stringent selection rules as opposed to the R3 approach. Both S- and P-wave $\bar{p}p$ initial states can annihilate into either three s-wave mesons or two s-wave mesons and one p-wave meson[45]. More quantitative support for the dominance of the planar diagrams A2 and A3 in the $\overline{N}N$ annihilation process can be found in refs.[43, 44, 45, 46].

	$^{11}S_0$	$^{31}S_0$	$^{13}S_1$	$^{33}S_1$	$^{11}P_1$	$^{31}P_1$	$^{13}P_0$	$^{33}P_0$	$^{13}P_1$	$^{33}P_1$	$^{13}P_2$	$^{33}P_2$
$\pi\pi$	-	-	-	+	-	-	+	-	-	-	+	-
$\pi^0\eta$	-	-	-	-	-	-	-	+	-	-	-	+
$\eta\eta$	-	-	-	-	-	-	+	-	-	-	+	-
$\rho\rho$	+	-	-	+	-	+	+	-	-	-	+	-
$\rho^0\omega$	-	+	-	-	-	-	-	+	-	+	-	+
$\omega\omega$	+	-	-	-	-	+	+	-	-	-	+	-
$\pi\rho$	-	+	+	-	+	-	-	-	-	+	-	+
$\pi^0\omega$	-	-	-	+	-	+	-	-	-	-	-	-
$\eta\rho^0$	-	-	-	+	-	+	-	-	-	-	-	-
$\eta\omega$	-	-	+	-	+	-	-	-	-	-	-	-

Table 2.7: $\overline{N}N$ annihilation into two s-wave meson in the A2 topology. + and - mean allowed and forbidden transitions, respectively.

Chapter 3

Transition Amplitude of the A2 Quark Diagram

In this chapter, we provide some details on how to calculate transition matrix elements for $\overline{N}N$ annihilation into two mesons in a quark model. First, we discuss the relevant $Q\overline{Q}$ dynamics, as defined in the so-called $^3P_0$ quark pair creation/destruction model. Then we introduce the nonrelativistic wave functions for QQQ baryon and $Q\overline{Q}$ meson states. Finally, we present the derivation of the transition amplitude in the A2 model.

3.1 The $^3P_0$ Quark Pair Creation Model

The dynamics of a $Q\overline{Q}$ vertex is in principle effectively described by either a vector ($^3S_1$) or a scalar ($^3P_0$) interaction. Both types of interactions find their parallels in quark models applied to the baryon and meson spectra, where the vector interaction corresponds to the effective one-gluon-exchange, the scalar one to the confinement interaction. A priori it is not clear whether there is a dominant type of vertex, with the $Q\overline{Q}$ creation/annihilation being a nonperturbative process. Phenomenological studies have shown that meson and baryon decay data can be well understood applying the scalar $^3P_0$ vertex[51]. The vector vertex $^3S_1$, based originally on a nonperturbative argument, fails to explain the meson decay data[59]. The same

picture prevails when analyzing the more complex $\overline{N}N$ annihilation process. Here the planar diagrams (A2 and A3), together with the $^3P_0$ vertex for the $Q\overline{Q}$ dynamics, can explain the experimental data by far the best. Strong coupling QCD supports the picture emerging from the phenomenology of hadronic transitions, that the scalar $^3P_0$ dynamics is the dominant nonperturbative process[52, 53, 54, 55].

In the $^3P_0$ model, the $Q\overline{Q}$ pair is created or destroyed with vacuum quantum numbers, i.e.

$$I^G(J^{PC}) = 0^+(0^{++}), \tag{3.1}$$

Since the vacuum has parity $P = +1$, the $Q\overline{Q}$ pair (with intrinsic negative parity) must be in an odd relative orbital angular momentum. To obtain zero total angular momentum, the $Q\overline{Q}$ pair has to be coupled to spin $S = 1$ which together with orbital angular momentum $L = 1$ couples to $J = 0$, hence $^3P_0$.

In a relativistic ansatz, the vertex is analogous to a scalar interaction for the Dirac spinors of the annihilating quark and antiquark. The vertex for the fermion-antifermion-vacuum interaction can be written in momentum space as

$$W_{ij} = \sqrt{\frac{m}{E_i}}\sqrt{\frac{m}{E_j}}\overline{v}_i(\vec{p}_i,\vec{\sigma}_i)\, u_j(\vec{p}_j,\vec{\sigma}_j)\delta(\vec{p}_i+\vec{p}_j), \tag{3.2}$$

where $E_i = \sqrt{p_i^2 + m^2}$, m is the mass of the quark/antiquark and the δ-function indicates momentum conservation. The Dirac spinors for the quark (u_i) and antiquark (v_j) are defined as

$$v_i(\vec{p}_i,\vec{\sigma}_i) = \sqrt{\frac{E_i+m}{2m}}\begin{pmatrix} \frac{\vec{\sigma}_i\cdot\vec{p}_i}{E_i+m}\bar{\chi}_i \\ \bar{\chi}_i \end{pmatrix} \tag{3.3}$$

$$u_j(\vec{p}_j,\vec{\sigma}_j) = \sqrt{\frac{E_j+m}{2m}}\begin{pmatrix} \chi_j \\ \frac{\vec{\sigma}_j\cdot\vec{p}_j}{E_j+m}\chi_j \end{pmatrix} \tag{3.4}$$

with

$$\overline{v}_i = v^\dagger\gamma_4 \tag{3.5}$$

where χ and $\bar{\chi}$ are 2-component spinors respectively for quark and antiquark, defined

as:

$$\begin{aligned} \chi(\text{spin up}) &= \begin{pmatrix} 1 \\ 0 \end{pmatrix} \quad \chi(\text{spin down}) = \begin{pmatrix} 0 \\ -1 \end{pmatrix} \\ \bar{\chi}(\text{spin up}) &= \begin{pmatrix} 0 \\ -1 \end{pmatrix} \quad \bar{\chi}(\text{spin up}) = \begin{pmatrix} 1 \\ 0 \end{pmatrix} \end{aligned} \tag{3.6}$$

Inserting eq. 3.3 - 3.5 into eq. 3.2 we obtain

$$W_{ij} = \frac{m}{2E} [\, \chi_i^\dagger (\vec{\sigma}_i \cdot \vec{p}_i - \vec{\sigma}_j \cdot \vec{p}_j) \chi_j \,] \, \delta(\vec{p}_i + \vec{p}_j). \tag{3.7}$$

In the nonrelativistic approximation, namely $E \simeq m$, we have

$$W_{ij} = \frac{1}{2} \chi_i^\dagger V_{ij} \chi_j. \tag{3.8}$$

with

$$\begin{aligned} V_{ij} &= (\vec{\sigma}_i \cdot \vec{p}_i - \vec{\sigma}_j \cdot \vec{p}_j) \, \delta(\vec{p}_i + \vec{p}_j) \\ &= \vec{\sigma}_{ij} \cdot (\vec{p}_i - \vec{p}_j) \, \delta(\vec{p}_i + \vec{p}_j) \end{aligned} \tag{3.9}$$

where $\vec{\sigma}_{ij}$ defined as

$$\vec{\sigma}_{ij} = \frac{\vec{\sigma}_i + \vec{\sigma}_j}{2} \tag{3.10}$$

It can be easily proven that

$$\begin{aligned} \langle \bar{b} | \sigma_{ij}^{-1} | a \rangle &= -\sqrt{2} \delta_{a,\bar{b}} \delta_{a,1/2} \\ \langle \bar{b} | \sigma_{ij}^{0} | a \rangle &= \sqrt{2} \delta_{a,-\bar{b}} \\ \langle \bar{b} | \sigma_{ij}^{1} | a \rangle &= -\sqrt{2} \delta_{a,\bar{b}} \delta_{a,-1/2} \end{aligned} \tag{3.11}$$

where σ_{ij}^{μ} are defined as

$$\begin{aligned} \sigma_{ij}^{1} &= -\frac{1}{\sqrt{2}} (\sigma_{ij}^{x} + i \, \sigma_{ij}^{y}) \\ \sigma_{ij}^{0} &= \sigma_{ij}^{z} \\ \sigma_{ij}^{-1} &= \frac{1}{\sqrt{2}} (\sigma_{ij}^{x} - i \, \sigma_{ij}^{y}) \end{aligned} \tag{3.12}$$

The operation of the $\vec{\sigma}_{ij}$ could be understand as that it operates a quark state to an antiquark state, or that it projects a quark-antiquark pair onto a spin-1 state. We may write eqs. (3.11) in the form

$$\langle 0,0|\sigma_{ij}^{\mu}|[\bar{\chi}_i \otimes \chi_j]_{JM}\rangle = (-1)^M \sqrt{2}\delta_{J,1}\delta_{M,-\mu} \tag{3.13}$$

For the flavor a quark-antiquark pair which annihilates into vacuum must have zero isospin. So we may introduce an unit operator $\mathbf{1}^F$ with the property

$$\langle 0,0|\hat{\mathbf{1}}^F|T,T_z\rangle = \sqrt{2}\delta_{T,0}\delta_{T_z,0} \tag{3.14}$$

Finally one may write the $^3P_0$ operator in the form

$$V_{ij} = \lambda \sum_{\mu}(-1)^{1-\mu} \langle 0,0|_{ij}^{S} \langle 0,0|_{ij}^{F} \sigma_{ij}^{-\mu} \mathbf{1}_{ij}^{F} Y_{1\mu}(\vec{p}_i - \vec{p}_j)\, \delta(\vec{p}_i + \vec{p}_j) \tag{3.15}$$

where λ is the effective coupling strength. The operator does project a general state onto a $^3P_0$ state which takes the form

$$\begin{aligned} |0,0\rangle^{\text{spin-spatial}} &= \sum_{\mu,\nu}\langle 11,\mu\nu|0,0\rangle|1,\mu\rangle^{\text{spin}} Y_{1\nu}(\vec{q}) \\ &= \sum_{mu} \frac{(-1)^{1-\mu}}{\sqrt{3}}|1,\mu\rangle^{\text{spin}} Y_{1\nu}(\vec{q}) \end{aligned} \tag{3.16}$$

Conventionally, the $^3P_0$ operator is expressed as

$$V_{ij} = \frac{\lambda}{\sqrt{3}} \sum_{\mu}(-1)^{1-\mu} \langle 0,0|_{ij}^{S} \langle 0,0|_{ij}^{F} \sigma_{ij}^{-\mu} \mathbf{1}_{ij}^{F} Y_{1\mu}(\vec{p}_i - \vec{p}_j)\, \delta(\vec{p}_i + \vec{p}_j) \tag{3.17}$$

with the two body matrix elements given by

$$\langle 0,0|\sigma_{ij}^{\mu}|[\bar{\chi}_i \otimes \chi_j]_{JM}\rangle = (-1)^M \sqrt{2}\delta_{J,1}\delta_{M,-\mu} \tag{3.18}$$

$$\langle 0,0|\hat{\mathbf{1}}^F|T,T_z\rangle = \sqrt{2}\delta_{T,0}\delta_{T_z,0} \tag{3.19}$$

3.2 Nucleon-Antinucleon Wave Function

In the quark model, a baryon is composed of three quarks, with total wave function antisymmetric. Since baryons must be colorless, the total wave functions should take the form

$$\Phi = \underset{R}{\square\square\square} \oplus \underset{SF}{\square\square\square} \oplus \underset{C}{\begin{array}{|c|}\hline\ \\ \hline\ \\ \hline\ \\ \hline\end{array}}$$

The spin-flavor part takes the form:

$$\Psi^{(SF)}_{S_z T_z} = \frac{1}{\sqrt{2}} \sum_{J_{23}=0,1} \left| \left(\frac{1}{2}^{(2)} \otimes \frac{1}{2}^{(3)} \right)_{J_{23}} \otimes \frac{1}{2}^{(1)} \right\rangle^{\text{Spin}}_{1/2,S_z} \left| \left(\frac{1}{2}^{(2)} \otimes \frac{1}{2}^{(3)} \right)_{J_{23}} \otimes \frac{1}{2}^{(1)} \right\rangle^{\text{Flavor}}_{1/2,T_z} \tag{3.20}$$

For the harmonic oscillator interaction

$$V(r) = \frac{1}{2}\mu\omega^2 r^2 \tag{3.21}$$

one may write the spatial wave function in momentum space in the form

$$\Psi(\vec{p}_1,\vec{p}_2,\vec{p}_3) = N_B \exp\left[-\frac{1}{2}a^2\left(\frac{\vec{p}_2-\vec{p}_3}{\sqrt{2}}\right)^2\right] \cdot\exp\left[-\frac{1}{2}a^2\left(\frac{\vec{p}_2+\vec{p}_3-2\vec{p}_1}{\sqrt{6}}\right)^2\right] \tag{3.22}$$

where $N_B = 3^{4/3}a^3/\pi^{3/2}$ with $a = 1/(\sqrt{6}\mu\omega)$.

Put the spin and spatial parts totether, one obtains the initial proton-antiproton wave function as follows:

$$\begin{aligned}
&\Psi_{S,S_z;T,T_z}(\vec{k}_1,\vec{k}_2;\vec{p}_1,\vec{p}_2,\vec{p}_3;\vec{p}_4,\vec{p}_5,\vec{p}_6) \\
&= \frac{N_B^2}{2}\delta(\vec{k}_1-\vec{p}_1-\vec{p}_2-\vec{p}_3)\delta(\vec{k}_2-\vec{p}_4-\vec{p}_5-\vec{p}_6) \\
&\exp\left[-\frac{1}{2}a^2\left(\frac{\vec{p}_2-\vec{p}_3}{\sqrt{2}}\right)^2\right] \exp\left[-\frac{1}{2}a^2\left(\frac{\vec{p}_2+\vec{p}_3-2\vec{p}_1}{\sqrt{6}}\right)^2\right] \\
&\exp\left[-\frac{1}{2}a^2\left(\frac{\vec{p}_5-\vec{p}_6}{\sqrt{2}}\right)^2\right] \exp\left[-\frac{1}{2}a^2\left(\frac{\vec{p}_5+\vec{p}_6-2\vec{p}_4}{\sqrt{6}}\right)^2\right] \\
&\sum_{J_{34},J_{56}} \left| \left[\left(\frac{1}{2}^{(2)} \otimes \frac{1}{2}^{(3)} \right)_{J_{23}} \otimes \frac{1}{2}^{(1)} \right]_{1/2} \otimes \left[\left(\frac{1}{2}^{(5)} \otimes \frac{1}{2}^{(6)} \right)_{J_{56}} \otimes \frac{1}{2}^{(4)} \right]_{1/2} \right\rangle^{\text{Spin}}_{SS_z}
\end{aligned}$$

$$\left|\left[\left(\frac{1}{2}^{(2)} \otimes \frac{1}{2}^{(3)}\right)_{J_{23}} \otimes \frac{1}{2}^{(1)}\right]_{1/2} \otimes \left[\left(\frac{1}{2}^{(5)} \otimes \frac{1}{2}^{(6)}\right)_{J_{56}} \otimes \frac{1}{2}^{(4)}\right]_{1/2}\right\rangle^{\text{Flavor}}_{TT_z} \tag{3.23}$$

3.3 Meson Wave Function

In the quark-antiquark interaction of harmonic oscillator type, the momentum space wave functions for s-wave and p-wave mesons are

$$\begin{aligned}
\Phi_s(\vec{p}) &= N_s \exp\left(-\frac{1}{2}b^2p^2\right) \frac{1}{\sqrt{4\pi}}|S, S_z\rangle \\
\Phi_p(\vec{p}) &= N_p\,(bp) \exp\left(-\frac{1}{2}b^2p^2\right) \\
&\quad \cdot \sum_{S_z,m} C(S1J, S_z m J_z)|S, S_z\rangle Y_{1m}(\hat{p})
\end{aligned} \tag{3.24}$$

where $\vec{p}$ is the relative momentum with $\vec{p} = \frac{1}{2}(\vec{p}_1 - \vec{p}_2)$, and $N_s = 2b^{3/2}/\pi^{1/4}$, $N_p = 2(2/3)^{1/2}b^{3/2}/\pi^{1/4}$ with $b^2 = 1/(\mu\omega)$.

The root-mean-square radii for mesons and baryons are defined in terms of the size parameters as follows:

For a s-wave meson

$$\begin{aligned}
\langle r^2\rangle_s^{1/2} &= \frac{1}{2}\sqrt{\langle\,\Phi_s \mid r^2 \mid \Phi_s\rangle} \\
&= \frac{1}{2}\sqrt{\frac{3}{2}}b \;\simeq\; 0.5 \text{ fm}
\end{aligned} \tag{3.25}$$

For a p-wave meson

$$\begin{aligned}
\langle r^2\rangle_p^{1/2} &= \frac{1}{2}\sqrt{\langle\,\Phi_p \mid r^2 \mid \Phi_p\rangle} \\
&= \frac{1}{2}\sqrt{\frac{5}{2}}b \;\simeq\; 0.64 \text{ fm}
\end{aligned} \tag{3.26}$$

For the nucleon

$$\begin{aligned}
\langle r^2\rangle_N^{1/2} &= \frac{1}{\sqrt{3}}\sqrt{\langle\,\Psi \mid \xi_1^2 \mid \Psi\rangle} \\
&= a \;\simeq\; 0.61 \text{ fm}
\end{aligned} \tag{3.27}$$

In practice, a and b are fitted to the nucleon and meson sizes. Here we choose $a = 3.1\text{GeV}^{-1}$ and $b = 4.1\text{GeV}^{-1}$

3.4 $\overline{N}N$ Annihilation into two Mesons in the A2 Model

The transition amplitude for $\overline{N}N$ annihilation into two mesons in the A2 diagram, see Fig. 3.1, is defined as

$$T_{A2} = \int \prod_{i=1}^{4} d\vec{q}_i' \prod_{i=1}^{6} d\vec{q}_i \; \Psi^{\dagger}_{M_1 M_2} \, O_{A2} \, \Psi_{\overline{N}N} \tag{3.28}$$

where $\Psi_{M_1 M_2}$ and $\Psi_{\overline{N}N}$ are the final two-meson and initial $\overline{N}N$ wave functions, respectively. The operator O_{A2} is defined as

$$O_{A2} = \lambda_{A2} \, \delta(\vec{q}_1 - \vec{q}\,'_1)\delta(\vec{q}_4 - \vec{q}\,'_4) V_{25}({}^3P_0) V_{36}({}^3P_0) V^{\dagger}_{2'3'}({}^3P_0) \tag{3.29}$$

In order to evaluate the transition amplitude for certain initial and final states, we expand the total transition amplitude T_{A2} in partial waves

$$T_{A2} = \sum_{JMLS} \sum_{jmls} T^{JMLS}_{jlms} Y^{JM}_{LS}(\hat{k}) Y^{jm*}_{ls}(\hat{p}), \tag{3.30}$$

where $J(j)$, $M(m)$, $L(l)$, and $S(s)$ denote the total angular momentum, its projection, the orbital angular momentum and total spin of the $\overline{N}N$ $(M_1 M_2)$ system, Y^{JM}_{LS} and Y^{jm}_{ls} are the vector spherical harmonics

$$\begin{aligned} Y^{JM}_{LS}(\hat{k}) &= \sum_{M_S} \langle LS, M_L M_S | J, M \rangle \, |S, M_S\rangle Y_{LM_L}(\hat{k}) \\ Y^{jm}_{ls}(\hat{p}) &= \sum_{m_s} \langle ls, m_l m_s | j, m \rangle \, |s, m_s\rangle Y_{lm_l}(\hat{p}) \end{aligned} \tag{3.31}$$

The partial wave transition amplitude for $\overline{N}N$ annihilation into two s-wave mesons takes the form

$$\begin{aligned} T^{JMLS}_{jlms}(k,p) &= \int d\hat{p}\, d\hat{k}\, T_{A2} Y^{JM*}_{LS}(\hat{k}) Y^{jm}_{ls}(\hat{p}) \\ &= \sum_{M_S, m_s} \sum_{\mu,\nu,\gamma} \langle LS, M_L M_S) | J, M \rangle \, \langle j, m | ls, m_l m_s \rangle \\ &\quad \cdot T^{\text{Spatial}}_{LM_L, lm_l, \mu\nu\gamma} T^{\text{Spin-Flavor}}_{SM_S, s_1 s_2 s m_s, T T_z, \mu\nu\gamma} \end{aligned} \tag{3.32}$$

with

$$T^{\text{Spin-Flavor}}_{SM_S,s_1s_2sm_s,TT_z,\mu\nu\gamma} = \langle M_1M_2|^{SF}\frac{1}{3\sqrt{3}}(-1)^{1+\mu+\nu+\gamma} \cdot\hat{O}^S_{-\mu}\hat{O}^S_{-\nu}\hat{O}^S_{-\gamma}\hat{O}^F\hat{O}^F\hat{O}^F\left|\overline{N}N\right\rangle^{SF}$$

and

$$\begin{aligned}
T^{\text{Spatial}}_{LM_L,lm_l,\mu\nu\gamma} = {} & \lambda_{A2}N_B^2N_s^2\int\prod_{i=1}^{4}d\vec{q}_i'\prod_{i=1}^{6}d\vec{q}_i\,d\hat{k}d\hat{p}\,Y^*_{LM_L}(\hat{k})\,Y_{lm_l}(\hat{p}) \\
& \cdot\exp\left\{-\frac{a^2}{2}\left[\left(\frac{\vec{q}_2-\vec{q}_3}{\sqrt{2}}\right)^2+\left(\frac{\vec{q}_2+\vec{q}_3-2\vec{q}_1}{\sqrt{6}}\right)^2\right]\right\} \\
& \cdot\exp\left\{-\frac{a^2}{2}\left[\left(\frac{\vec{q}_5-\vec{q}_6}{\sqrt{2}}\right)^2+\left(\frac{\vec{q}_5+\vec{q}_6-2\vec{q}_4}{\sqrt{6}}\right)^2\right]\right\} \\
& \cdot\delta\left(\vec{q}_1+\vec{q}_2+\vec{q}_3+\vec{q}_4+\vec{q}_5+\vec{q}_6\right) \\
& \cdot\delta\left(\frac{1}{2}\left[\left(\vec{q}_1+\vec{q}_2+\vec{q}_3\right)-\left(\vec{q}_4+\vec{q}_5+\vec{q}_6\right)\right]-\vec{k}\right) \\
& \cdot\exp\left[-\frac{b^2}{8}\left(\vec{q}_1'-\vec{q}_2'\right)^2\right]\exp\left[-\frac{b^2}{8}\left(\vec{q}_3'-\vec{q}_4'\right)^2\right] \\
& \cdot\delta\left(\frac{1}{2}\left[\left(\vec{q}_1'+\vec{q}_2'\right)-\left(\vec{q}_3'+\vec{q}_4'\right)\right]-\vec{p}\right) \\
& \cdot\delta\left(\vec{q}_1-\vec{q}_1'\right)\delta\left(\vec{q}_4-\vec{q}_4'\right)\delta\left(\vec{q}_2'+\vec{q}_3'\right) \\
& \delta\left(\vec{q}_2+\vec{q}_5\right)\delta\left(\vec{q}_3+\vec{q}_6\right) \\
& \cdot Y_{1\mu}(\vec{q}_3-\vec{q}_6)\,Y_{1\nu}(\vec{q}_2-\vec{q}_5)\,Y^*_{1\gamma}\left(\vec{q}_2'-\vec{q}_3'\right)
\end{aligned} \tag{3.33}$$

First, we evaluate the spatial part of the transition amplitude in eq. 3.33. To simplify the calculation, we make the following transformation

$$\begin{aligned}
\vec{q}_2 &= a_1\vec{Q}_1+a_2\vec{Q}_2+b_1\vec{k}+b_2\vec{p} \\
\vec{q}_3 &= a_1\vec{Q}_1-a_2\vec{Q}_2+b_1\vec{k}+b_2\vec{p}
\end{aligned} \tag{3.34}$$

where

$$\begin{aligned}
a_1 = \left[\frac{b^2+2a^2}{2(2b^2+3a^2)}\right]^{1/2},\quad a_2 = \left[\frac{b^2+2a^2}{2a^2}\right]^{1/2} \\
b_1 = \frac{a^2+b^2}{2b^2+3a^2},\quad b_2 = -\frac{b^2}{2(2b^2+3a^2)}
\end{aligned} \tag{3.35}$$

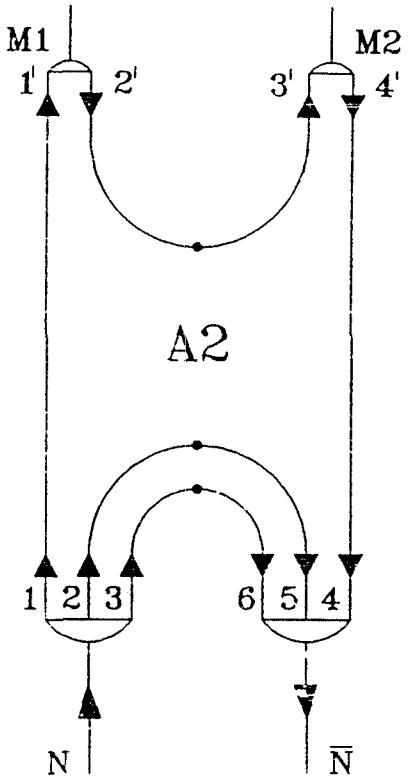

Fig. 3.1 Nucleon–antinucleon annihilation into two mesons in the A2 diagram.

Due to the δ-functions in eq. (3.33), most of the integrations can be easily carried out. One may express $T^{\rm Spatial}$ in the new coordinates $\{\vec{p}, \vec{k}, \vec{Q}_1, \vec{Q}_2\}$

$$\begin{aligned} T^{\rm Spatial} &= \lambda_{A2} N_B^2 N_s^2 \, |Det(A)|^3 \int d\vec{Q}_1 d\vec{Q}_2 \, d\hat{k} d\hat{p} \\ &\cdot \exp\left[-d_{A2}\left(\frac{3}{4}p^2 + \frac{1}{3}k^2 + \vec{p}\cdot\vec{k}\right)\right] \\ &\cdot \exp\left[-(b^2+2a^2)(Q_1^2+Q_2^2)\right] \, Y^*_{LM_L}(\hat{k})\, Y_{lm_l}(\hat{p}) \\ &\cdot 2Y_{1\mu}\left(a_1\vec{Q}_1 - a_2\vec{Q}_2 + b_1\vec{k} + b_2\vec{p}\right) \\ &\cdot 2Y_{1\nu}\left(a_1\vec{Q}_1 + a_2\vec{Q}_2 + b_1\vec{k} + b_2\vec{p}\right) \\ &\cdot 2Y^*_{1\gamma}\left(2a_1\vec{Q}_1 - (b_1+2b_2)\vec{k} + (3b_1+4b_2)\vec{p}\right) \end{aligned} \tag{3.36}$$

where

$$\begin{aligned} d_{A2} &= \frac{a^2 b^2}{2b^2+3a^2} \\ |\,Det(A)| &= -\frac{(b^2+2a^2)^3}{a^3(2b^2+3a^2)^{3/2}}. \end{aligned} \tag{3.37}$$

The integrations in eq. (3.36) can be carried out analytically by using the following formulae

$$\exp(-d_{A2}\vec{p}\cdot\vec{k}) = 4\pi \sum_{l'=0}^{\infty} \sum_{m'=-l'}^{l'} i^{l'} j_{l'}(-id_{A_2}kp) Y_{l'm'}(\hat{p}) Y^*_{l'm'}(\hat{k}) \tag{3.38}$$

$$Y_{1\mu}(a\vec{x} + b\vec{y}) = ax\, Y_{1\mu}(\hat{x}) + by\, Y_{1\mu}(\hat{y}) \tag{3.39}$$

$$\int d\Omega\, Y_{1\mu} Y_{1\nu} Y^*_{1\gamma} = 0 \tag{3.40}$$

$$\begin{aligned} \int d\Omega\, Y_{l_1 m_1} Y_{l_2 m_2} Y^*_{l_3 m_3} &= \sqrt{\frac{(2l1+1)(2l_2+1)}{4\pi(2l_3+1)}} \\ &\cdot \langle l_1 l_2, 00 | l_3, 0\rangle \langle l_1 l_2, m_1 m_2 | l_3, -m_3\rangle \end{aligned} \tag{3.41}$$

$$\int d\Omega\, Y_{l_1 m_1} Y_{l_2 m_2} Y_{l_3 m_3} Y_{l_4 m_4}$$

$$= \sum_{l=\max(|l_2-l_1|,|l_4-l_3|)}^{\min(l_2+l_1,l_4+l_3)} \sum_{m=-l}^{l} \sqrt{\frac{(2l_1+1)(2l_2+1)}{4\pi(2l+1)}}$$
$$\cdot\sqrt{\frac{(2l_3+1)(2l_4+1)}{4\pi(2l+1)}}\langle l_1 l_2, 00|l,0\rangle\langle l_1 l_2, m_1 m_2|l,m\rangle$$
$$\cdot\langle l_3 l_4, 00|l,0\rangle\langle l_3 l_4, m_3 m_4|l,-m\rangle(-1)^{-m} \tag{3.42}$$

$$\int d\Omega\, Y_{l_1 m_1} Y_{l_2 m_2} Y_{l_3 m_3} Y_{l_4 m_4} Y_{l_5 m_5}$$
$$= \sum_{l=|l_2-l_1|}^{|l_2+l_1|} \sum_{l'=|l_4-l_3|}^{|l_4+l_3|} \sum_{m=-l}^{l} \sum_{m'=-l'}^{l'} \sqrt{\frac{(2l_1+1)(2l_2+1)}{4\pi(2l+1)}}$$
$$\cdot\sqrt{\frac{(2l_3+1)(2l_4+1)}{4\pi(2l'+1)}}\sqrt{\frac{(2l+1)(2l_5+1)}{4\pi(2l'+1)}}$$
$$\cdot\langle l_1 l_2, 00|l,0\rangle\langle l_1 l_2, m_1 m_2|l,m\rangle$$
$$\cdot\langle l_3 l_4, 00|l',0\rangle\langle l_3 l_4, m_3 m_4|l',m'\rangle$$
$$\cdot\langle l l_5, 00|l',0\rangle\langle l l_5, m m_5|l',-m'\rangle \tag{3.43}$$

An easy way to evaluate the spin-flavor part of the $A2$ transition amplitude is to first recouple the quark spins and flavors using the formulas

$$|(j_1 \otimes j_2)_{J_{12}} \otimes (j_3 \otimes j_4)_{J_{34}}\rangle_{J,M}$$
$$= \sum_{J_{13},J_{24}} \langle (j_1 j_3)_{J_{13}}, (j_2 j_4)_{J_{24}}; JM|(j_1 j_2)_{J_{12}}, (j_3 j_4)_{J_{34}}; JM\rangle$$
$$\cdot|(j_1 \otimes j_3)_{J_{13}} \otimes (j_2 \otimes j_4)_{J_{24}}\rangle_{J,M} \tag{3.44}$$

with

$$\langle (j_1 j_3)_{J_{13}}, (j_2 j_4)_{J_{24}}; JM|(j_1 j_2)_{J_{12}}, (j_3 j_4)_{J_{34}}; JM\rangle$$
$$= \sqrt{(2J_{12}+1)(2J_{34}+1)(2J_{13}+1)(2J_{24}+1)} \cdot \begin{Bmatrix} j_1 & j_2 & J_{12} \\ j_3 & j_4 & J_{34} \\ J_{13} & J_{24} & J \end{Bmatrix} \tag{3.45}$$

The $\overline{N}N$ spin-flavor wave function may be rewritten as

$$
\begin{aligned}
&|\overline{N}N\rangle_{TT_z}^{SM_S} \\
&= \frac{1}{2}\sum_{J_{34},J_{56}} \left|\left[\left(\frac{1}{2}^{(2)}\otimes\frac{1}{2}^{(3)}\right)_{J_{23}}\otimes\frac{1}{2}^{(1)}\right]_{1/2}\otimes\left[\left(\frac{1}{2}^{(5)}\otimes\frac{1}{2}^{(6)}\right)_{J_{56}}\otimes\frac{1}{2}^{(4)}\right]_{1/2}\right\rangle_{SS_z}^{\text{Spin}} \\
&\quad\cdot\left|\left[\left(\frac{1}{2}^{(2)}\otimes\frac{1}{2}^{(3)}\right)_{J_{23}}\otimes\frac{1}{2}^{(1)}\right]_{1/2}\otimes\left[\left(\frac{1}{2}^{(5)}\otimes\frac{1}{2}^{(6)}\right)_{J_{56}}\otimes\frac{1}{2}^{(4)}\right]_{1/2}\right\rangle_{TT_z}^{\text{Flavor}} \\
&= \frac{1}{2}\sum_{J_{23},J_{56}}\sum_{g,h,i,j}\sum_{g_t,h_t,i_t,j_t} \\
&\quad\cdot\left\langle (J_{23}J_{56})\,g,\left(\frac{1}{2}\frac{1}{2}\right)h;S\middle|\left(J_{23}\frac{1}{2}\right)\frac{1}{2},\left(J_{56}\frac{1}{2}\right)\frac{1}{2};S\right\rangle \\
&\quad\cdot\left\langle\left(\frac{1}{2}\frac{1}{2}\right)i,\left(\frac{1}{2}\frac{1}{2}\right)j;g\middle|\left(\frac{1}{2}\frac{1}{2}\right)J_{23},\left(\frac{1}{2}\frac{1}{2}\right)J_{56};g\right\rangle \\
&\quad\cdot\left\langle (J_{23}J_{56})\,g_t,\left(\frac{1}{2}\frac{1}{2}\right)h_t;T\middle|\left(J_{23}\frac{1}{2}\right)\frac{1}{2},\left(J_{56}\frac{1}{2}\right)\frac{1}{2};T\right\rangle \\
&\quad\cdot\left\langle\left(\frac{1}{2}\frac{1}{2}\right)i_t,\left(\frac{1}{2}\frac{1}{2}\right)j_t;g_t\middle|\left(\frac{1}{2}\frac{1}{2}\right)J_{23},\left(\frac{1}{2}\frac{1}{2}\right)J_{56};g_t\right\rangle \\
&\quad\cdot\left|\left[\left(\frac{1}{2}^{(2)}\otimes\frac{1}{2}^{(5)}\right)_{i}\otimes\left(\frac{1}{2}^{(3)}\otimes\frac{1}{2}^{(6)}\right)_{j}\right]_{g}\otimes\left(\frac{1}{2}^{(1)}\otimes\frac{1}{2}^{(4)}\right)_{h}\right\rangle_{SS_z}^{Spin} \\
&\quad\cdot\left|\left[\left(\frac{1}{2}^{(2)}\otimes\frac{1}{2}^{(5)}\right)_{i_t}\otimes\left(\frac{1}{2}^{(3)}\otimes\frac{1}{2}^{(6)}\right)_{j_t}\right]_{g_t}\otimes\left(\frac{1}{2}^{(1)}\otimes\frac{1}{2}^{(4)}\right)_{h_t}\right\rangle_{TT_z}^{Flavor}
\end{aligned}
\tag{3.46}
$$

For the $^3P_0$ quark-antiquark operator, one has

$$i = j = 1, \text{ and } i_t = j_t = 0 \tag{3.47}$$

hence

$$
\begin{aligned}
&\left\langle\left(\frac{1}{2}\frac{1}{2}\right)i_t,\left(\frac{1}{2}\frac{1}{2}\right)j_t;g_t\middle|\left(\frac{1}{2}\frac{1}{2}\right)J_{23},\left(\frac{1}{2}\frac{1}{2}\right)J_{56};g_t\right\rangle \\
&= \left\langle\left(\frac{1}{2}\frac{1}{2}\right)0,\left(\frac{1}{2}\frac{1}{2}\right)0;g_t\middle|\left(\frac{1}{2}\frac{1}{2}\right)J_{23},\left(\frac{1}{2}\frac{1}{2}\right)J_{56};g_t\right\rangle \\
&= \frac{1}{2}\delta_{g_t,0}\delta_{J_{23},J_{56}}\sqrt{2J_{23}+1}
\end{aligned}
\tag{3.48}
$$

and

$$\left\langle (J_{23}J_{56})\,g_t,\left(\frac{1}{2}\frac{1}{2}\right)h_t;T\middle|\left(J_{23}\frac{1}{2}\right)\frac{1}{2},\left(J_{56}\frac{1}{2}\right)\frac{1}{2};T\right\rangle$$

$$= \left\langle (J_{23}J_{56})\,0, \left(\frac{1}{2}\frac{1}{2}\right) h_t; T \middle| \left(J_{23}\frac{1}{2}\right)\frac{1}{2}, \left(J_{56}\frac{1}{2}\right)\frac{1}{2}; T \right\rangle$$

$$= \delta_{T,h_t}\frac{2}{\sqrt{2J_{23}+1}}(-1)^{T+J_{23}+1}\begin{Bmatrix} 1/2 & 1/2 & T \\ 1/2 & 1/2 & J_{23} \end{Bmatrix} \tag{3.49}$$

Finally, the $\overline{N}N$ spin-flavor wave function takes the form

$$|\overline{N}N\rangle^{SS_z}_{TT_z} = \left| \left[\left(\frac{1}{2}^{(2)} \otimes \frac{1}{2}^{(5)}\right)_0 \otimes \left(\frac{1}{2}^{(3)} \otimes \frac{1}{2}^{(6)}\right)_0 \right]_0 \otimes \left(\frac{1}{2}^{(1)} \otimes \frac{1}{2}^{(4)}\right)_T \right\rangle^{Flavor}_{TT_z}$$
$$\cdot \sum_{g=0,2} F(T,S,g)$$
$$\cdot \left| \left[\left(\frac{1}{2}^{(2)} \otimes \frac{1}{2}^{(5)}\right)_1 \otimes \left(\frac{1}{2}^{(3)} \otimes \frac{1}{2}^{(6)}\right)_1 \right]_g \otimes \left(\frac{1}{2}^{(1)} \otimes \frac{1}{2}^{(4)}\right)_S \right\rangle^{Spin}_{SS_z} \tag{3.50}$$

with

$$F(T,S,g) = \frac{1}{2}\sum_{J_{23}=0,1}(-1)^{T+J_{23}+1}\begin{Bmatrix} 1/2 & 1/2 & T \\ 1/2 & 1/2 & J_{23} \end{Bmatrix}$$
$$\cdot \left\langle (J_{23}J_{23})\,g, \left(\frac{1}{2}\frac{1}{2}\right) S; S \middle| \left(J_{23}\frac{1}{2}\right)\frac{1}{2}, \left(J_{23}\frac{1}{2}\right)\frac{1}{2}; S \right\rangle$$
$$\cdot \left\langle \left(\frac{1}{2}\frac{1}{2}\right) 1, \left(\frac{1}{2}\frac{1}{2}\right) 1; g \middle| \left(\frac{1}{2}\frac{1}{2}\right) J_{23}, \left(\frac{1}{2}\frac{1}{2}\right) J_{23}; g \right\rangle \tag{3.51}$$

Note that the sum over g in eq. 3.50 takes values only 0 and 2. This stems from the property of the $9j$-symbol

$$\begin{Bmatrix} 1/2 & 1/2 & 1 \\ 1/2 & 1/2 & 1 \\ J_{23} & J_{23} & g \end{Bmatrix} = (-1)^{2+2+2J_{23}+g}\begin{Bmatrix} 1/2 & 1/2 & 1 \\ 1/2 & 1/2 & 1 \\ J_{23} & J_{23} & g \end{Bmatrix} \tag{3.52}$$

The spin wave function of the two-meson final state may be written as

$$\left| \left(\frac{1}{2}^{(1')} \otimes \frac{1}{2}^{(2')}\right)_{\bar{S}_1} \otimes \left(\frac{1}{2}^{(4')} \otimes \frac{1}{2}^{(3')}\right)_{\bar{S}_2} \right\rangle_{\bar{S}\bar{S}_z}$$
$$= \sum_{S',S''} \left\langle \left(\frac{1}{2}\frac{1}{2}\right) S', \left(\frac{1}{2}\frac{1}{2}\right) S''; \bar{S} \middle| \left(\frac{1}{2}\frac{1}{2}\right) \bar{S}_1, \left(\frac{1}{2}\frac{1}{2}\right) \bar{S}_2; \bar{S} \right\rangle$$

$$\cdot\left|\left(\frac{1}{2}^{(1')}\otimes\frac{1}{2}^{(4')}\right)_{S'}\otimes\left(\frac{1}{2}^{(2')}\otimes\frac{1}{2}^{(3')}\right)_{S''}\right\rangle_{\bar{S}\bar{S}_z}$$

$$= \sqrt{(2\bar{S}_1+1)(2\bar{S}_2+1)}\sum_{S',S''}\sqrt{(2S'+1)(2S''+1)}\left\{\begin{array}{ccc}1/2 & 1/2 & \bar{S}_1\\ 1/2 & 1/2 & \bar{S}_2\\ S' & S'' & \bar{S}\end{array}\right\}$$

$$\cdot\left|\left(\frac{1}{2}^{(1')}\otimes\frac{1}{2}^{(4')}\right)_{S'}\otimes\left(\frac{1}{2}^{(2')}\otimes\frac{1}{2}^{(3')}\right)_{S''}\right\rangle_{\bar{S}\bar{S}_z} \tag{3.53}$$

Due to the dynamics of $^3P_0$ operator one has $S''=1$, hence

$$\left|\left(\frac{1}{2}^{1'}\otimes\frac{1}{2}^{2'}\right)_{\bar{S}_1}\otimes\left(\frac{1}{2}^{4'}\otimes\frac{1}{2}^{3'}\right)_{\bar{S}_2}\right\rangle_{\bar{S}\bar{S}_z}$$

$$= \sum_{S'}G(\bar{S},\bar{S}_1,\bar{S}_2;S')\left|\left(\frac{1}{2}^{(1')}\otimes\frac{1}{2}^{(4')}\right)_{S'}\otimes\left(\frac{1}{2}^{2'}\otimes\frac{1}{2}^{(3')}\right)_{1}\right\rangle_{\bar{S}\bar{S}_z} \tag{3.54}$$

$$G(\bar{S}_1,\bar{S}_2,\bar{S};S')$$

$$= \sqrt{3}\sqrt{(2\bar{S}_1+1)(2\bar{S}_2+1)(2S'+1)}\left\{\begin{array}{ccc}1/2 & 1/2 & \bar{S}_1\\ 1/2 & 1/2 & \bar{S}_2\\ S' & 1 & \bar{S}\end{array}\right\} \tag{3.55}$$

Note in the above equations and also the following equations that $\bar{S}_i$, $\bar{S}$, $\bar{S}_z$ stand for the spin of the ith-meson, the total spin of the two-meson system and the projection of the total spin, respectively.

Using the wave functions in eqs. (3.50) and (3.54) and considering the opreation properties of the $^3P_0$ operator, we can easily evaluate the spin part of the transition amplitude. The main steps are as below:

$$
\begin{aligned}
& T^{spin}(S, S_z; \bar{S}_1, \bar{S}_2, \bar{S}; \mu, \nu, \gamma; T) \\
= & \sum_{\bar{S}'} G(\bar{S}, \bar{S}_1, \bar{S}_2; \bar{S}') \left\langle \left(\frac{1}{2}^{(1')} \otimes \frac{1}{2}^{(4')} \right)_{\bar{S}'} \otimes \left(\frac{1}{2}^{(2')} \otimes \frac{1}{2}^{(3')} \right)_1 \right|_{\bar{S}\bar{S}_z} \\
& \cdot \frac{(-1)^{1+\mu+\nu+\gamma}}{3\sqrt{3}} \hat{O}^S_{-\mu,25} \hat{O}^S_{-\nu,36} \hat{O}^{S\dagger}_{-\gamma,2'3'} \cdot \sum_{g=0,2} F(T, S, g) \cdot \\
& \cdot \left| \left[\left(\frac{1}{2}^{(2)} \otimes \frac{1}{2}^{(5)} \right)_1 \otimes \left(\frac{1}{2}^{(3)} \otimes \frac{1}{2}^{(6)} \right)_1 \right]_g \otimes \left(\frac{1}{2}^{(1)} \otimes \frac{1}{2}^{(4)} \right)_S \right\rangle^{Spin}_{SS_z} \\
= & \frac{(-1)^{1+\mu+\nu+\gamma}}{3\sqrt{3}} \sum_{g=0,2} \sum_{\bar{S}'} F(T, S, g) G(\bar{S}_1, \bar{S}_2, \bar{S}, \bar{S}') \\
& \cdot \sum_{M_{25}, M_{36}} \sum_{M_g, M_{14}} \sum_{M_{1'4'}, M_{2'3'}} \\
& \cdot \langle \bar{S}' 1, M_{1'4'} M_{2'3'} | \bar{S}, \bar{S}_z \rangle \langle 11, M_{25} M_{36} | g M_g \rangle \langle gS, M_g M_{14} | S S_z \rangle \\
& \cdot \left\langle \frac{1}{2}^{(1')} \otimes \frac{1}{2}^{(4')} \right|_{\bar{S}', M_{1'4'}} \left\langle \frac{1}{2}^{(2')} \otimes \frac{1}{2}^{(3')} \right|_{1, M_{2'3'}} \hat{O}^S_{-\mu,25} \hat{O}^S_{-\nu,34} \hat{O}^{S\dagger}_{-\gamma,2'3'} \\
& \cdot \left| \frac{1}{2}^{(2)} \otimes \frac{1}{2}^{(5)} \right\rangle_{1, M_{25}} \left| \frac{1}{2}^{(3)} \otimes \frac{1}{2}^{(6)} \right\rangle_{1, M_{36}} \left| \frac{1}{2}^{(1)} \otimes \frac{1}{2}^{(4)} \right\rangle_{S, M_{14}} \\
= & \frac{2\sqrt{2}}{3} \sqrt{2S+1} \sqrt{(2\bar{S}_1 + 1)(2\bar{S}_2 + 1)} \\
& \cdot \begin{Bmatrix} 1/2 & 1/2 & \bar{S}_1 \\ 1/2 & 1/2 & \bar{S}_2 \\ S & 1 & \bar{S} \end{Bmatrix} \delta_{\mu+\nu-\gamma, S_z - \bar{S}_z} \langle S1, \bar{S}_z - \gamma, \gamma | \bar{S}, \bar{S}_z \rangle \\
& \cdot \sum_{g=0,2} F(T, S, g) \langle gS, \mu + \nu, S_z - \mu - \nu | S, S_z \rangle \langle 11, \mu\nu | g, \mu + \nu \rangle
\end{aligned}
\tag{3.56}
$$

Here we have used

$$
\left\langle \frac{1}{2}^{(1')} \otimes \frac{1}{2}^{(4')} \right|_{\bar{S}', M_{1'4'}} \cdot \left| \frac{1}{2}^{(1)} \otimes \frac{1}{2}^{(4)} \right\rangle_{S, M_{14}} = \delta_{S, \bar{S}'} \, \delta_{M_{1'4'}, M_{14}}
$$

$$
\langle 0, 0 | \hat{O}_{1\mu} | J, M \rangle = (-1)^M \sqrt{2} \; \delta_{J,1} \delta_{M,-\mu} \tag{3.57}
$$

We are now ready to write the spin-spatial part of the transition amplitude

$$
\begin{aligned}
& T^{\text{Spin-Spatial}}(J,M,L,S;J',M',L',S';k,p) \\
= & \sum_{S'_z,S_z}\sum_{\mu,\nu,\gamma}\langle LS,L_zS_z|J,M\rangle\langle J',M'|L'S',L'_zS'_z\rangle \\
& \cdot T^{\text{Spatial}}(LL_z,L'L'_z,\mu\nu\gamma)\,T^{\text{Spin}}(SS_z,S'_1S'_2S'S'_z,TT_z,\mu\nu\gamma) \\
\\
= & \frac{2\sqrt{2}}{3}\sqrt{(2S+1)(2S'_1+1)(2S'_2+1)}\begin{Bmatrix} 1/2 & 1/2 & S'_1 \\ 1/2 & 1/2 & S'_2 \\ S & 1 & S' \end{Bmatrix} \\
& \cdot\sum_{g=0,2}F(S,T,g)\sum_{S_z,S'_z}\sum_{\mu,\nu,\gamma}\cdot\langle LS,M-S_z,S_z|JM\rangle \\
& \langle J'M'|L'S',M'-S'_z,S'_z\rangle\langle S1,S'_z-\gamma,\gamma|S',S'_z\rangle \\
& \cdot\langle gS,\mu+\nu,S_z-\mu-\nu|S,S_z\rangle\langle 11,\mu\nu|g,\mu+\nu\rangle\,\delta_{\mu+\nu-\gamma,S_z-S'_z} \\
& \cdot T^{\text{Spatial}}(L,L_z=M-S_z,L',L'_z=M'-S'_z,\mu,\nu,\gamma,)
\end{aligned}
\tag{3.58}
$$

where $J(J')$, $M(M')$, $L(L')$, and $S(S')$ stand respectively for the total angular momentum, its projection, total orbital angular momentum, total spin of the $\overline{N}N$ (M_1M_2) system.

Let consider the flavor part of the transition amplitude. We need first to couple the two-meson final state to isospin eigenstates

$$
\begin{aligned}
& \left|\frac{1}{2}^{(1')}\otimes\frac{1}{2}^{(2')}\right\rangle_{T_1,T_{z1}}\left|\frac{1}{2}^{(4')}\otimes\frac{1}{2}^{(3')}\right\rangle_{T_2,-T_{z1}} \\
= & \sum_{T',T'_z}\langle T',T'_z|T_1T_2,T_{1z},-T_{1z}\rangle\left|\left(\frac{1}{2}^{(1')}\otimes\frac{1}{2}^{(2')}\right)_{T_1}\otimes\left(\frac{1}{2}^{(4')}\otimes\frac{1}{2}^{(3')}\right)_{T_2}\right\rangle_{T',T'_z} \\
= & \sum_{T',T'_z}\langle T',T'_z|T_1T_2,T_{1z},-T_{1z}\rangle \\
& \cdot\sum_{T_a,T_b}\left\langle\left(\frac{1}{2}\frac{1}{2}\right)T_a,\left(\frac{1}{2}\frac{1}{2}\right)T_b;T'\middle|\left(\frac{1}{2}\frac{1}{2}\right)T_1,\left(\frac{1}{2}\frac{1}{2}\right)T_2;T'\right\rangle \\
& \cdot\left|\left(\frac{1}{2}^{(1')}\otimes\frac{1}{2}^{(4')}\right)_{T_a}\otimes\left(\frac{1}{2}^{(2')}\otimes\frac{1}{2}^{(3')}\right)_{T_b}\right\rangle_{T',T'_z}
\end{aligned}
$$

$$= \frac{3}{\sqrt{2}} \sum_{T',T'_z} (-1)^{1+T_2+T'} \langle T', T'_z | T_1 T_2, T_{1z}, -T_{1z} \rangle \cdot \left\{ \begin{array}{ccc} 1/2 & 1/2 & T' \\ T_2 & T_1 & 1/2 \end{array} \right\}$$
$$\cdot \left| \left(\frac{1}{2}^{(1')} \otimes \frac{1}{2}^{(4')} \right)_{T'} \otimes \left(\frac{1}{2}^{(2')} \otimes \frac{1}{2}^{(3')} \right)_0 \right\rangle_{T',T'_z} \tag{3.59}$$

Here we have set $T_b = 0$, and used

$$\left\{ \begin{array}{ccc} 1/2 & 1/2 & T_a \\ 1/2 & 1/2 & 0 \\ T_1 & T_2 & T' \end{array} \right\} = \delta_{T',T_a} \frac{(-1)^{1+T_2+T'}}{\sqrt{2(2T'+1)}} \left\{ \begin{array}{ccc} 1/2 & 1/2 & T_a \\ T_2 & T_1 & 1/2 \end{array} \right\} \tag{3.60}$$

The flavor part of the A2 transition amplitude is derived as:

$$\begin{aligned} & T^{Flavor}(T, T_z = 0; T_1, T_{1z}, T_2, T_{2z}) \\ = & \frac{3}{\sqrt{2}} \sum_{T',T'_z} (-1)^{1+T_2+T'} \langle T', T'_z | T_1 T_2, T_{1z}, -T_{1z} \rangle \cdot \left\{ \begin{array}{ccc} 1/2 & 1/2 & T' \\ T_2 & T_1 & 1/2 \end{array} \right\} \\ & \cdot \left\langle \left(\frac{1}{2}^{(1')} \otimes \frac{1}{2}^{(4')} \right)_{T'} \otimes \left(\frac{1}{2}^{(2')} \otimes \frac{1}{2}^{(3')} \right)_0 \right|_{T',T'_z} \hat{O}^F_{25} \hat{O}^F_{36} \hat{O}^{F\dagger}_{2'3'} \\ & \cdot \left| \left[\left(\frac{1}{2}^{(2)} \otimes \frac{1}{2}^{(5)} \right)_0 \otimes \left(\frac{1}{2}^{(3)} \otimes \frac{1}{2}^{(6)} \right)_0 \right]_0 \otimes \left(\frac{1}{2}^{(1)} \otimes \frac{1}{2}^{(4)} \right)_T \right\rangle^{Flavor}_{TT_z} \\ = & 6(-1)^{1+T_2+T} \langle T_1 T_2, T_{1z}, -T_{1z} | T, 0 \rangle \cdot \left\{ \begin{array}{ccc} 1/2 & 1/2 & T \\ T_2 & T_1 & 1/2 \end{array} \right\} \end{aligned} \tag{3.61}$$

where T and T_z are respectively the total isospin spin and its projection of the initial $\overline{N}N$ system. T_i and T_{iz} are the isospin and its projection of the ith meson of the two-meson final state.

We have evaluated all parts of the transition amplitude of the process of $\overline{N}N$ annihilation into two s-wave mesons in the A2 quark diagram. It is straightforward to derive the transition amplitude of the A2 diagram

$$T^{JMLS}_{jlms}(k,p) = T^{\text{Flavor}}_{T_1,T_2,T_{1z},T_{2z};T} T^{\text{Spin-Spatial}}_{J,M,L,S;j,l,m,s} \tag{3.62}$$

with

$$T^{\text{Spin-Spatial}}_{J,M,L,S;j,l,m,s}(p,k) = \sum_{M_S,m_s} \sum_{\mu,\nu,\gamma} \langle LS, M_L M_S) | J, M \rangle \langle j, m | ls, m_l m_s \rangle$$

$$\cdot T^{\rm Spatial}(LM_L, lm_l, \mu\nu\gamma)\ \cdot T^{\rm Spin}(SM_S, s_1 s_2 s m_s, T, \mu\nu\gamma)$$

$$= N_{A2}\, F_0\, e^{-d_{a2}\left(\frac{1}{3}k^2+\frac{3}{4}p^2\right)} \cdot T \tag{3.63}$$

and

$$\begin{aligned} T &= i^L j_L(x)\left[p\,F_1A_1 + p\,F_2A_2 + p^3F_3A_3\right] \\ &+ i^l j_l(x)\left[k\,F_4A_4 + k^3F_5A_5\right] \\ &+ i^{L-1} j_{L-1}(x)\left[F_6A_6 + F_7A_7\right]p^2k \\ &+ i^{L+1} j_{L+1}(x)\left[F_8A_8 + F_9A_9\right]p^2k \\ &+ i^{l-1} j_{l-1}(x)\left[F_{10}A_{10} + F_{11}A_{11}\right]pk^2 \\ &+ i^{l+1} j_{l+1}(x)\left[F_{12}A_{12} + F_{13}A_{13}\right]pk^2 \end{aligned} \tag{3.64}$$

$$\begin{aligned} x &= -id_{A2}pk \\ N_{A2} &= \lambda_{A2}N_B^2N_s^2\frac{4}{\sqrt{4\pi}}\left(\frac{\pi}{\frac{3}{2}a^2+b^2}\right)^{3/2}\left(\frac{\pi}{2a^2}\right)^{3/2} \\ A_i &= A_i(a,b) \\ F_i &= F_i(J,M,L,S;j,m,l,s,s_1,s_2;T) \end{aligned} \tag{3.65}$$

where $J(j)$, $M(m)$, $L(l)$ and $S(s$ are respectively the total angular momentum, its projection, total orbital angular momentum and total spin of the initial $\overline{N}N$ state (the final two-meson state). s_i is the spin of the ith meson, and T the total isospin of the system.

It should be pointed out that the form of the transition amplitude in eq. (3.64) holds not only for the final states with two s-wave mesons, but also for final states with one s-wave and one p-wave mesons and with two p-wave mesons, and so on. The coefficient $A\cdot$ are also general, depending only on the size parameters a and b. However, the coefficients F_i vary with different initial and final states. As an example, we show in Table 3.1 the coeficient F_i for the process of $\overline{N}N$ annihilation to two s-wave mesons;

3.5 Optical Potential of A2 Diagram

In order to supplement the elastic medium and long-ranged meson-exchange part of the $\overline{N}N$ interaction with a short-ranged annihilation potential we have to work out the optical potential as defined in the A2/A3 quark model. We start with the definition of the $\overline{N}N$ Hilbert space as P-space, the Hilbert space of two and three meson states as Q-space. The corresponding projection operators P and Q satisfy the relations

$$PQ = 0, \tag{3.66}$$

$$QP = 0, \tag{3.67}$$

$$P+Q = 1. \tag{3.68}$$

We define H and $\mid \psi \rangle$ as the Hamilton operator and the eigenfunction of the full coupled channel system. Projecting onto the $\overline{N}N$ and mesonic subspaces we obtain following coupled system of equations:

$$(E - PHP)\, P \mid \psi \rangle = PHQ\, Q \mid \psi \rangle \tag{3.69}$$

$$(E - QHQ)\, Q \mid \psi \rangle = QHP\, P \mid \psi \rangle \tag{3.70}$$

where E is the total energy eigenvalue. The effective one-body equation for the $\overline{N}N$ system is derived from the above equations as

$$(E - PHP - PHQ\, G\, QHP)\; P \mid \psi \rangle = 0 \tag{3.71}$$

with

$$G = \frac{1}{E - QHQ}, \tag{3.72}$$

where G is the Greens function for the two and three meson intermediate states. When neglecting the final state interaction between the mesons, the Greens function will take the form

$$\langle \alpha \mid G \mid \beta \rangle = \frac{\delta_{\alpha\beta}}{E - \sum_i E_i + i\varepsilon} \tag{3.73}$$

where E_i is the energy of the ith meson.

In eq. 3.71, the term PHP includes the kinetic energy and the elastic meson-exchange potential of the $\overline{N}N$ system. The term $PHQGQHP$ is the optical potential due to annihilation into two and three mesons. In our calculation, we treat the meson kinematics relativistically and use Lorentz invariant phase space. The potential due to the A2 diagram is obtained as

$$\begin{aligned} V_{A2}(\vec{k},\vec{k}') &\equiv \langle \vec{k}' \mid PHQGQHP \mid \vec{k} \rangle \\ &= \sum_{\alpha\beta} \langle \vec{k}' \mid PHQ \mid \alpha \rangle \langle \alpha \mid G \mid \beta \rangle \langle \beta \mid QHP \mid \vec{k} \rangle \\ &= \sum_{rt} \sum_{JMSLL'} Y_{L'S}^{JM*}(\hat{k}')\, Y_{LS}^{JM}(\hat{k}) \\ &\quad \cdot \int \frac{d\vec{p}_1}{E_r} \frac{d\vec{p}_2}{E_t} \delta(\vec{p}_1 + \vec{p}_2) \sum_{jmls} \frac{T_{jmls}^{JML'S*}\, T_{jmls}^{JMLS}}{E - E_r - E_t + i\varepsilon} \end{aligned} \tag{3.74}$$

where the summation r, s runs over all possible two-meson states. In the partial wave basis α of the $\overline{N}N$ system, where $\alpha = \{LSJMT\}$, the optical potential takes the form

$$V_\alpha(k,k') = \sum_{rt} \int \frac{d\vec{p}}{E_r E_t} \sum_{jmls} \frac{T_{jmls}^{\alpha *}(\vec{p},k')\, T_{jmls}^{\alpha}(\vec{p},k)}{E - E_r - E_t + i\varepsilon}. \tag{3.75}$$

With the operator identity

$$\frac{1}{E - E_r - E_t + i\varepsilon} = Pr \frac{1}{E - E_r - E_t} - i\pi\, \delta(E - E_r - E_t) \tag{3.76}$$

where Pr stands for the principle value, the complex optical potential V_α can be separated into a real and an imaginary part. For the imaginary part of the A2 potential we obtain immediately

$$\mathrm{Im}V_\alpha(k,k') = -8\pi \frac{p(E)}{E} \sum_{rt} \sum_{jmls} T_{jmls}^{\alpha *}(p(E),k')\, T_{jlms}^{\alpha}(p(E),k) \tag{3.77}$$

with the momentum p related to the total energy E as

$$E = \sqrt{m_r^2 + \vec{p}^{\,2}} + \sqrt{m_t^2 + \vec{p}^{\,2}} \tag{3.78}$$

where m_r and m_t are the masses of the final state mesons.

In practice, we include in the case of the A2 model contributions from all possible two-meson annihilation channels, which are combinations of two s-wave (s) mesons

or one s- and one p-wave (p) meson. The s and p mesons considered here are listed as folows:

$$s = (Q\overline{Q})_{l=0} = \begin{cases} \pi, \eta, \eta' & J^{PC} = 0^{-+} \\ \rho, \omega & J^{PC} = 1^{--} \end{cases} \tag{3.79}$$

$$p = (Q\overline{Q})_{l=1} = \begin{cases} \delta(a_0(980)), \epsilon(f_0(1400)) & J^{PC} = 0^{++} \\ B(b(1235)), H(h_1(1170)) & J^{PC} = 1^{+-} \\ A_1(a_1(1260)), D(f_1(1285)) & J^{PC} = 1^{++} \\ A_2(a_2(1320)), f(f_2(1270)) & J^{PC} = 2^{++} \end{cases} \tag{3.80}$$

For $\overline{N}N$ scattering most of the two-meson channels considered in the A2 model are already opened. Therefore, when considering the finite widths of mesons, it has little influence on the results for the potential. For the $\overline{N}N$ bound state problem, however, fewer and fewer channels contribute to the imaginary potential as the energy of the state decreases. Then a few meson channels dominantly determine the behavior of the potential for this particular state. In a proper determination of the annihilation potential, the finite meson widths have to be introduced into the calculation. The optical potential of eq. 3.75 is rewritten as

$$\begin{aligned} V_\alpha(k,k') = & \sum_{rt} \int dm_r\, dm_t f(m_r,\Gamma_r) f(m_t,\Gamma_t) \\ & \cdot \int \frac{d\vec{p}}{\sqrt{m_r^2+\vec{p}^{\,2}}\sqrt{m_t^2+\vec{p}^{\,2}}} \sum_{jmls} \frac{T^{\alpha *}_{jmls}(p,k')\, T^{\alpha}_{jmls}(p,k)}{E - \sqrt{m_r^2+\vec{p}^{\,2}} - \sqrt{m_t^2+\vec{p}^{\,2}} + i\varepsilon} \end{aligned}$$

where $f(m_r,\Gamma_r)$ is the mass distribution of the meson r, with mass m_r and width Γ_r. The explicit form of these mass distribution functions can be found, for example, in Ref.[45].

	F_0	F_1	F_2	F_3	F_4	F_5	F_6
$^{13}P_0 \to ^1 S_0$	$\frac{\sqrt{2}}{36}$	15	15	-18	45	-18	10
$^{33}P_0 \to ^1 S_0$	$\frac{\sqrt{2}}{108}$	3	39	-18	45	-18	2
$^{13}S_1 \to ^1 P_1$	$\frac{\sqrt{6}}{108}$	-15	-15	18	-45	18	0
$^{33}S_1 \to ^1 P_1$	$\frac{\sqrt{6}}{324}$	-3	-39	18	-45	18	0
$^{13}D_1 \to ^1 P_1$	$-\frac{\sqrt{3}}{270}$	-75	-75	90	-225	90	-54
$^{33}D_1 \to ^1 P_1$	$-\frac{\sqrt{3}}{810}$	-15	-195	90	-225	90	-18
$^{13}P_2 \to ^1 D_2$	$\frac{\sqrt{5}}{450}$	-75	-75	90	-225	90	-20
$^{33}P_2 \to ^1 D_2$	$\frac{\sqrt{5}}{1350}$	-15	-195	90	-225	90	-40
$^{13}F_2 \to ^1 D_2$	$-\frac{\sqrt{30}}{2100}$	-175	-175	210	-525	210	-130
$^{33}F_2 \to ^1 D_2$	$\frac{\sqrt{30}}{6300}$	35	455	-210	525	-210	50

	F_7	F_8	F_9	F_{10}	F_{11}	F_{12}	F_{13}
$^{13}P_0 \to ^1 S_0$	10	8	8	0	0	-18	-18
$^{33}P_0 \to ^1 S_0$	26	16	-8	0	0	-18	-18
$^{13}S_1 \to ^1 P_1$	0	-18	-18	10	10	8	8
$^{33}S_1 \to ^1 P_1$	0	-18	-18	2	26	16	-8
$^{13}D_1 \to ^1 P_1$	-54	-36	-36	20	20	70	70
$^{33}D_1 \to ^1 P_1$	-126	-72	36	40	-20	50	110
$^{13}P_2 \to ^1 D_2$	-20	-70	-70	54	54	36	36
$^{33}P_2 \to ^1 D_2$	20	-50	-110	18	126	72	-36
$^{13}F_2 \to ^1 D_2$	-130	-80	-80	56	56	154	154
$^{33}F_2 \to ^1 D_2$	290	160	-80	-112	56	-98	-266

Table 3.1: Coefficients F_i in eq. (3.64) for $\overline{N}N$ annihilation into two s-wave mesons. The notation of the quantum numbers in the initial and final states is $(^{(2T+1)(2S+1)}L_J \to ^{2s+1} l_{j=J})$.

Chapter 4

$\overline{N}N$ Atomic States

Replacing an electron orbiting around a nucleus in an atom with a heavier, negatively charged particle has opened up new windows in nuclear and particle physics. In the last three decades "muonic" [60] and "pionic" [61] atoms have been the focus of much theoretical and experimental efforts at various "pion factories" (LAMPF, PSI, TRIUMF). More recently the even heavier, negatively charged, antiproton $\overline{p}$ has become available in sufficient numbers to probe the nucleus at much smaller distances. Very low-energetic $\overline{p}$ can be "trapped" to form "antiprotonic atoms". These allow to study the interference of QED and QCD on the one hand, and the strong interaction (QCD) in the form of the annihilation into mesons, with unprecedented sensitivity, on the other hand. The simplest antiprotonic atom is the antiprotonic hydrogen atom known as "protonium". The $\overline{p}p$ system can have quantum numbers unavailable to the e^+e^- system and, therefore, is particularly suited to study "exotic" (i.e. non-$\overline{Q}Q$) mesons. We employ here a powerful and well-documented mathematical method (not previously applied to $\overline{N}N$ bound states), known in atomic physics as Sturmian function approach. With this method $\overline{N}N$ atomic states, arising from the interference of the long-ranged Coulomb interaction with the short-ranged strong interaction of QCD, can reliably be evaluated. Unlike the traditionally used Numerov method, the here employed Sturmian function approach can also be applied to non-local potentials (like the Bonn potential) and to the atomic states with higher angular momenta.

4.1 Brief History of $\overline{N}N$ Atoms

In recent years several experiments have been carried out at the low-energy antiproton ring LEAR at CERN to study the properties of protonium. In these experiments low energetic antiprotons are captured into the Coulomb field of the proton via Auger electron emission, after deceleration to a kinetic energy of a few eV [62]. In the case of hydrogen, $\bar{p}$ are captured into orbits of $n_{\bar{p}} \approx 40$ and cascade rapidly to the $1s$ and $2p$ levels (by X-ray emission), from which the $\bar{p}p$ system annihilates mostly into multi-meson final states (occasionally those multi-meson states are observed to be correlated via πf_2, $\pi\pi f_2$ etc). The strong interaction shifts the Coulombic binding energies of the $1s$ and $2p$ states and adds a finite width describing the annihilation from this state. For a $\bar{p}p$ atom the purely Coulombic $1s$ Bohr radius is calculated to be 57.6 fm with a binding energy of $E_{1s} = 12.49$ keV. The electromagnetic energies for the Lyman $K_\alpha(2p \rightarrow 1s)$, Balmer $L_\alpha(3d \rightarrow 2p)$ and Paschen $M_\alpha(4f \rightarrow 3d)$ transitions have been calculated; they are 9.367, 1.735 and 0.607 keV, respectively. The strong interaction splits the $1s$ state into $^1S_0$ and $^3S_1$, and the $2p$ state into $^3P_0$, $^3P_2$, $^1P_1$ and $^3P_1$. In principle, these energy levels can be determined by measuring the emitted X-rays in the electromagnetic transitions. It is, however, extremely difficult to measure such small energy splittings (less than 0.5 keV). Therefore, the first experiments [63] delivered only spin-averaged data, since the experimental resolution was not sufficient to separate the transitions to the $^1S_0$ and $^3S_1$ levels. Recent measurements [64] at LEAR yielded the first information on the spin dependence of the $1s$ protonium energy shift and width. Listed in Table 4.1 are the experimental data over a decade, including the most recent results from LEAR.

Theoretical interest in the properties of protonium arose long before the first experiments were performed. Bryan and Phillips [67] first studied the scattering lengths of the $\bar{p}p$ annihilation at rest in their model of $\overline{N}N$ interaction. From the scattering lengths, the energy shifts and widths of $\overline{N}N$ atoms can be derived via Truemans' formula [68]. Later, the energy shift and width of protonium states were investigated by other groups using the either original Truemans' formula [69, 70] or an improved Truemans' approach [71], or a WKB approximation [72] or an iteration technique which, however, neglected the $\overline{n}n$ component [73]. More accurate studies

ΔE_{1s}(keV)	Γ_{1s}(keV)	Refs.
-0.50± 0.30	< 1.0	Ahmad *et al.* (1985) [63]
-0.70± 0.15	1.60± 0.40	Ziegler *et al.* (1988) [63]
-0.75± 0.06	0.90± 0.18	Baker *et al.* (1988) [63]
-0.73± 0.05	1.13± 0.09	Van Eijk *et al.* (1988) [63]
-0.62± 0.10	1.13± 0.17	Bacher *et al.* (1989) [63]
-0.73± 0.02	1.12± 0.06	Heitliner *et al.* (1993) [64]
-0.85± 0.04($^3SD_1$)	0.77± 0.15 ($^3SD_1$)	
-0.440± 0.075 ($^1S_0$)	1.20± 0.25 ($^1S_0$)	M. Augsburger (1999) [65]
-0.785± 0.035 ($^3SD_1$)	0.940± 0.080 ($^3SD_1$)	
ΔE_{2p}(meV)	Γ_{2p}(meV)	Refs.
-	45± 10	Bacher *et al.* (1989) [63]
-	32± 10	Bacher *et al.* (1989) [63]
-	34± 2.9	K. Heitliner *et al.* (1993) [64]
-	30.8± 3.0	M. Augsburger *et al.* (1999) [65]
139 ± 28 ($^3P_0$)	120 ± 25 ($^3P_0$)	D. Gotta *et al.* (1999) [66]
-	38 ± 9 ($^3P_2$, $^1P_1$, $3P_3$)	

Table 4.1: Experimental ΔE_s, Γ_s, ΔE_p and Γ_p for $N\overline{N}$ atoms

of the protonium properties were carried out in the matrix Numerov algorithm [74, 75]. All these theoretical predictions for the energy shifts and widths of protonium states are consistent with available experimental data. In order to quantitatively evaluate the photon and pion emission in the reaction of protonium decay to $\overline{N}N$ deep bound states, Dover *et al.* [76] explictly worked out the wave function of the $\overline{N}N$ $^1S_0$ and $^3S_1$ atomic states in the Numerov approach. In their calculation, the coupling of the $^3D_1$ and $^3S_1$ states is neglected. Using the numerical method developed in Ref. [75], they recalculate, in a later work [77], the wave functions of $\overline{N}N$ atomic states with the tensor coupling included. However, the wave function of $\overline{N}N$ atomic states for non-local $\overline{N}N$ potentials has not yet been evaluated in an

accurate numerical method which takes into account the two length scales involved, the $\overline{p}p$ and $\overline{n}n$ component coupling and the tensor coupling of the nuclear force. In the present work, we solve the Schrödinger equation for $\overline{N}N$ bound states employing a properly adapted numerical method. The method accounts for both the strong *short* range nuclear potential (local and non-local) and the *long* range Coulomb force and provides directly the wave function of the protonium system and of the $\overline{N}N$ deep bound states with complex eigenvalues $E = E_R - i\frac{\Gamma}{2}$. Details of this method can be found below, in section 3.

The protonium states also provide a new tool for meson spectroscopy, which is still an active field exhibiting many open questions. The physics of mesons is far from complete although the quark model has been remarkably successful in understanding and classifying most of the experimentally well-established mesons as $Q\overline{Q}$ bound states. However, in recent years there has been a variety of experiments, for example πN scattering, $\overline{N}N$ annihilation, J/Ψ decay and e^+e^- annihilation, which suggest the existence of new mesons which do not fit into the usual $\overline{Q}Q$ multiplets of flavor $SU(N_f)$. These new meson states might be glueballs ggg, hybrids $Q\overline{Q}g$ or four quark-antiquark $Q^2\overline{Q}^2$ states as well as more "conventional" resonances such as $\overline{N}N$ bound states and meson-meson molecules. Recent reviews, concerning the status of non-$\overline{Q}Q$ states, are found in Ref. [78].

4.2 The Schrödinger Equation for $\overline{N}N$ Atomic States

A correct treatment of $\overline{N}N$ atomic states must include the coupling of the proton-antiproton ($\overline{p}p$) and neutron-antineutron ($\overline{n}n$) configurations. We define the Hilbert spaces of proton-antiproton and neutron-antineutron as P_1 and P_2 spaces, respectively. The Hilbert space of two- and three-meson channels is defined as Q space. The corresponding projection operators P_1, P_2 and Q satisfy the relation:

$$P_1 + P_2 + Q = 1\,, \tag{4.1}$$

$$P_1P_2 = P_2P_1 = 0\,, \tag{4.2}$$

$$P_1Q = QP_1 = 0\,, \tag{4.3}$$

$$P_2Q = QP_2 = 0\,. \tag{4.4}$$

The Hamilton operator of the full coupled-channel problem is given by H with the corresponding wave function $|\psi\rangle$ defined in the complete Hilbert space. Analogous to the procedure of Chapter 3, we eliminate the two- and three-meson channels resulting in the coupled set of equations for the $\bar{p}p$ and $\bar{n}n$ wave function:

$$\begin{aligned}(E - P_1HP_1)\,P_1\,|\,\psi\rangle &= P_1HQ\,G\,QHP_1\,P_1\,|\,\psi\rangle \\ &+ P_1HP_2\,P_2\,|\,\psi\rangle + P_1HQ\,G\,QHP_2\,P_2\,|\,\psi\rangle \qquad (4.5)\end{aligned}$$

$$\begin{aligned}(E - P_2HP_2)\,P_2\,|\,\psi\rangle &= P_2HQ\,G\,QHP_2\,P_2\,|\,\psi\rangle \\ &+ P_2HP_1\,P_1\,|\,\psi\rangle + P_2HQ\,G\,QHP_1\,P_1\,|\,\psi\rangle \qquad (4.6)\end{aligned}$$

where E is the energy eigenvalue and G is the Greens function for two- and three-meson intermediate states, defined as:

$$G = \frac{1}{E - QHQ}. \qquad (4.7)$$

The interaction terms in eq.4.5 and eq.4.6 are given as:

$$P_1HP_1 = H_0^p + V_c + V_{\bar{p}p\to\bar{p}p}\,, \qquad (4.8)$$

$$P_2HP_2 = H_0^n + V_{\bar{n}n\to\bar{n}n}\,, \qquad (4.9)$$

$$P_1HP_2 = P_2HP_1 = V_{\bar{p}p\to\bar{n}n}\,, \qquad (4.10)$$

where

$$V_{\bar{n}n\to\bar{n}n} = V_{\bar{p}p\to\bar{p}p}\,, \qquad (4.11)$$

$$H_0^p = \sqrt{m_p^2 + k^2}\,, \qquad (4.12)$$

$$H_0^n = \sqrt{m_n^2 + k^2}\,, \qquad (4.13)$$

$$V_{\bar{p}p\to\bar{p}p} = \frac{1}{2}\,(V^0 + V^1)\,, \qquad (4.14)$$

$$V_{\bar{p}p\to\bar{n}n} = \frac{1}{2}\,(V^0 - V^1)\,, \qquad (4.15)$$

where V_c is the Coulomb interaction, V^0 and V^1 are the potentials due to meson-exchange for the isospin $I = 0$ and 1 $\overline{N}N$ states, respectively. The mass of the proton and neutron are denoted as m_p and m_n.

$P_iHQGQHP_j$ are the optical potentials W_{ij} for $\overline{N}N$ annihilation into two and three mesons given in the isospin basis as:.

$$\begin{aligned} W_{\bar{p}p\to\bar{p}p} &= P_1HQGQHP_1 \\ &= P_2HQGQHP_2 \\ &= \frac{1}{2}(W^0+W^1), \end{aligned} \tag{4.16}$$

$$\begin{aligned} W_{\bar{p}p\to\bar{n}n} &= P_1HQGQHP_2 \\ &= P_2HQGQHP_1 \\ &= \frac{1}{2}(W^0-W^1), \end{aligned} \tag{4.17}$$

where W^0 and W^1 are the annihilation potentials for isospin $I=0$ and 1 $\overline{N}N$ states in the A2 and A3 model, respectively.

As an example, we give the final equation for spin-triplet $\overline{N}N$ states in the $\{J,L,S\}$ basis as

$$\begin{pmatrix} H_{11} & H_{12} \\ H_{21} & H_{22} \end{pmatrix} \begin{pmatrix} \Psi_{\bar{p}p} \\ \Psi_{\bar{n}n} \end{pmatrix} = E_b \begin{pmatrix} \Psi_{\bar{p}p} \\ \Psi_{\bar{n}n} \end{pmatrix} \tag{4.18}$$

with

$$H_{11} = \begin{pmatrix} P^2/2\mu + V_c^{L_1L_1} + V_{\bar{p}p\to\bar{p}p}^{L_1L_1} + W_{\bar{p}p\to\bar{p}p}^{L_1L_1} & V_{\bar{p}p\to\bar{p}p}^{L_1L_2} + W_{\bar{p}p\to\bar{p}p}^{L_1L_2} \\ V_{\bar{p}p\to\bar{p}p}^{L_2L_1} + W_{\bar{p}p\to\bar{p}p}^{L_2L_1} & P^2/2\mu + V_c^{L_2L_2} + V_{\bar{p}p\to\bar{p}p}^{L_2L_2} + W_{\bar{p}p\to\bar{p}p}^{L_2L_2} \end{pmatrix}$$

$$H_{12} = \begin{pmatrix} V_{\bar{p}p\to\bar{n}n}^{L_1L_1} + W_{\bar{p}p\to\bar{n}n}^{L_1L_1} & V_{\bar{p}p\to\bar{n}n}^{L_1L_2} + W_{\bar{p}p\to\bar{n}n}^{L_1L_2} \\ V_{\bar{p}p\to\bar{n}n}^{L_2L_1} + W_{\bar{p}p\to\bar{n}n}^{L_2L_1} & V_{\bar{p}p\to\bar{n}n}^{L_2L_2} + W_{\bar{p}p\to\bar{n}n}^{L_2L_2} \end{pmatrix}$$

$$H_{21} = \begin{pmatrix} V_{\bar{p}p\to\bar{n}n}^{L_1L_1} + W_{\bar{p}p\to\bar{n}n}^{L_1L_1} & V_{\bar{p}p\to\bar{n}n}^{L_2L_1} + W_{\bar{p}p\to\bar{n}n}^{L_2L_1} \\ V_{\bar{p}p\to\bar{n}n}^{L_1L_2} + W_{\bar{p}p\to\bar{n}n}^{L_1L_2} & V_{\bar{p}p\to\bar{n}n}^{L_2L_2} + W_{\bar{p}p\to\bar{n}n}^{L_2L_2} \end{pmatrix}$$

$$H_{22} = \begin{pmatrix} P^2/2\mu + 2\delta m + V_{\bar{p}p\to\bar{p}p}^{L_1L_1} + W_{\bar{p}p\to\bar{p}p}^{L_1L_1} & V_{\bar{p}p\to\bar{p}p}^{L_1L_2} + W_{\bar{p}p\to\bar{p}p}^{L_1L_2} \\ V_{\bar{p}p\to\bar{p}p}^{L_2L_1} + W_{\bar{p}p\to\bar{p}p}^{L_2L_1} & P^2/2\mu + 2\delta m + V_{\bar{p}p\to\bar{p}p}^{L_2L_2} + W_{\bar{p}p\to\bar{p}p}^{L_2L_2} \end{pmatrix}$$

and

$$\Psi_{\bar{p}p} = \begin{pmatrix} \Psi_{\bar{p}p}^{L_1} \\ \Psi_{\bar{p}p}^{L_2} \end{pmatrix}, \qquad \Psi_{\bar{n}n} = \begin{pmatrix} \Psi_{\bar{n}n}^{L_1} \\ \Psi_{\bar{n}n}^{L_2} \end{pmatrix}, \tag{4.19}$$

where $\delta m = m_n - m_p$, $\mu = m_p/2$, $V_c = -\alpha/r$, $L_1 = J-1$, $L_2 = J+1$, J is the total angular momentum and $E_b = E - 2m_p$, the binding energy of $\overline{N}N$ atomic states.

4.3 Complete set of Sturmian functions

In principle, one could solve Eq. (4.18) through expanding the $\overline{N}N$ wave functions $\Psi_{\bar{p}p}$ and $\Psi_{\bar{n}n}$ in any complete set of orthonormal functions. The complete set of harmonic oscillator wave functions is widely applied to bound state problems since they have analytical forms both in coordinate and momentum spaces. Bound state problems with only the strong interaction or only the Coulomb force can be well solved in the regime of harmonic oscillator wave functions, by choosing the oscillator length being of order 1 fm or 100 fm, respectively. Detailed investigations [79], however, have shown that the harmonic oscillator wave function approach fails to describe $\overline{N}N$ atomic states which are dominated by the long-ranged Coulomb force and influenced by the short-ranged strong interaction. The reason is that two very different oscillator lengths are involved to describe the $\overline{N}N$ deep bound state *and* the atomic state.

The Sturmian function method was first used in atomic physics to evaluate the binding energy and wave function of atoms [80, 81]. It was pointed out that the method is much more powerful than the approach using harmonic oscillator and hydrogen wave functions. Subsequently, the method was applied to various physical problems such as electromagnetic collisions [82], binding energies of nuclei [83, 84] and bound and resonant states in special potentials [85, 86]. The Sturmian functions are very similar to the hydrogen wave functions, and are, therefore, also named Coulomb-Sturmian functions. In coordinate space the Sturmians $S_{nl}(r)$, which are used in the present work, satisfy the second order differential equation [82]

$$\left(\frac{d^2}{dr^2} - \frac{l(l+1)}{r^2} + \frac{2b(n+l+1)}{r} - b^2\right) S_{nl}(r) = 0\,. \tag{4.20}$$

By solving Eq. (4.20), one finds

$$S_{nl}(r) = \left[\frac{n!}{(n+2l+1)!}\right]^{\frac{1}{2}} (2br)^{l+1} exp(-br) L_n^{2l+1}(2br)\,, \tag{4.21}$$

where $L_n^{2l+1}(x)$ are associated Laguerre polynomials defined as

$$L_n^k(x) = (-1)^k \frac{d^k}{dx^k}[L_{n+k}(x)] \tag{4.22}$$

that is

$$L_n^{2l+1}(x) = \sum_{m=0}^{n} (-1)^m \frac{(n+2l+1)!}{(n-m)!(2l+1+m)!m!} x^m \tag{4.23}$$

The Sturmians are orthogonal and form a complete set with respect to the weight function $1/r$, which follows from the corresponding $1/r$ potential term in Eq. (4.20),

$$\int_0^\infty r^2 dr \frac{S_{nl}(r)}{r} \frac{1}{r} \frac{S_{n'l}(r)}{r} = \delta_{nn'} . \tag{4.24}$$

Thus radial functions $R_l(r)$ can be expanded in the complete set of the Sturmian functions $S_{nl}(r)$,

$$R_l(r) = \sum_n a_{nl} \frac{S_{nl}(r)}{r} . \tag{4.25}$$

The Sturmian functions can be defined in momentum space as

$$\begin{aligned} S_{nlm}(\vec{p}) &\equiv S_{nl}(p) Y_{lm}(\theta_p, \phi_p) \\ &= \frac{1}{(2\pi)^{3/2}} \int dr\, d\Omega\, S_{nl}(r) Y_{lm}(\theta, \phi) e^{-i\vec{p}\cdot\vec{r}} \end{aligned} \tag{4.26}$$

One can derive the momentum form analytically

$$\begin{aligned} S_{nl}(p) &= \left[\frac{2^{4l+3}(n+l+1)\, n!\, (l!)^2}{b\,(n+2l+1)!}\right]^{1/2} \\ &\cdot \frac{(p/b)^l}{[(p/b)^2+1]^{l+1}} C_n^{l+1}\left(\frac{(p/b)^2-1}{(p/b)^2+1}\right) \end{aligned} \tag{4.27}$$

where $C_t^s(x)$ are the Gegenbauer polynomials. It is very convenient to have such a complete set to study interactions in momentum space.

Inserting Eq. (4.25) into Eq. (4.18) does not lead to a diagonal form on the right hand side of Eq. (4.18) unlike the case of the harmonic oscillator wave functions. The matrices on both sides of Eq. (4.18) must be simultaneously diagonalized. Note that the Sturmians have analytical form [82] in momentum space. One is allowed to deal with strong interactions in momentum space with the complete set

of the Sturmians as easily as with the set of the harmonic oscillator wave functions. The matrix elements of the Coulomb interaction as well as the kinetic term can be evaluated analytically according to Eq. (4.20) and Eq. (4.24).

Because almost all bound-state hydrogentic wave functions are close to zero energy, the innermost zeros of the functions are insensitive to the principle quantum number. This accounts for that the bound hydrogen functions do not form a complete set; the continuum is needed to analyze the region between the origin and the limiting first zero. Unlike hydrogen functions, the first node of the Sturmian functions continues to move closer to the origin with increasing the principle number n. This is the key point why a short-ranged nuclear force can easily be taken into account for $\overline{N}N$ atomic state problem by using complete sets of the Sturmian functions.

The parameter b is the length scale entering the Sturmian functions in eqs. (4.20) and (4.21), in the same way as the corresponding parameter enters the harmonic oscillator functions. For $\overline{N}N$ deep bound states one should use $1/b$ of order 1 fm while the atomic states without strong interactions require $1/b$ of order 10^2 fm. However, for protonium accounting for both the strong interaction and the Coulomb force, one must use a $1/b$ between the two values used for the above cases. Using a complete basis of, for example, 200 Sturmian functions (100 for the $L = J - 1$ wave, and another 100 for the $L = J + 1$) with $1/b = 5 - 500$ fm, one can precisely reproduce the analytical $1s$ and $2p$ wave functions of the $\overline{N}N$ system subject to only the Coulomb interaction. Using the same basis with $1/b = 0.1 - 30$ fm, the wave functions of $\overline{N}N$ deep bound states can be precisely evaluated. The $\overline{N}N$ deep bound states can be evaluated in the complete set of the harmonic oscillator wave functions, and also in the complete set of Sturmian functions with a more suitable length parameter, for example $1/b = 1$ fm. From the above investigation, a length parameter $1/b$ around 20 fm is suitable for the protonium problem.

We have compared our numerical method with the traditionally used method, namely the Numerov approach [75], applied to the $\overline{N}N$ atomic problem in for example the Kohno-Weise potential. The binding energies and widths presented in Ref. [75] for the states $^1S_0$, $^3P_0$, $^3S_1$ and $^3SD_1$ are well reproduced in the Sturmian function approach. Wave functions for these states are also compared in the two

approaches. It is found that at short distance the outputs in the two approaches are quite consistent, and that the discrepancies between the wave functions evaluated in the two methods become more and more obvious as the relative distance between nucleon and antinucleon increases, especially the imaginary part of the $^1S_0$ and $^3S_1$ wave functions.

Finally, it should be pointed out that the Numerov method can not be applied to a non-local potential, for example the Bonn potential which is given in momentum space, and it is not easy to handle atomic states with higher angular momentum [87], for example the state $^3PF_2$. Therefore it is essential to use a precise numerical method, applied not only to local but also to non-local potentials, to handle the $\overline{N}N$ atomic state problem from a more general point of view. In principle, there is no limit to the accuracy in the evaluation of the $\overline{N}N$ atomic states in the Sturmian function approach. One is allowed to use larger and larger complete bases of the Sturmian functions until the theoretical results converge.[1] And the $\overline{N}N$ atomic states with higher angular momenta can be easily handled in the approach.

4.4 Energy Shifts and Widths of $\overline{N}N$ Atomic States

Eq.4.18 is solved numerically by expanding $\Psi_{\bar{p}p}$ and $\Psi_{\bar{n}n}$ in a complete set of Sturmian functions. Theoretical predictions for energy shifts and widths of $\overline{N}N$ atomic states are presented in Table 4.2 for two models:

Model A: The elastic part is taken from the Paris potential[27, 28, 29] with a short range regularization according to

$$V_{\overline{N}N}(r) = \begin{cases} \sum_i G_i V^i_{NN}(r) & r > r_0 \\ \\ \sum_i G_i V^i_{NN}(r_0) & r \leq r_0 \end{cases} \tag{4.28}$$

The annihilation part is the optical potential due to the A2 and A3 quark models.

Model B: Here we apply the energy dependent meson-exchange potential OBEPT (one-boson exchange energy-dependent potential)[26] of the Bonn group with the

[1] There is no CPU problem, most university computers are capable enough.

modified nucleon-meson coupling constants $g_\omega^2/4\pi = 10$ and $g_\sigma^2/4\pi = 5$ (see Ref. [79] for a detailed discussion). No short range regularization is applied, in consistency with the claim of the Bonn group that meson exchange should be taken seriously even for small separation distance of the $\overline{N}N$ system. The annihilation part is described by the microscopic A2 and A3 models. The short range cut-off r_0 in Model A and the effective strength parameters λ_{A2} and λ_{A3} for the processes of nucleon-antinucleon annihilation into two and three mesons are fitted to the $\overline{N}N$ scattering cross sections[47]. The cutoff r_0 is chosen as $r_0 = 0.8$ fm, which closes to the annihilation radius as deduced from the convolution of the baryon number distribution in the $\overline{N}N$ system[88].

It is found that Model A yields the correct width Γ_{1s} with a somewhat small value for the energy shift ΔE_{1s}. Model B fares better in obtaining a reasonable value for ΔE_{1s}, however underestimates the corresponding width.

	Model A		Model B		Date [65]	
	$^1S_0$	$^3S_1 - ^3D_1$	$^1S_0$	$^3S_1 - ^3D_1$	$^1S_0$	$^3S_1 - ^3D_1$
ΔE_{1s}(keV)	0.37	-0.70	-0.38	-0.60	-0.440± 0.075	-0.785± 0.035
Γ_{1s}(keV)	0.47	1.38	0.21	0.49	1.20± 0.25	0.940± 0.080

Table 4.2: The energy shifts and widths of 1s $\overline{N}N$ atomic states.

In model A, the energy shifts ΔE_{1s} mainly stem from the π-exchange potential. The π-contribution of the meson-exchange potential evaluated for a pure $\bar{p}p$ state gives[23]

$$^1S_0 \qquad V(r) = -3\,V_\sigma(r) \tag{4.29}$$

$$^3S_1 \qquad V(r) = V_\sigma(r) \tag{4.30}$$

$$^3D_1 \qquad V(r) = V_\sigma(r) - 2\,V_T(r) \tag{4.31}$$

where the positive quantities $V_\sigma(r)$ and $V_T(r)$ are the spin-spin and tensor components of the π-exchange potential. For the evaluation we used

$$|\,\bar{p}p\,\rangle = -\frac{1}{\sqrt{2}}\,(\,|\,\overline{N}N(I=0)\,\rangle + |\,\overline{N}N(I=1)\,\rangle\,). \tag{4.32}$$

Based on the previous equations, we can qualitatively predict the signs of the energy shifts of the various 1s states. The $^1S_0$ protonium state will shift down with respect to the pure Coulomb state, while the pure $^3S_1$ state is shifted upward. Including tensor force mixing the $^3SD_1$ state will move down a little compared to the pure $^3S_1$ state. Above arguments are in agreement with the results of model A:

$$\Delta E(^1S_0) = 0.37 \ keV \tag{4.33}$$

$$\Delta E(^3S_1) = -0.96 \ keV \tag{4.34}$$

$$\Delta E(^3S_1 - ^3D_1) = -0.70 \ keV \tag{4.35}$$

A more complete analysis of level shifts in the protonium states based on the use of the Paris potential (as our model A) is in line with our arguments that the π-exchange is the dominant component. In the case of model B (using the Bonn potential) where the energy shift $\Delta E(^1S_0)$ is negative, hence we have a repulsive effect, no such simple analysis can be made.

For comparison, we present here also the theoretical results of the energy shift and width of the $\overline{N}N$ atomic states in the potential Paris98[89]. It is clear that the predictions of Paris98 are much more reasonable than our models A and B. Paris98 is a phenomelogical $\overline{N}N$ potential, it fits to the existent $\overline{N}N$ data the best. Paris98 was worked out in 1997, based on the Paris NN potential and the Paris94 $\overline{N}N$ potential[90].

	$^1S_0$		$^3SD_1$		$^3P_0$	
	ΔE(eV)	Γ(eV)	ΔE(eV)	Γ(eV)	ΔE(meV)	Γ(meV)
Paris98	-766	484	-680	663	62	114
Data[65, 66]	-440± 75	1200± 250	-785± 35	940± 80	139 ± 28	120 ± 25

4.5 Summary and Discussions

In this work we have evaluated $\overline{N}N$ atomic bound states as based on a microscopically derived $\overline{N}N$ interaction in the Sturmian function method. The medium and

long ranged elastic part of the $\overline{N}N$ interaction resulted from meson-exchange, obtained by G-parity transformation of a realistic meson-exchange NN potential. To reflect the uncertainties in the meson-exchange part, we applied different versions as given by the Bonn and Paris groups. In describing the short ranged annihilation part of the $\overline{N}N$ interaction, we used a nonrelativistic quark model, which naturally takes into account the multitude of mesonic annihilation channels, while at the same time possessing only a small number of fit parameters, i.e. the corresponding strength parameters of the respective two- and three-meson transitions. Here we used a quark model, where the annihilation mechanism is determined by planar quark line diagrams (denoted as A2 and A3), while the respective $Q\overline{Q}$ interaction is described by the nonperturbative $^3P_0$ dynamics. The basis for the use of this particular model is founded in the analysis of two- and three-meson production data for $\overline{N}N$ annihilation at rest and in flight. A phenomenological approach has been adopted, in which the dominant annihilation topology (rearrangement versus creation/destruction of $Q\overline{Q}$ pairs) and the spin-flavor dependence of the effective $Q\overline{Q}$ creation/destruction operator ($^3P_0$ versus one gluon $^3S_1$, color $\{8\}$ vertex) has been determined. $\overline{N}N$ annihilation leads to a rich ensemble of final states, whose relative branching ratios provide constraints on dynamical models. The observed branching ratios display a significant dependence on L, the relative orbital angular momentum of the $\overline{N}N$ system, indicating a dynamical content which goes beyond simple statistical models. These Dynamical Selection Rules (DSR) provide key signatures for the underlying annihilation mechanism. Different annihilation topologies linked with a specific $Q\overline{Q}$ operators lead to distinct predictions of DSR in the various models. Comparison with experiment then allows to rule out certain models. The phenomenological analysis indicates that the A2 and A3 models are the dominant processes in $\overline{N}N$ annihilation into mesons. The nonlocal, state- and energy-dependent potential arising from the A2 and A3 transition processes consists of an imaginary part, describing the annihilation flux into mesonic final states, and a dispersive real part, which in general is attractive. In setting up the absolute contribution of the short ranged annihilation potential, as determined by the respective two- and three-meson transition strength constants λ_{A2} and λ_{A3}, we fitted these parameters to the experimental $\overline{N}N$ scattering cross sections. Thus, all the predictions for the $\overline{N}N$ atomic bound

state sector are parameter free.

$\overline{N}N$ atoms are states where the Coulomb interaction between proton and antiproton is the dominant component. The presence of the strong interaction, inducing dramatic short-ranged distortions in the pure $\bar{p}p$ wave function, leads to a shift in the energy levels and an additional width due to annihilation. The theoretical predictions for the spin-averaged binding energies and widths of $\overline{N}N$ atomic states are agreeable with the experimental data, where at this level no definite preference for a particular model can be made. When considering more detailed obseevables, such as the binding energy of the $^1S_0$ atomic $\overline{N}N$ state, differences are sizable, which can be traced to the different versions of the meson-exchange potential (Paris versus Bonn) used. From the predictions for the width of the $^1S_0$ atomic state we find that the contribution from the A2 and A3 processes to the imaginary part of the optical potential in this particular partial wave is somewhat too small. To elucidate this point in more detail one should look at particular two-meson production branching ratios in $\overline{N}N$ annihilation from the atom, where specific isospin components of the atomic wave function can be explicitly tested.

The Sturmian function approach is first introduced to evaluate the $\overline{N}N$ atomic states in this work. The method is much more powerful, accurate and much easier to use than all other methods in history. It can be applied to solve the $\overline{N}N$ bound state problem for local and non-local potentials, accounting for both the strong short range nuclear interaction and the long range Coulomb force and provides directly the wave function of protonium and $\overline{N}N$ deep bound states with complex eigenvalues.

Chapter 5

Electron-Position annihilation into Nucleon-Antinucleon Pairs

Experimental data on the reaction $e^+e^- \to \bar{n}n$ from the FENICE collaboration [91] and the earlier data on the reaction $e^+e^- \to \bar{p}p$ [92] and also the data on the time-reversed reaction $\bar{p}p \to e^+e^-$ [93] indicate in Fig. 5.1 that $\sigma(e^+e^- \to \bar{n}n)/\sigma(e^+e^- \to \bar{p}p) > 1$ at energies around the threshold $E_{cm} \sim 2$ GeV. Averaging over the available data on both the direct and time-reversed reactions, one finds

$$\frac{\sigma(e^+e^- \to \bar{p}p)}{\sigma(e^+e^- \to \bar{n}n)} = 0.66^{+0.16}_{-0.11}. \tag{5.1}$$

That the ratio is less than one is quite puzzling.

In a naive perturbative description of e^+e^- annihilation into baryons the virtual time-like photon first decays into a $\bar{q}q$ pair, then the $\bar{q}q$ pair is dressed by two additional quark-antiquark pairs excited out of the vacuum to form a baryon pairs. The dressing process does not distinguish between u and d quarks at high momentum transfers in the description of perturbative QCD since gluon couplings are flavor blind. In the conventional perturbative picture, theorefore, the only difference between the proton and neutron productions comes from the different electric charges of the primary $\bar{q}q$ pairs. One expects to get

$$\frac{\sigma(e^+e^- \to \bar{p}p)}{\sigma(e^+e^- \to \bar{n}n)} > 1 \tag{5.2}$$

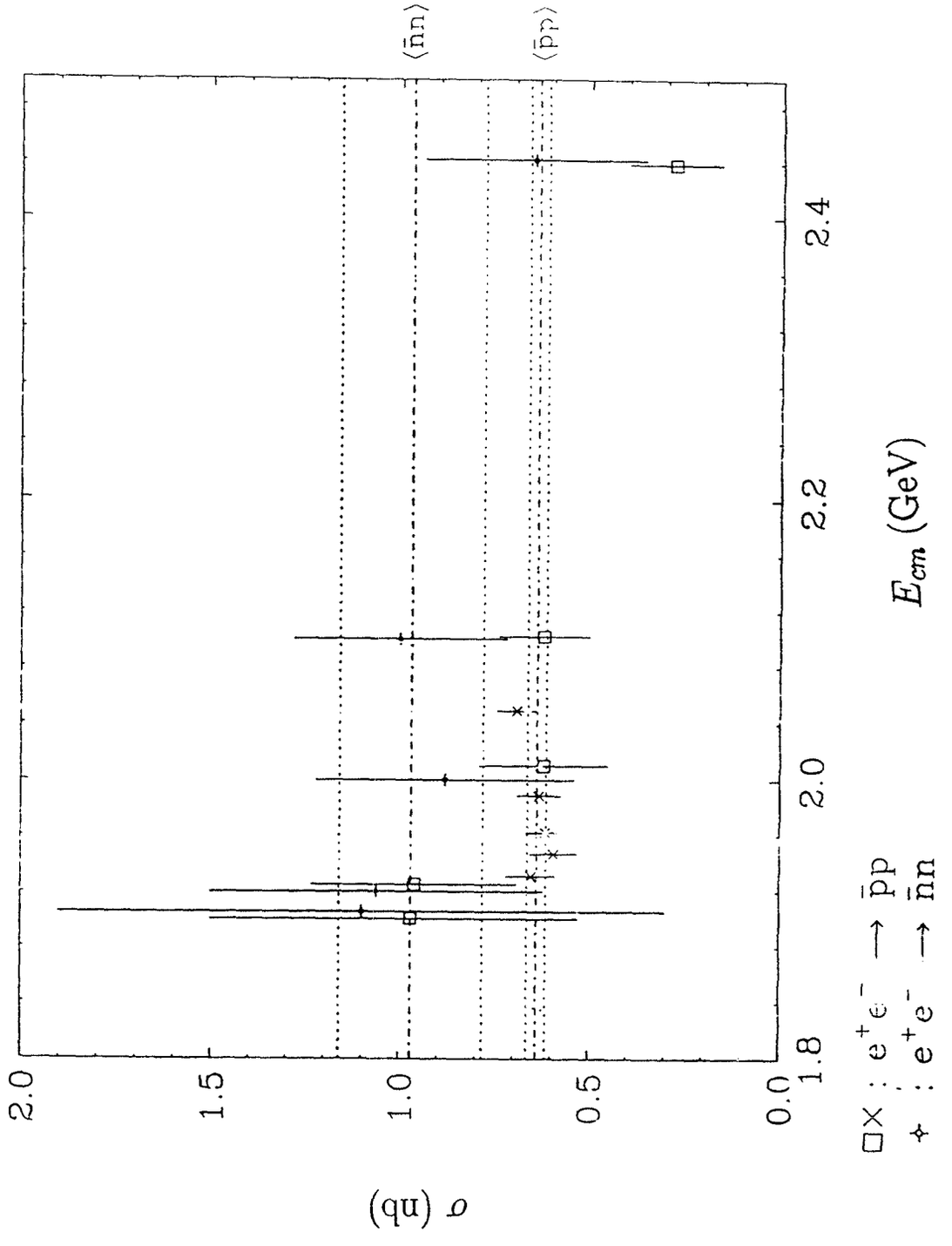

Fig. 5.1 Measured total cross sections of the reaction $e^+e^- \rightarrow \overline{N}N$. $\langle \overline{n}n \rangle$ and $\langle \overline{p}p \rangle$ stand for the averaged data over the available energies at threshold.

at large momentum transfers if it is true that the u contribution dominates in the proton and the d in the neutron.

The total perturbative cross section σ_{pt} in the center-of-mass system is obtained by superposing the amplitudes with different flavor quarks in the primary $\bar{q}q$ pair and squaring,

$$\sigma(e^+e^- \to \overline{N}N) \propto \left| \sum_{q \in N} Q_q A_q^N(s) \right|^2 \tag{5.3}$$

where Q_q is the charge of quarks and $A_a^N(s)$ denotes the amplitude at $s = E_{CM}^2$ for making the baryon N with a given primary flavor quark q. These amplitudes are determined by the baryon wave functions. In the simplest case that

$$A_u^p = A_u^n = A_d^p = A_d^n, \tag{5.4}$$

one gets

$$\frac{\sigma(e^+e^- \to \bar{p}p)}{\sigma(e^+e^- \to \bar{n}n)} = 1.5 \tag{5.5}$$

In this work we study the reactions in a nonperturbative quark model, considering both one-step process (the primary $\bar{q}q$ pair is produced by the virtual photon and dressed by two additional quark-antiquark pairs to form a baryon pair) and two-step process (the primary $\bar{q}q$ pair forms first a meson, then the the meson decays into a baryon pair). Here below we first work out the wave functions of the final state nucleon and antinucleon and the intermediate mesons. Those wave functions are essential for our calculations.

5.1 Nucleon and Meson Wave Functions

In the quark model, a baryon is composed of three quarks, with total wave function antisymmetric. Since baryons must be colorless, the total wave functions should take the form

$\Phi =$ 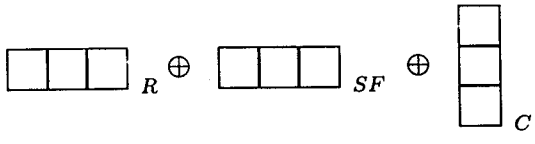 $_R \oplus$ $_{SF} \oplus$ $_C$

The spin-flavor part:

$$\Psi^{(SF)}_{S_z T_z} = \frac{1}{\sqrt{2}} \sum_{J_{23}=0,1} \left| \left(\frac{1}{2}^{(2)} \otimes \frac{1}{2}^{(3)} \right)_{J_{23}} \otimes \frac{1}{2}^{(1)} \right\rangle^{\text{Spin}}_{1/2,S_z} \cdot \left| \left(\frac{1}{2}^{(2)} \otimes \frac{1}{2}^{(3)} \right)_{J_{23}} \otimes \frac{1}{2}^{(1)} \right\rangle^{\text{Flavor}}_{1/2,T_z} \tag{5.6}$$

The spatial wave function in momentum space:

$$\Psi(\vec{p}_1,\vec{p}_2,\vec{p}_3) = N_B \exp\left[-\frac{1}{2} a^2 \left(\frac{\vec{p}_2 - \vec{p}_3}{\sqrt{2}} \right)^2 \right] \cdot \exp\left[-\frac{1}{2} a^2 \left(\frac{\vec{p}_2 + \vec{p}_3 - 2\vec{p}_1}{\sqrt{6}} \right)^2 \right] \tag{5.7}$$

for the harmonics oscillator interaction

$$V(r) = \frac{1}{2} \mu \omega^2 r^2 \tag{5.8}$$

where $N_B = 3^{4/3} a^3/\pi^{3/2}$ with $a = 1/(\sqrt{6}\mu\omega)$.

The initial proton-antiproton wave function:

$$\begin{aligned}
&\Psi_{S,S_z;T,T_z}(\vec{k}_1,\vec{k}_2;\vec{p}_1,\vec{p}_2,\vec{p}_3;\vec{p}_4,\vec{p}_5,\vec{p}_6) \\
&= \frac{N_B^2}{2} \delta(\vec{k}_1 - \vec{p}_1 - \vec{p}_2 - \vec{p}_3) \delta(\vec{k}_2 - \vec{p}_4 - \vec{p}_5 - \vec{p}_6) \\
&\exp\left[-\frac{1}{2} a^2 \left(\frac{\vec{p}_2 - \vec{p}_3}{\sqrt{2}} \right)^2 \right] \exp\left[-\frac{1}{2} a^2 \left(\frac{\vec{p}_2 + \vec{p}_3 - 2\vec{p}_1}{\sqrt{6}} \right)^2 \right] \\
&\exp\left[-\frac{1}{2} a^2 \left(\frac{\vec{p}_5 - \vec{p}_6}{\sqrt{2}} \right)^2 \right] \exp\left[-\frac{1}{2} a^2 \left(\frac{\vec{p}_5 + \vec{p}_6 - 2\vec{p}_4}{\sqrt{6}} \right)^2 \right] \\
&\sum_{J_{34},J_{56}} \left| \left[\left[\left(\frac{1}{2}^{(2)} \otimes \frac{1}{2}^{(3)} \right)_{J_{23}} \otimes \frac{1}{2}^{(1)} \right]_{1/2} \otimes \left[\left(\frac{1}{2}^{(5)} \otimes \frac{1}{2}^{(6)} \right)_{J_{56}} \otimes \frac{1}{2}^{(4)} \right]_{1/2} \right\rangle^{\text{Spin}}_{SS_z} \right. \\
&\left. \left| \left[\left[\left(\frac{1}{2}^{(2)} \otimes \frac{1}{2}^{(3)} \right)_{J_{23}} \otimes \frac{1}{2}^{(1)} \right]_{1/2} \otimes \left[\left(\frac{1}{2}^{(5)} \otimes \frac{1}{2}^{(6)} \right)_{J_{56}} \otimes \frac{1}{2}^{(4)} \right]_{1/2} \right\rangle^{\text{Flavor}}_{TT_z} \right.
\end{aligned}$$

In the quark-antiquark interaction of harmonic oscillator type, the momentum space wave functions for $3S$ and $2D$ vector mesons are as follows:

$$\Phi_s(\vec{p}) = N_s \exp\left(-\frac{1}{2} b^2 p^2 \right) \left(\frac{15}{4} - 5b^2p^2 + b^4p^2 \right) \left[\frac{1}{2}^{(1)} \otimes \frac{1}{2}^{(2)} \right]_1$$

$$\Phi_p(\vec{p}) = N_d \exp\left(-\frac{1}{2}b^2p^2\right)(bp)^2\left(\frac{7}{2}-b^2p^2\right)\left[\left(\frac{1}{2}^{(1)}\otimes\frac{1}{2}^{(2)}\right)_1\otimes Y_2(\hat{p})\right]_1 \quad (5.10)$$

where $\vec{p}$ is the relative momentum with $\vec{p}=\frac{1}{2}(\vec{p}_1-\vec{p}_2)$,
and $N_s=\left(\frac{2b^3}{15\pi^{3/2}}\right)^{1/2}$, $N_d=\left(\frac{32b^3}{105\pi^{1/2}}\right)^{1/2}$

5.2 Two-Step Process Dominant

The effective strength parameter λ in the $^3P_0$ vertex

$$V_{ij} = \lambda\sum_{\mu}(-1)^{1+\mu}\langle 0,0|^S_{ij}\langle 0,0|^F_{ij}\sigma^{-\mu}_{ij}\,1^F_{ij}\,Y_{1\mu}(\vec{p}_i-\vec{p}_j)\,\delta(\vec{p}_i+\vec{p}_j) \quad (5.11)$$

may vary largely from one reaction to another since it accounts for various effects in a reaction. In our case the λ in the one-step process might be very much differ from that in the two-step process. Therefore, to investigate whether the one-step process or the two-step process is dominant, we will carry out the following studies step by step: (1) determine the length parameter b for the ρ meson by the reaction of $\rho\rightarrow e^+e^-$; (2) determine the effective strength parameter λ in the $^3P_0$ vertex for the process $\rho\rightarrow\pi^+\pi^-$; (3) study the reaction $e^+e^-\rightarrow\pi^+\pi^-$.

5.2.1 The Length Parameter b

We study here the electromagnetic decay process $\rho\rightarrow e^+e^-$, shown in Fig. 5.2.

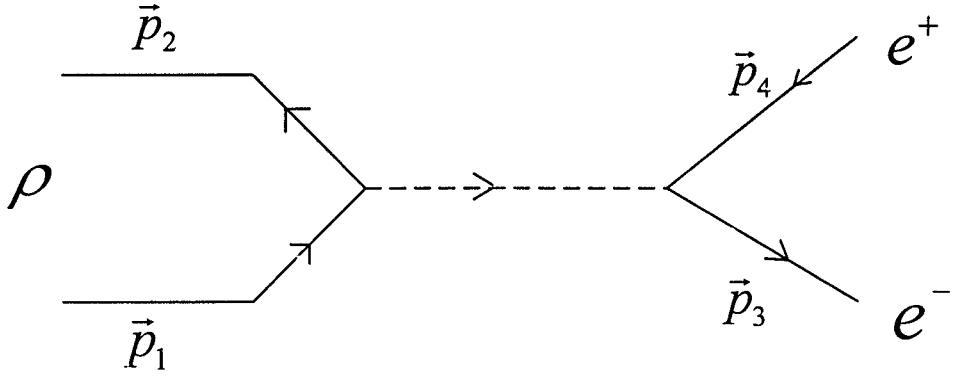

Fig. 5.2 The vector meson ρ decays into an electron-position pair.

The transition amplitude of the process may be written in general

$$M = \langle e^+e^-|T|q\bar{q}\rangle\langle q\bar{q}|V\rangle \tag{5.12}$$

where $|V\rangle$ is the wave function of a vector meson, and $\langle e^+e^-|T|q\bar{q}\rangle$ the transition amplitude of the quark-antiquark to electron-position. We have

$$|V\rangle = \psi_{spatial}\psi_{color}\psi_{flavor}\psi_{spin} \tag{5.13}$$

with

$$\psi_{color} = \frac{1}{\sqrt{3}}|q\rangle_\beta|\bar{q}\rangle_\beta \tag{5.14}$$

$$\psi_{flavor} = \left[\frac{1}{2}^{(1)} \otimes \frac{1}{2}^{(2)}\right]_{II_z} \tag{5.15}$$

$$\psi_{spin} = \left[\frac{1}{2}^{(1)} \otimes \frac{1}{2}^{(2)}\right]_{SS_z} \tag{5.16}$$

and the spatial part $\psi_{spatial}$ depending on the momenta $\vec{p}_1$ and $\vec{p}_2$ only. S and I are respectively the spin and isospin of the vector meson. In the center-of-mass system, that is, $\vec{p}_1 + \vec{p}_2 = 0$ and $\vec{p} = (\vec{p}_1 + \vec{p}_2)/2$, we have $\psi_{spatial} \equiv \psi(\vec{p})$, obeying the following relations:

$$\begin{aligned}
\phi(\vec{x}) &= \int \frac{d^3p}{(2\pi)^{3/2}} e^{i\vec{p}\cdot\vec{x}}\psi(\vec{p}) \\
\psi(\vec{p}) &= \int \frac{d^3x}{(2\pi)^{3/2}} e^{-i\vec{p}\cdot\vec{x}}\phi(\vec{x}) \\
\int d^3x|\phi(\vec{x})|^2 &= \int d^3p|\phi(\vec{p})|^2 = 1
\end{aligned} \tag{5.17}$$

The matrix elements of $\langle q\bar{q}|V\rangle$ are derived as follows:

$$\begin{aligned}
\langle q\bar{q}|V\rangle_{colcr} &= \langle q|_\alpha\langle\bar{q}|_\alpha\frac{1}{\sqrt{3}}|q\rangle_\beta|\bar{q}\rangle_\beta = \frac{1}{\sqrt{3}} \\
\langle q\bar{q}|V\rangle_{flavor} &= \left[\left\langle\frac{1}{2}t_q\right|\left\langle\frac{1}{2}t_{\bar{q}}\right|\right]\left|\frac{1}{2}^{(1)} \otimes \frac{1}{2}^{(2)}\right\rangle_{II_z} = C\left(\frac{1}{2}\frac{1}{2}I; t_q t_{\bar{q}} I_z\right) \\
\langle q\bar{q}|V\rangle_{spin} &= \left[\left\langle\frac{1}{2}t_q\right|\left\langle\frac{1}{2}t_{\bar{q}}\right|\right]\left|\frac{1}{2}^{(1)} \otimes \frac{1}{2}^{(2)}\right\rangle_{SS_z} = C\left(\frac{1}{2}\frac{1}{2}S; m_q m_{\bar{q}} S_z\right)
\end{aligned} \tag{5.18}$$

where $C(j_1, j_2 J, m_1, m_2 m)$ are the Clebsch-Gordon coefficients, and t_q ($t_{\bar{q}}$) and m_q ($m_{\bar{q}}$) are respectively the isospin and spin projections of quark (antiquark).

The transition amplitude for the process $q\bar{q} \to e^+e^-$ could be evaluated in the standard method developed in the electrodynamics. We have

$$\begin{aligned} T_{q\bar{q}\to e^+e^-} &\equiv \langle e^+e^-|T|q\bar{q}\rangle \\ &= e_q e(2\pi)^4\delta^{(4)}(p_1+p_2-p_3-p_4)\frac{1}{(2\pi)^6}\left(\frac{1}{8E_qE_{\bar{q}}E_{e^-}E_{e^+}}\right)^{1/2} \\ &\quad \bar{u}_e(p_3, m_{e^-})\gamma^\mu v_e(p_4, m_{e^+})\frac{-1}{s}\bar{v}_q(p_2, m_{\bar{q}})\gamma_\mu u_q(p_1, m_q) \end{aligned} \tag{5.19}$$

where $s = (p_1+p_2)^2$, and e_q is the charge of quark. The transition amplitude for the decay process $V \to e^+e^-$ is thus derived as

$$\begin{aligned} M &= \sum_i \sum_{m_q m_{\bar{q}}} \sum_{t_q t_{\bar{q}}} \int d^3p_1 d^3p_2\, \delta^{(3)}(\vec{p}_1+\vec{p}_2)\psi(\vec{p}_1,\vec{p}_2) \\ &\quad \frac{1}{\sqrt{3}} C\left(\frac{1}{2}\frac{1}{2} I; t_q t_{\bar{q}} I_z\right) C\left(\frac{1}{2}\frac{1}{2} S; m_q m_{\bar{q}} S_z\right) T_{q\bar{q}\to e^+e^-} \end{aligned} \tag{5.20}$$

where the sum over i is to take into account all the possible quark colors, and the delta function $\delta^{(3)}(\vec{p}_1+\vec{p}_2)$ implies that we work in the rest-meson frame.

The decay width of the process $V \to e^+e^-$ is defined as

$$\Gamma = \int d^3p_3 d^3p_4 \Delta\Gamma \tag{5.21}$$

with

$$\Delta\Gamma = (2\pi)^4\delta^{(3)}(\vec{p}_3+\vec{p}_4)\delta(E_1+E_2-E_3+E_4)\left(\frac{1}{8E_qE_{\bar{q}}E_{e^-}E_{e^+}}\right)\frac{1}{(2\pi)^6}|M|^2 \tag{5.22}$$

Due to the delta functions $(\vec{p}_3+\vec{p}_4)\delta(E_1+E_2-E_3+E_4)$, one can easily carry out the integrations and obtain

$$\Gamma = \frac{1}{(2\pi)^2}\frac{p_f}{M_V^3}\int d\Omega |T|^2 \tag{5.23}$$

where p_f is the momentum of the final electron, M_V the mass of the initial meson, and the integration is over the angles of the final electron.

In the small quark momentum $\vec{p}$ approximation, one gets

$$\Gamma = \frac{16\pi\alpha^2 Q^2}{M_v^2}|\phi(0)|^2 \tag{5.24}$$

where Q^2 is the squared sum of the charges of the quarks in the meson, $\phi(0)$ is the amplitude of the meson wave function at origin in the coordinate space. $Q^2 = 1/2$ for ρ, $1/18$ for ω and $1/9$ for ϕ.

In the harmonic oscillator interaction, the spatial part of the wave functions of the lightest mesons (like π, ρ, ω and ϕ) takes the form

$$\phi(r) = \frac{1}{(b^2\pi)^{3/4}} e^{-b^2 r^2/2} \tag{5.25}$$

hence

$$\phi(0) = \frac{1}{(b^2\pi)^{3/4}} \tag{5.26}$$

Substitute the $\phi(0)$ with the Q^2 for ρ together into eq. (5.24), we get the final result for the decay width of the process $\rho \to e^+e^-$

$$\Gamma_{\rho\to e^+e^-} = \frac{8\alpha^2}{\sqrt{\pi} b^3 M_\rho^2} \tag{5.27}$$

Input $M_\rho = 0.77$ GeV, $\alpha = 1/137$ and the experimental value 6.85 keV for the $\Gamma_{\rho\to e^+e^-}$, we get

$$b \approx 4.0 \text{ GeV}^{-1} \tag{5.28}$$

Now we have the length parameter b.

5.2.2 $\rho \to \pi^+\pi^-$ Process

We study here the reaction $\rho \to \pi^+\pi^-$ shown in Fig. 5.3 in order to determine the effective strength parameter λ in the $^3P_0$ vertex

$$V_{ij} = \lambda \sum_\mu (-1)^{1+\mu} \langle 0,0|^S_{ij} \langle 0,0|^F_{ij} \sigma^{-\mu}_{ij} \mathbf{1}^F_{ij} Y_{1\mu}(\vec{p}_i - \vec{p}_j)\delta(\vec{p}_i + \vec{p}_j) \tag{5.29}$$

The transition amplitude of the reaction of one meson decay into two meson in the $^3P_0$ model is defined as

$$T = \langle f|V_{45}|i\rangle \tag{5.30}$$

where $|i\rangle$ and $|f\rangle$ are respectively the initial and final states. For simplicity, we consider here only the S-wave mesons, that is, all the mesons involved have orbital angular momentum equal to 0. The initial state is simply the one meson wave function, taking the form

$$|i\rangle = N \exp\left(-\frac{1}{8} b^2(\vec{p}_1 - \vec{p}_2)^2\right) \left[\frac{1}{2}^{(1)} \otimes \frac{1}{2}^{(2)}\right]_{s_i,m_i} \left[\frac{1}{2}^{(1)} \otimes \frac{1}{2}^{(2)}\right]_{t_i,mt} \tag{5.31}$$

We have the spin $s_i = 1$ and the isospin $t_i = 1$ for the ρ mesom, and the isospin projection $t_z = 0$ for ρ^0. Here we have employed the harmonic oscillator interaction between quark and antiquark.

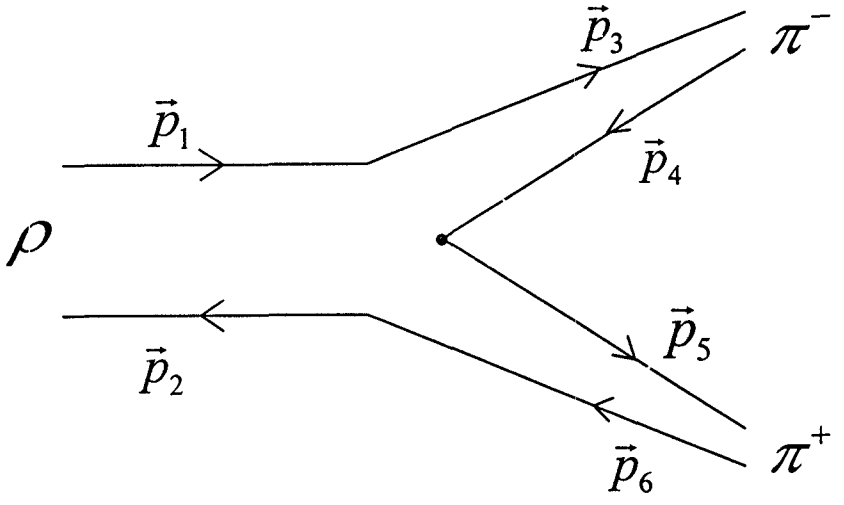

Fig. 5.3 The vector meson ρ decays into $\pi^+\pi^-$ in the $^3P_0$ quark model.

We must couple the wave functions of the two final mesons to form the final state $|f\rangle$. For two S-wave mesons we have

$$\begin{aligned}|f\rangle &= N_1 N_2 \exp\left(-\frac{1}{8}b^2(\vec{p}_3-\vec{p}_4)^2\right)\exp\left(-\frac{1}{8}b^2(\vec{p}_5-\vec{p}_6)^2\right)\\ &\cdot\left[\left[\frac{1}{2}^{(3)}\otimes\frac{1}{2}^{(4)}\right]_{s_1,m_1}\otimes\left[\frac{1}{2}^{(5)}\otimes\frac{1}{2}^{(6)}\right]_{s_2,m_2}\right]_{s_f,m_f}\\ &\cdot\left[\left[\frac{1}{2}^{(3)}\otimes\frac{1}{2}^{(4)}\right]_{t_1,mt_1'}\otimes\left[\frac{1}{2}^{(5)}\otimes\frac{1}{2}^{(6)}\right]_{t_2,mt_2'}\right]_{t_f,mt'}\end{aligned} \tag{5.32}$$

The transition amplitude may be expressed in the form

$$T = T_{color}T_{flavor}T_{spin}T_{spatial} \tag{5.33}$$

with

$$\begin{aligned}T_{color} &= \frac{1}{\sqrt{3}}\langle q_3|_i\langle\bar{q}_4|_i\frac{1}{\sqrt{3}}\langle q_5|_j\langle\bar{q}_6|_j\frac{1}{\sqrt{3}}|q_1\rangle_k|\bar{q}_2\rangle_k\\ &= \frac{1}{3\sqrt{3}}\delta_{ik}\delta_{jk}\delta_{ij}\\ &= \frac{1}{\sqrt{3}}\end{aligned} \tag{5.34}$$

$$\begin{aligned}T_{flavor} &= \left[\left\langle\frac{1}{2}^{(3)}\otimes\frac{1}{2}^{(4)}\right|_{t_1,mt_1'}\otimes\left\langle\frac{1}{2}^{(5)}\otimes\frac{1}{2}^{(6)}\right|_{t_2,mt_2'}\right]_{t_f,mt'}O_F^{45}\left|\frac{1}{2}^{(1)}\otimes\frac{1}{2}^{(2)}\right\rangle_{t_i,mt}\\ &= \sqrt{2}\left\langle\left(\tfrac{1}{2}\tfrac{1}{2}\right)t,\left(\tfrac{1}{2}\tfrac{1}{2}\right)0;tt_z\right|\left(\tfrac{1}{2}\tfrac{1}{2}\right)t_1,\left(\tfrac{1}{2}\tfrac{1}{2}\right)t_2;tt_z\right\rangle\end{aligned} \tag{5.35}$$

$$\begin{aligned}T_{spin} &= \left[\left\langle\tfrac{1}{2}^{(3)}\otimes\tfrac{1}{2}^{(4)}\right|_{s_1,m_1}\otimes\left\langle\tfrac{1}{2}^{(5)}\otimes\tfrac{1}{2}^{(6)}\right|_{s_2,m_2}\right]_{s_f,m_f}(-1)^{1+\mu}\sigma_{-\mu}^{45}\left|\tfrac{1}{2}^{(1)}\otimes\tfrac{1}{2}^{(2)}\right\rangle_{s_i,m_i}\\ &= -\sqrt{2}\,C(s_im_i,1\mu,s_fm_f)\left\langle\left(\tfrac{1}{2}\tfrac{1}{2}\right)s_i,\left(\tfrac{1}{2}\tfrac{1}{2}\right)1;s_im_i\right|\left(\tfrac{1}{2}\tfrac{1}{2}\right)s_1,\left(\tfrac{1}{2}\tfrac{1}{2}\right)s_2;s_fm_f\right\rangle\end{aligned} \tag{5.36}$$

where the factor $\left\langle\left(\frac{1}{2}\frac{1}{2}\right)\alpha,\left(\frac{1}{2}\frac{1}{2}\right)\beta;JJ_z\right|\left(\frac{1}{2}\frac{1}{2}\right)\alpha',\left(\frac{1}{2}\frac{1}{2}\right)\beta';JJ_z\right\rangle$ is related to the Wigner $9j$-symbol as in Chapter 3. Note that we have rewritten t_i and t_f as t and mt and mt' as t_z due to the isospin conservation.

Unlike the color, flavor and spin wave functions, the spatial wave functions of mesons depend on the interactions between quark and antiquarks. Here in our calculation we employ the harmonic oscillator interaction, and the the transition amplitude is derived as

$$\begin{aligned} T_{spatial} &= \int \prod d^3p_i \delta(\vec{p}_1 - \vec{p}_3)\delta(\vec{p}_2 - \vec{p}_6) Y^*_{1\mu}(\vec{p}_4 - \vec{p}_5)\delta(\vec{p}_4 + \vec{p}_5)\delta(\vec{p}_1 + \vec{p}_2) \\ &\quad \cdot\delta(\vec{p}_3 + \vec{p}_4 - \vec{k}) N_1 N_2 N \exp\left(-\frac{1}{8} b^2(\vec{p}_3 - \vec{p}_4)^2\right) \\ &\quad \cdot\exp\left(-\frac{1}{8} b^2(\vec{p}_5 - \vec{p}_6)^2\right) \exp\left(-\frac{1}{8} b^2(\vec{p}_1 - \vec{p}_2)^2\right) \\ &= N_1 N_2 N \int d^3p_1 \exp\left[-\frac{3}{2} b^2(\vec{p}_1 - \frac{1}{3}\vec{k})^2 - \frac{b^2}{12}k^2\right] \left[2kY^*_{1\mu}(\hat{k}) + 2p_1 Y^*_{1\mu}(\hat{p}_1)\right] \\ &= N_1 N_2 N(4\pi)\left(\frac{4}{3}k\right) Y^*_{1\mu}(\hat{k}) \exp\left[-\frac{b^2}{12}k^2\right] \int q^2 dq \exp\left[-\frac{3}{2}b^2 q^2\right] \end{aligned} \tag{5.37}$$

Note here that we have worked in the center-of-mass system and assigned the outgoing mesons the momentum $\vec{k}$.

Using the two body phase factor

$$dQ = \frac{E_1 E_2 k}{\sqrt{s}} d\Omega_k \tag{5.38}$$

one can derive the decay width for one meson to two mesons

$$\Gamma = 2\pi \frac{E_1 E_2 k}{\sqrt{s}} \int d\Omega_k |T|^2 \tag{5.39}$$

In the rest frame of ρ meson for the reaction $\rho^0 \to \pi^+\pi^-$, we have $\sqrt{s} = M_\rho = 0.77$ GeV, $E_1 = E_2 = \sqrt{k^2 + M_\pi}$ with $M_\pi = 0.14$ GeV. We suppose, for simplicity, that the ρ and π mesons have the same length parameter b, that is

$$N = N_1 = N_2 = \left(\frac{b^2}{\pi}\right)^{3/4} \tag{5.40}$$

Let $b = 4.0$ GeV^{-1} as determined in the previous section, and take the experimental value $\Gamma = 0.15$ GeV for the decay width of $\rho^0 \to \pi^+\pi^-$, one finds that the effective strength parameter λ is predicted as

$$\lambda \approx 1.6 \tag{5.41}$$

5.2.3 e^-e^+ to $\pi^-\pi^+$ reaction

The reaction $e^-e^+ \to \pi^-\pi^+$ may result from the processes:
(1) The e^-e^+ pair annihilates into a virtual time-like photon, the virtual photon decays into a $\bar{q}q$ pair, the $\bar{q}q$ pair is dressed by an additional quark-antiquark pair pumped out of the vacuum to form a meson pair, as shown in Fig. 5.4a. The transition amplitude might be expresses formally as

$$T_1 = \langle \pi^-\pi^+|V(^3P_0)|\bar{q}q\rangle\langle\bar{q}q|T|e^+e^-\rangle \tag{5.42}$$

where $\langle\bar{q}q|T|e^+e^-\rangle$ is simply the transition amplitude of e^-e^+ to a primary quark pair while $\langle\pi^-\pi^+|V(^3P_0)|\bar{q}q$ denotes the amplitude of the process of a $\bar{q}q$ pair to a $\pi^-\pi^+$ pair. $V(^3P_0)$ is the effective vertex for creation and destruction of a quark-antiquark pair in the nonrelativistic quark model $^3P_0$.
(2) The e^-e^+ pair annihilates into a virtual time-like photon, the virtual photon decays into a $\bar{q}q$ pair, the $\bar{q}q$ pair first form a vector meson, then the vector meson decay into a meson pair. We refer the first process as one step reaction and the second two step reaction, as shown in Fig. 5.4b. The transition amplitude of the two step process take formally the form

$$T_2 = \langle \pi^-\pi^+|V(^3P_0)|\rho\rangle\langle\rho|G|\rho\rangle\langle\rho|\bar{q}q\rangle\langle\bar{q}q|T|e^+e^-\rangle \tag{5.43}$$

where $\langle\rho|\bar{q}q\rangle$ is simplify the wave function of the intermediate meson ρ^0, $\langle\rho|G|\rho\rangle$ the Green function describing the propagation of the intermediate meson, and $\langle\pi^-\pi^+|V(^3P_0)|\rho\rangle$ the transition amplitude of ρ^0 annihilation into the $\pi^-\pi^+$ pair.

Based on the works in previous sections for the reactions $\rho^0 \to \pi^-\pi^+$ and $\rho^0 \to e^-e^+$, it is straightforward to work out the transition amplitude of the reaction e^-e^+ to $\pi^-\pi^+$ in the two step model

$$\begin{aligned} T_2 &= \int d^3p_\rho\, T_{\rho^0\to\pi^-\pi^+}\frac{\delta^{(3)}(\vec{p}_\rho)}{E-E_\rho}T_{e^-e^+\to\rho^0} \\ &= T_{\rho^0\to\pi^-\pi^+}\frac{1}{E-M_\rho}T_{e^-e^+\to\rho^0} \end{aligned} \tag{5.44}$$

The differential cross section might be written in the symbolic form

$$d\sigma = \frac{|T|^2}{F}dQ \tag{5.45}$$

where dQ is the Lorentz invariant phase factor

$$dQ = (2\pi)\delta(E_f - E_i)\delta(\vec{p}_{\pi^+} + \vec{p}_{\pi^+})d^3p_{\pi^+}\, d^3p_{\pi^-}, \tag{5.46}$$

and the incident flux F is for a general frame

$$\begin{aligned} F &= |\vec{v}_{\pi^+} - \vec{v}_{\pi^-}| \\ &= 4\sqrt{(p_{\pi^+} \cdot p_{\pi^-})^2 - m_{\pi^-}^2 m_{\pi^-}^2} \end{aligned} \tag{5.47}$$

In the center-of-mass frame one can easily derive

$$dQ = (2\pi)\frac{p_f\sqrt{s}}{4}d\Omega_f \tag{5.48}$$

$$F = = 4p_i\sqrt{s} \tag{5.49}$$

where $p_i = |\vec{p}_{e^+}| = |\vec{p}_{e^-}|$, $p_f = |\vec{p}_{\pi^+}| = |\vec{p}_{\pi^-}|$, and $s = (E_{e^-} + E_{e^+})^2$.

The total cross section of the reaction e^-e^+ to $\pi^-\pi^+$ is finally derived

$$\begin{aligned} \sigma &= \frac{(2\pi)p_f}{16p_i}\int d\Omega_f |T|^2 \\ &= \frac{(2\pi)p_f}{16p_i}|T(l=1)|^2 \end{aligned} \tag{5.50}$$

Note that only the P-wave contributes to the process since the spin of the intermediate meson ρ has spin 1. There is no free parameter since the length parameter and the effective strength parameter have been nailed down respectively by the processes $\rho^0 \to e^-e^+$ and $\rho^0 \to \pi^+\pi^-$. We present in Fig. 5.5 the prediction for the cross section of the reaction e^-e^+ to $\pi^-\pi^+$ in the model of the two step process. It is found that there is no room for the one step process. The discrepancy between the theoretical prediction and the experimental data [94] at higher energies could be understood by considering the mixture of the ρ and ω mesons.

One may conclude that the two step process is dominant over the one step process.

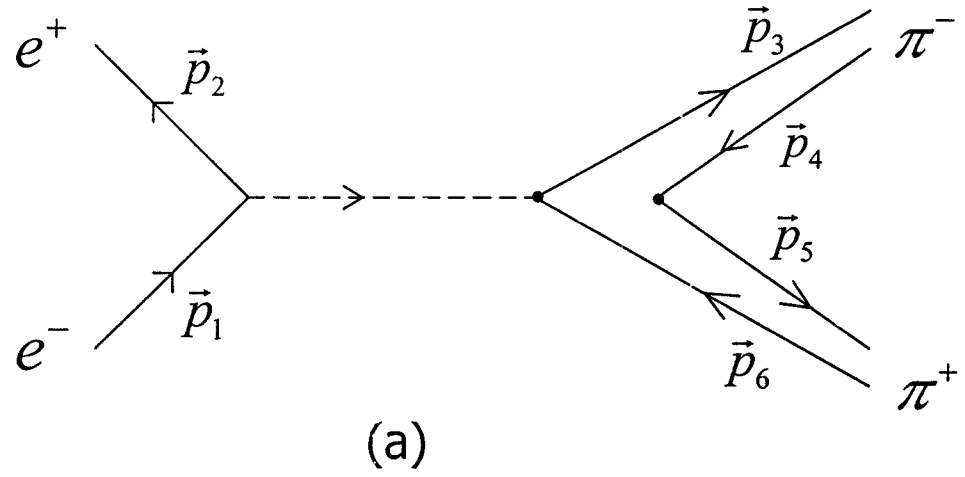

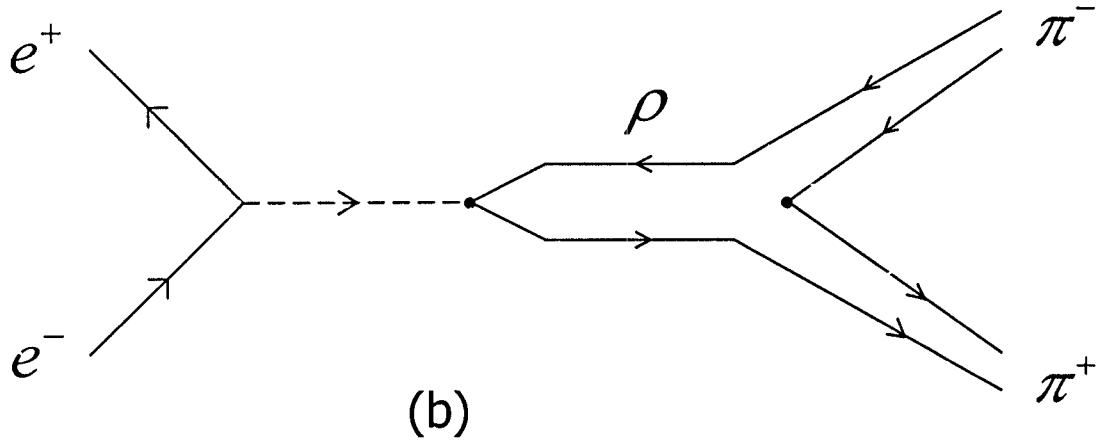

Fig. 5.4 The reaction $e^+e^- \rightarrow \pi^+\pi^-$ in the one-step process (a), and the two-step process (b).

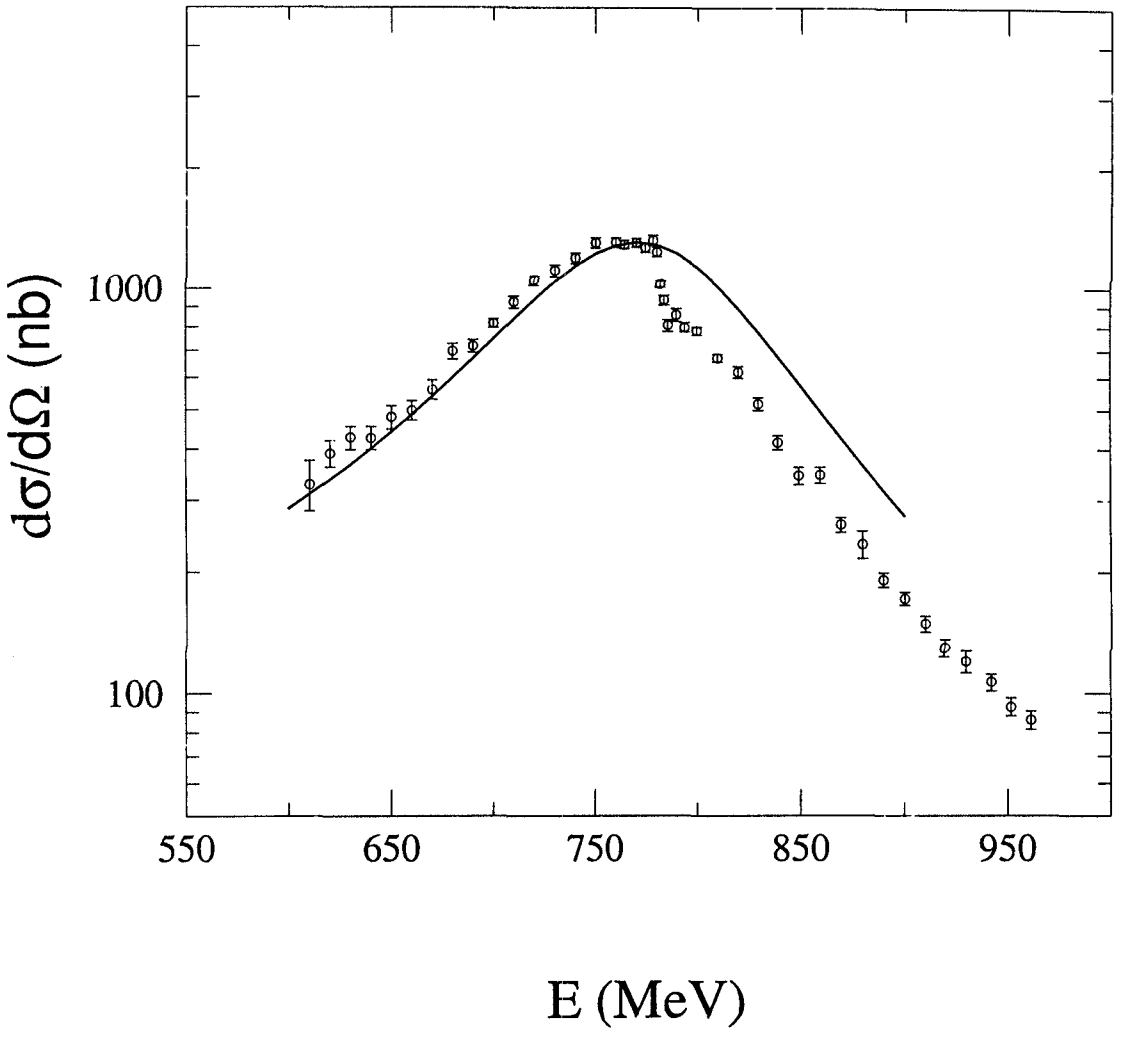

Fig. 5.5 Theoretical prediction (solid line) for the reaction $e^+e^- \rightarrow \pi^+\pi^-$ in the $^3P_0$ model against the experimental data (circles).

5.3 e^-e^+ to $\overline{N}N$

It might be reasonable to suppose that for the $e^-e^+ \to \overline{N}N$ reaction the two step process is dominant over the one step process, just like in the reaction of e^-e^+ to two mesons.

Here we study the two-step process in Fig. 5.6 that an e^-e^+ pair annihilates into a virtual time-like photon, and the photon decays into a $\bar{q}q$ pair, then the $\bar{q}q$ pair forms a virtual vector meson, finally the virtual vector meson is dressed by two additional quark-antiquark pairs pumped out of the vacuum to form a baryon pairs. The meson $\rho(2150)$ with the quantum number $I^G(J^{PC}) = 1^+(1^{--})$ is a good candidate for such an intermediate state.

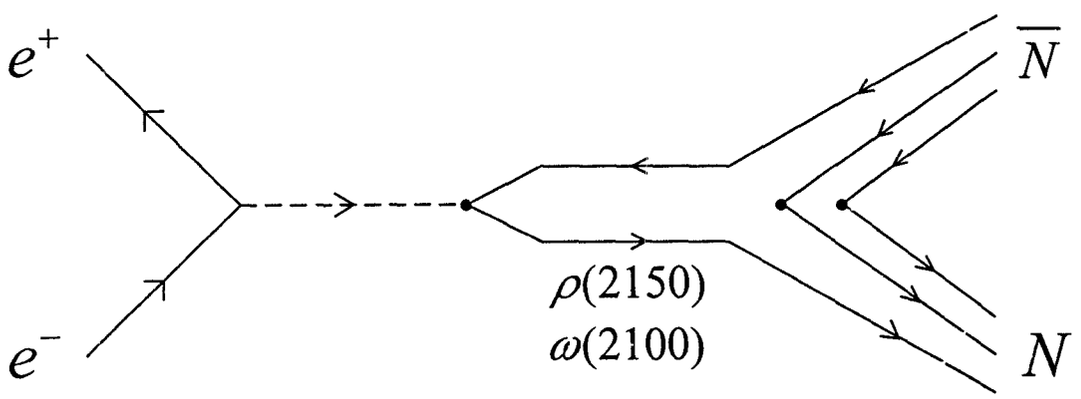

Fig. 5.6 Electron-position annihilation into nucleon-antinucleon pairs in a two-step process via intermediate vector meson states.

The transition amplitude in such a two step process takes the form

$$T = \langle \overline{N}N|V(^3P_0)|V\rangle\langle V|G|V\rangle\langle V|\bar{q}q\rangle\langle \bar{q}q|T|e^+e^-\rangle \tag{5.51}$$

Here $\langle V|\bar{q}q\rangle$ is simplify the wave function of the intermediate vector meson which can be both isospin $I = 0$ and 1 states, $\langle V|G|V\rangle$ the Green function describing the propagation of the intermediate vector meson, and $\langle \overline{N}N|V(^3P_0)|V\rangle$ the transition amplitude of the intermediate meson annihilation into a nucleon-antinucleon pair. What one needs to evaluate is the transition amplitude $\langle \overline{N}N|V(^3P_0)|V\rangle$ since other factors have been calculated in previous sections.

The transition amplitude of the reaction $\langle \overline{N}N|V(^3P_0)|V\rangle$ might be written in the form

$$\begin{aligned}\langle \overline{N}N|V(^3P_0)|V\rangle &\equiv \langle \overline{N}N|V_{25}V_{36}|V\rangle \\ &= \sum_{S'_z} C(L\,J_z - S'_z, S'S'_z, 1J_z)\cdot M_{color}M_{sf}M_{spatial}\end{aligned} \tag{5.52}$$

where the Clebsch-Gordon coefficient $C(L\,J_z - S'_z, S'S'_z, 1J_z)$ results from the spin-orbital coupling of the intermediate meson having the orbital angular momentum $L = 0, 2$ and spin S'. The V_{ij} is defined as in eq. (5.29). Using the wave functions defined in previous sections, one may derive for the color part

$$\begin{aligned}M_{color} &= \frac{1}{\sqrt{6}}\epsilon_{ijk}\langle q_1|_i\langle q_2|_j\langle q_3|_k\frac{1}{\sqrt{6}}\epsilon_{i'j'k'}\langle \bar{q}_4|_{i'}\langle \bar{q}_5|_{j'}\langle \bar{q}_6|_{k'}\frac{1}{\sqrt{3}}|q_7\rangle_\alpha|\bar{q}_8\rangle_\alpha \\ &= \frac{1}{6\sqrt{3}}\epsilon_{ijk}\epsilon_{i'j'k'}\delta_{jj'}\delta_{kk'}\delta_\alpha\delta_{\alpha i'} \\ &= \frac{1}{\sqrt{3}},\end{aligned} \tag{5.53}$$

for the spin-flavor part

$$\begin{aligned}M_{sf} = &\left\langle \frac{1}{2}^{(7)} \otimes \frac{1}{2}^{(8)}\right|_{S'S'_z}(-1)^{1+\mu}\sigma^{25}_{-\mu}\mathbf{1}^F_{25}(-1)^{1+\nu}\sigma^{36}_{-\nu}\mathbf{1}^F_{36} \\ &\frac{1}{2}\sum_{J_{23},J_{56}}\left|\left[\left(\frac{1}{2}^{(2)}\otimes\frac{1}{2}^{(3)}\right)_{J_{23}}\otimes\frac{1}{2}^{(1)}\right]_{1/2}\otimes\left[\left(\frac{1}{2}^{(5)}\otimes\frac{1}{2}^{(6)}\right)_{J_{56}}\otimes\frac{1}{2}^{(4)}\right]_{1/2}\right\rangle^{\text{Spin}}_{SS_z} \\ &\left|\left[\left(\frac{1}{2}^{(2)}\otimes\frac{1}{2}^{(3)}\right)_{J_{23}}\otimes\frac{1}{2}^{(1)}\right]_{1/2}\otimes\left[\left(\frac{1}{2}^{(5)}\otimes\frac{1}{2}^{(6)}\right)_{J_{56}}\otimes\frac{1}{2}^{(4)}\right]_{1/2}\right\rangle^{\text{Flavor}}_{TT_z}\end{aligned}$$

$$
\begin{aligned}
= \; & 2\sum_{J_{23}}\sum_{g} C(1\mu, 1\nu, g\,\mu+\nu) C(g\,\mu+\nu, S'S'_z, SS_z) \\
& \cdot \left\langle (J_{23}J_{23})\, g, \left(\frac{1}{2}\frac{1}{2}\right) S'; S \middle| \left(J_{23}\frac{1}{2}\right)\frac{1}{2}, \left(J_{23}\frac{1}{2}\right)\frac{1}{2}; S \right\rangle \\
& \cdot \left\langle \left(\frac{1}{2}\frac{1}{2}\right) 1, \left(\frac{1}{2}\frac{1}{2}\right) 1; g \middle| \left(\frac{1}{2}\frac{1}{2}\right) J_{23}, \left(\frac{1}{2}\frac{1}{2}\right) J_{23}; g \right\rangle \\
& \cdot \left\langle (J_{23}J_{23})\, 0, \left(\frac{1}{2}\frac{1}{2}\right) T; T \middle| \left(J_{23}\frac{1}{2}\right)\frac{1}{2}, \left(J_{23}\frac{1}{2}\right)\frac{1}{2}; T \right\rangle \\
& \cdot \left\langle \left(\frac{1}{2}\frac{1}{2}\right) 0, \left(\frac{1}{2}\frac{1}{2}\right) 0; 0 \middle| \left(\frac{1}{2}\frac{1}{2}\right) J_{23}, \left(\frac{1}{2}\frac{1}{2}\right) J_{23}; 0 \right\rangle
\end{aligned} \tag{5.54}
$$

and for the spatial part

$$
\begin{aligned}
M_{spatial} = & \int \prod d^3q_i \, \Psi^*_{N\overline{N}} Y_{1\mu}(\vec{q}_2 - \vec{q}_5)\delta^{(3)}(\vec{q}_2 + \vec{q}_5) Y_{1\nu}(\vec{q}_3 - \vec{q}_6)\delta^{(3)}(\vec{q}_3 - \vec{q}_6) \\
& \cdot \Psi_m(\vec{q}_7 - \vec{q}_8)\delta^{(3)}(\vec{q}_1 - \vec{q}_7)\delta^{(3)}(\vec{q}_4 - \vec{q}_8)\delta^{(3)} \\
& \cdot (\vec{q}_1 + \vec{q}_2 + \vec{q}_3 - \vec{k})\delta^{(3)}(\vec{q}_4 + \vec{q}_5 + \vec{q}_6 + \vec{k})
\end{aligned} \tag{5.55}
$$

where $\Psi_{N\overline{N}}$ is the spatial wave function of the final $N\overline{N}$ state

$$
\begin{aligned}
\Psi_{N\overline{N}} = & \exp\left[-\frac{1}{2}a^2\left(\frac{\vec{q}_2 - \vec{q}_3}{\sqrt{2}}\right)^2\right] \exp\left[-\frac{1}{2}a^2\left(\frac{\vec{q}_2 + \vec{q}_3 - 2\vec{q}_1}{\sqrt{6}}\right)^2\right] \\
& \exp\left[-\frac{1}{2}a^2\left(\frac{\vec{q}_5 - \vec{q}_6}{\sqrt{2}}\right)^2\right] \exp\left[-\frac{1}{2}a^2\left(\frac{\vec{q}_5 + \vec{q}_6 - 2\vec{q}_4}{\sqrt{6}}\right)^2\right]
\end{aligned}
$$

and Ψ_m the spatial wave function of the intermediate meson with

$$
\Psi_s(\vec{p}) = N_s \exp\left(-\frac{1}{2}b^2p^2\right)\left(\frac{15}{4} - 5b^2p^2 + b^4p^2\right) \tag{5.57}
$$

$$
\Psi_d(\vec{p}) = N_d \exp\left(-\frac{1}{2}b^2p^2\right)(bp)^2\left(\frac{7}{2} - b^2p^2\right) Y_{2L_z}(\hat{p}) \tag{5.58}
$$

In the above equations Ψ_s and Ψ_d are respectively for S-wave and D-wave mesons.

At the $\overline{N}N$ threshold, that is, $k \approx 0$, one may evaluate $M_{spatial}$ analytically. For the process with the intermediate vector meson being S-wave, we obtain

$$
\begin{aligned}
M_{spatial} = & \lambda^2 \cdot 4 \cdot (4\pi) \cdot 8 \cdot \delta_{\mu,-\nu}(-1)^\nu \cdot N_s N_b^2 \\
& \cdot \Big\{ f(2,\alpha)\left[\frac{15}{4}f(4,\beta) - 20b^2 f(4,\beta) + 14b^4 f(8,\beta)\right] \\
& - f(4,\alpha)\left[\frac{15}{4}f(2,\beta) - 20b^2 f(4,\beta) + 14b^4 f(6,\beta)\right]\Big\}
\end{aligned} \tag{5.59}
$$

For the process with the intermediate vector meson being D-wave, we have

$$M_{spatial} = \lambda^2 \cdot 16 \cdot (4\pi) \cdot 8 \cdot b^2 N_s N_b^2 \cdot I \cdot f(2,\alpha)\left[\frac{7}{2}f(6,\beta) - 4b^2 f(8,\beta)\right] \quad (5.60)$$

with

$$I = \frac{3}{\sqrt{5}}\frac{1}{\sqrt{4\pi}}C(10,10,20)C(1\mu,1\nu,2\,\mu+\nu) \quad (5.61)$$

In the above equations α and β are constants making up of the length parameters a and b

$$\begin{aligned} \alpha &= 2a^2 \\ \beta &= 2b^2 + 6a^2 \end{aligned} \quad (5.62)$$

The function $f(n,u)$ is defined as

$$f(n,u) = \int_0^\infty dx\, x^n e^{-ux^2} \quad (5.63)$$

We have now the transition amplitude of the process $V \to \overline{N}N$. The transition amplitude of the reaction $e^-e^+ \to \overline{N}N$ is derived by inserting into eq. (5.51) all the relevant parts which we have already in hands. Both the isospin 0 and 1 intermediate vector mesons will contribute to the process $e^-e^+ \to \overline{N}N$. The ratio of the cross sections of $e^-e^+ \to \overline{p}p$ to $e^-e^+ \to \overline{n}n$ take the form

$$\frac{\sigma(e^+e^- \to \overline{p}p)}{\sigma(e^+e^- \to \overline{n}n)} = \frac{|T(e^+e^- \to V(I=1) \to \overline{N}N) + T(e^+e^- \to V(I=0) \to \overline{N}N)|^2}{|T(e^+e^- \to V(I=1) \to \overline{N}N) - T(e^+e^- \to V(I=0) \to \overline{N}N)|^2} \quad (5.64)$$

The above equation indicates that the ratio will be 1 if only the $\rho(2150)$ is involved as the the intermediate meson. There are clues [94, 95] of the existence of an ω-like meson lying in the energy region of $\overline{N}N$ threshold. The vector meson has isospin 0, mass and width respectively around 2150 MeV and 240 MeV. The contribution of the $\omega(2150)$ should be included in our calculation.

The mesons $\rho(2150)$ and $\omega(2150)$ could be in the state $3S$ or $2D$ or the mixture of the $3S$ and $2D$ states. It is found in our numerical calculation that the experimental data prefer:

(1) The $\omega(2150)$ is in the $2D$ state;

(2) The $\rho(2150)$ is the mixture of the $3S$ and $2D$ states.

In our calculation we take the values of the parameters A, B and λ as predicted in the previous sections and works by other groups, that is $A = 3.0$ GeV^{-1}, $B = 4.0$ GeV^{-1}, and $\lambda = 1.6$. With the $\omega(2150)$ in the $2D$ state and the $\rho(2150)$ 25% in the $3S$ state and 75% in the $2D$ states, we derive

$$\begin{aligned} \sigma(e^+e^- \to \bar{p}p) &\approx 0.65 \text{ nb} \\ \sigma(e^+e^- \to \bar{n}n) &\approx 0.93 \text{ nb} \\ \frac{\sigma(e^+e^- \to \bar{p}p)}{\sigma(e^+e^- \to \bar{n}n)} &\approx 0.70 \end{aligned} \tag{5.65}$$

The results are consistent with the experimental data.

1S	$\rho(770)$	$\omega(782)$
2S	$\rho(1450)$	$\omega(1420)$
1D	$\rho(1700)$	$\omega(1650)$
3S or 2D	$\rho(2150)$	$\omega(2100)$?

5.4 Discussions

It is interesting to have a look at the Particle Table [96] to check how the *rho* and ω mesons come in pairs. For each ρ meson except for $\rho(2150)$, one always has one ω around with the similar mass, see Table 5.3. The work here strongly supports the argument that there exist a ω meson in the $^{13}D_1$ state with mass around 2100 MeV and width around 300 MeV.

Chapter 6

Looking Forward

It is honest to say that we have just performed researches in a small part of the particle-antiparticle physics in this project. Considering the exist and coming experimental data and the successes of our researches in proton-antiproton bound atomic states and electron-positron annihilation to nucleon-antinuclean pairs, we would like to suggest that the following topics are quite promising:

(1) $\pi\pi$ and KK atomic states, probably also deep bound states;

(2) e^-e^+ annihilation at threshold energies into meson pairs and baryon pairs like $\pi\pi$, KK, $N\overline{N}$, $\Delta\overline{\Delta}$, $\Lambda\overline{\Lambda}$, $\Sigma\overline{\Sigma}$, and so on;

(3) $\gamma\gamma$ annihilation at threshold energies into meson pairs and baryon pairs like $\pi\pi$, KK, $N\overline{N}$, $\Delta\overline{\Delta}$, $\Lambda\overline{\Lambda}$, $\Sigma\overline{\Sigma}$, and so on.

Bibliography

[1] G. 't Hooft, Nucl. Phys. B33(1971)173; B35(1971)167

[2] C.N. Yang and R.L. Mills, Phys. Rev. 96(1954)197

[3] S. Weinberg, Phys. Rev. Lett. 31(1973)494

[4] D.J. Gross and F. Wilczek, Phys. Rev. D8(1973)3633; D9(1974)980

[5] D.J. Gross and F. Wilczek, Phys. Rev. Lett. 30(1073)1343

[6] G. 't Hooft, Nucl. Phys. B75(1974)461

[7] T. DeGrand, R. L. Jaffe, K. Johnson and J. Kiskis, Phys. Rev. D12(1975)2060

[8] N. Isgar and G. Karl, Phys. Rev. D18(1978)4187

[9] A. De Rujula, H. Georgi and S.K. Glashow, Phys. Rev. D12(1975)147

[10] M. Oka and K. Yazaki, Prog. Theor. Phys. 66(1981)556; 572

[11] A. Faessler, F. Fernandez, G. Lübeck and K. Shimizu, Phys. Lett. B112(1982)201; Nucl. Phys. A402(1983)555

[12] A. Faessler and F. Fernandez, Phys. Lett, B124(1983)145

[13] O. Chamberlain, E. Segre, C. Wiegand and T. Ypsilantis Phys. Rev. 100(1955)947

[14] O. Chamberlain, *et al.* Phys. Rev. 102((1956)921

[15] G.B. Chadwick, *et al.* Phys. Rev. Lett. 10(1963)62

[16] C. Baltay, *et al.* Phys. Rev. B140(1965)1039

[17] M. Foster, *et al.* Nucl. Phys. B6(1968)107

[18] E. Fermi and C.N. Yang, Phys. Rev. 76(1949)1739

[19] R.P. Hamilton *et al.*, Phys. Rev. Lett. 44(1980)1182

[20] T. Kageyama *et al.*, Phys. Rev. D35(1987)2655

[21] W. Brückner *et al.*,Z. Phys. A335(1990)217

[22] R.A. Bryan and R.J.N. Phillips, Nucl. Phys. B5(1968)201

[23] W.W. Buck, C.B. Dover and J.M. Richard, Ann. Phys. 121(1979)47

[24] C.B. Dover and J.M. Richard, Ann. Phys. 121(1979)70

[25] C.B. Dover and J.M. Richard, Phy. Rev. C21(1980)1466

[26] R. Machleidt, K. Holinde and Ch. Elster, Phys. Rep. 149(1987)1

[27] W.N. Cottingham and R. Vinh Mau, Phys. Rev. 130(1963)735

[28] Man Chemtob, J.M. Durso and D.O. Riska, Nucl. Phys. B38(1971)141

[29] W.N. Cottingham, M. Locombe, B. Loiseau, J.M. Richard and R. Vinh Mau, Phys. Rev. B8(1973)800

[30] J. Côte, M. Lacombe, B. Loiseau, B. Moussallam, and R. Vinh Mau, Phys. Rev. Lett. 48(1982)1319

[31] M. Lacombe, B. Loiseau, B. Moussallam, and R. Vinh Mau, Phys. Rev. C29(1993)1800

[32] W.H. Barkas *et al.*, Phys. Rev. 105(1957)1037

[33] S.J. Orfanidis and V. Rittenberg, Nucl. Phys. B59(1973)570

[34] J. Vandermeulen, Lett. Nuovo Cim. 28(1980)60

[35] T. Hippchen J. Haidenbauer, K. Holinde and V. Mull, Phys. Rev. C44(1991)1323

[36] V. Mull, J. Haidenbauer, T. Hippchen and K. Holinde, Phys. Rev. C44(1991)1337

[37] J. Haidenbauer, T. Hippchen and R. Tegen, Phys. Rev. C44(1991)1812

[38] A.M. Green and J.A. Niskanen, Nucl. Phys. A412(1984)448; A430(1984)606

[39] J.A. Niskanen and A.M. Green, Nucl. Phys. A431(1984)593

[40] A.M. Green, V. Kuikka and J.A. Niskanen, Nucl. Phys. A446(1985)543

[41] M. Maruyama and T. Ueda, Nucl. Phys. A364(1981)297

[42] M. Maruyama and T. Ueda, Prog. Theor. Phys. 73(1985)1211; 74(1985)526

[43] M. Maruyama, S. Furui and A. Faessler, Nucl. Phys. A472(1987)643

[44] M. Maruyama, S. Furui, A. Faessler and R. Vinh Mau, Nucl. Phys. A473(1987)649

[45] T. Gutsche, M. Maruyama and A. Faessler, Nucl. Phys. A503(1989)737

[46] C.B. Dover, T. Gutsche, M. Maruyama and A. Faessler, Prog. Part. Nucl. Phys. 29(1992)87

[47] R. Thierauf, T. Gutsche, Y. Yan, A. Muhm and A. Faessler, Nucl. Phys. A588(1995)783

[48] E. Bauer, T. Gutsche, R. Thierauf, Y. Yan, A. Muhm and A. Faessler, Phys. Lett. B386(1996)50

[49] Y. Yan, T.Gutsche, R. Thierauf, A. Muhn and Amand Faessler, J. Phys. G23 (1997) 33.

[50] C.B. Dover, T. Gutsche and A. Faessler, Phys. Rev. C43(1991)379

[51] A. Le Yaouanc *et al.*, Phys. Rev. D8(1973)2223; D9(1974)1415; D11(1975)1272

[52] N. Isgur and J. Paton, Phys. Rev. D31(1985)2910

[53] R. Kokoski and N. Isgur, Phys. Rev. D35(1987)907

[54] H.G. Dosch and D. Gromes, Phys. Rev. D33(1986)1378; Z. Phys. C34(1987)139

[55] H.J. Weber, Phys. Lett. B218(1989)267

[56] B. May *et al.*, Z. Physik C46(1990)191

[57] P. Weidenauer *et al.*, Z. Physik C47(1991)353

[58] C. Amsler and F. Myhrer, Ann. Rev. Nucl. Part. Sci. 41(1991)219

[59] E.M. Henley, T. Oka and J.D. Vergados, Nucl. Phys. A476(1988)589

[60] V.W. Hugher, Ann. Rev. Nucl. Sci **16**, 445 (1966); C.S. Wu and L. Wilets, Ann. Rev. Nucl. Sci. **19**, 527 (1969).

[61] G. Backenstoss, Ann. Rev. Nucl. Sci. **20**, 467 (1970); E.H.S. Burhop, High Energy Physics, 3 (1969).

[62] J.S. Cohen and N.T. Padial, Phys. Rev. A**41**, 3460 (1990).

[63] S. Ahmad, *et al.*, Phys. Lett. **157B**, 333 (1985); M. Ziegler, *et al.*, Phys. Lett. **206B**, 151 (1988); C.W.E. Van Eijk, *et al.*, Nucl. Phys. **A486**, 604 (1988); C.A. Baker, *et al.*, Nucl. Phys. **A483** 631 (1988); R. Bacher, *et al.*, Z. Phys. A**334**, 93 (1989).

[64] K. Heitlinger, *et al.*, Z. Phys. **A342**, 359 (1992)

[65] M. Augsburger, *et al.*, Nucl. Phys. **A658**, 149 (1999)

[66] D. Gotta, *et al.*, Nucl. Phys. **A660**, 283 (1999)

[67] R.A. Bryan and R.J.N. Phillips, Nucl. Phys. **B5**, 201 (1968).

[68] T.L. Trueman, Nucl. Phys. **26**, 57 (1961).

[69] A.M. Green and S. Wycech, Nucl. Phys. **A377**, 441 (1982).

[70] W. Schweiger, J. Haidenbauer and W. Plessas, Phys. Rev. C **32**, 1261 (1985).

[71] J. Thaler, J. Phys. G **9**, 1009 (1983).

[72] W.B. Kaufmann and H. Pilkuhn, Phys. Rev. C **17**, 215 (1978); W.B. Kaufmann, Phys. Rev. C **19**, 440 (1979).

[73] M.A. Alberg, *et al.*, Phys. Rev. D **27**, 536 (1983).

[74] B. Moussallam, Z. Phys. A **325**, 1 (1986).

[75] J. Carbonell, G. Ihle and J.-M. Richard, Z. Phys. A**334**, 329 (1989).

[76] C.B. Dover, J.M. Richard and J. Garbonell, Ann, Phys. (N.Y.) **130**, 70 (1980)

[77] C.B. Dover, J.M. Richard and J. Garbonell, Phys. Rev. **C44**, 1281 (1991)

[78] T.H. Burnett and S.R. Sharpe, Ann. Rev. Nucl. Part. Sci. 40(1990) 327; K. Peters, Nucl. Phys. **A558**, 93c (1993); G. Kari, Nucl. Phys. **A558**, 113c (1993); C.B. Dover, Nucl. Phys. **A558**, 721c (1993); C. Amsler, 27th International Conference on High Energy Physics. Glasgow, July 1994.

[79] Y. Yan, Ph.D. Thesis, Universität Tübingen, 1994.

[80] E. Holoien, Phys. Rev. **104**, 1301 (1965).

[81] H. Schull and P.-O. Löwdin, J. Chem. Phys. **30**, 617 (1959).

[82] M. Rotenberg, Adv. At. Mol. Phys. **6**, 233 (1970).

[83] E. Truhlik, Nucl. Phys. **A296**, 134 (1978).

[84] B. Gyarmati, A.T. Kruppa and J. Révai, Nucl. Phys. **A326**, 119 (1979); B. Gyarmati and A.T. Kruppa, Nucl. Phys. **A378**, 407 (1982).

[85] B. Gyarmati, A.T. Kruppa, Z. Papp and G. Wolf, Nucl. Phys. **A417**, 393 (1984).

[86] K.F. Pál, J. Phys. A **18**, 1665 (1985).

[87] J. Carbonell, Private Communication.

[88] M.G. Meißner, N. Kaiser and W. Weise, Nucl. Phys. A466(1987)685

[89] B. El-Bennich, M. Lacombe, B. Loiseau and R. Vinh Mau, Phys. Rev. C59 (1998) 2313.

[90] M. Pignone, M. Lacombe, B. Loiseau and R. Vinh Mau, Phys. Rev. C50 (1994) 2710.

[91] A. Antonelli *et al.*, Nucl. Phys. B517, 3(1998).

[92] A. Antonelli *et al.*, Phys. Lett. B334, 431(1994), D. Bisello *et al.*, Z. Phys. C48, 23(1990)

[93] G. Bardin *et al.*, Nucl. Phys. B411, 3(1994)

[94] R.R. Akhmetshin *et al.*, Phys. Lett. **B527** (2002) 161.

[95] Anisovich *et al.*, Phys. Lett. **B476** (2000) 15.

[96] Anisovich *et al.*, Phys. Lett. **B507** (2001) 23.

[97] Review of Particle Physics, D.E. Groom *et al.*, Eur. Phys. J. C **15** (2000) 1

Biography

Dr. Yupeng Yan was born on April 2, 1962 in Inner Mongolia, P.R. China. He earned in 1994 Ph.D. in nuclear and particle physics from Prof. Amand Faessler in the Institute for Theoretical Physics, Tübingen Uiniversity, Germany. After some three years of research work as postdoctoral fellows in Tübingen University and University of the Witwatersrand in South Africa, he joined in 1997 the School of Physics, Suranaree University of Technology.